DISSERTATION

Global Soil Moisture Retrieval from ERS Scatterometer Data

ausgeführt zum Zwecke der Erlangung des akademischen Grades eines Doktors der technischen Wissenschaften unter der Leitung von

Univ.Prof. Dipl.-Ing. Dr.techn. Wolfgang Wagner
Institut für Photogrammetrie und Fernerkundung

eingereicht an der Technischen Universität Wien
Technisch Naturwissenschaftliche Fakultät

von

Klaus Scipal
Matr. Nr. 9225259

Große Sperlgasse 41/28
1020 Wien

Wien, am 21. Mai 2002

ABSTRACT

Soil moisture exerts a prominent control on the interactions between the hydrosphere, biosphere and atmosphere. Being basic to all surface bio-geophysical processes, an accurate assessment of the spatial and temporal variation of soil moisture is important for numerous applications and for answering diverse research questions. Given the crucial role that soil moisture plays in land-surface processes, it is desirable to monitor soil moisture with the same accuracy and frequency as other important environmental variables such as temperature, precipitation or wind.

However, currently only a few measurement networks exist, providing reliable data. The lack of a convincing approach to global soil moisture monitoring is by many felt as a pressing deficiency in related research disciplines. It is often stated, that microwave remote sensing might overcome the limitations of traditional methods.

The objective of this thesis was to apply a novel approach to monitor soil moisture on a global scale. The retrieval is based on ERS scatterometer data, a low resolution active microwave instrument operated in C-band, flown onboard of ERS-1 and ERS-2 satellites. The method can be regarded as a combination of an empirical model to describe basic scattering properties of the land surface and a simple change detection method to retrieve geophysical parameters.

The method has been applied successfully to global land surfaces of various climates. The distinct effect of different climatic regimes on the scattering properties of the land surface has been indicated. Derived parameters, describing scattering properties of the land surface, closely follow characteristic climate and vegetation patterns. Based, on a detail study of global scattering properties problematic concepts of the physical model were identified and will lead to an improvement of the method.

Validation of retrieved soil moisture indicated a high accuracy. The error of soil moisture estimates is in the range of 5-7 vol%. The data set can therefore be used in a number of applications related to the global hydrosphere, biosphere and atmosphere.

ZUSAMMENFASSUNG

Bodenfeuchte ist eine wesentliche Komponente des globalen Ökosystems und übt einen wichtigen Einfluss auf die Wechselwirkungen zwischen der Hydrosphäre der Biosphäre und der Atmosphäre aus. Aufgrund der Bedeutung von Bodenfeuchte für alle bio- und geophysikalischen Prozesse, ist genaue Information über die Variabilität dieser geophysikalischen Größe für viele Bereiche wichtig. Im Gegensatz zu einer Vielzahl von geophysikalischen Größen wie Temperatur, Niederschlag oder Wind, die in hoher Präzision und Dichte gemessen werden, wird Bodenfeuchte nur von wenigen Meßsysteme adäquat gemessen.

Das Fehlen geeigneter Daten und Meßsysteme wird von allen betroffenen Wissenschaften als großes Defizit gesehen. Der Entwicklung von neuen innovativen Methoden kommt daher größte Bedeutung zu. Fernerkundung, im speziellen Radar Fernerkundung, wird generell als möglicher Lösungsansatz gesehen.

Ziel dieser Arbeit war die globale Anwendung einer neuen innovativen Methode zur Beobachtung von Bodenfeuchte. Grundlage der Methode sind ERS Scatterometer Daten. Der ERS scatterometer ist ein C-band Radarsensor mit einer Auflösung von 50x50 km² der seit 1992 an Bord der Europäischen Fernerkundungssatelliten ERS-1 und ERS-2 die Erde beobachtet. Die Methode zur Analyse der Daten basiert auf einem empirischen Modell mit dem das grundlegende Streuverhalten der Erdoberfläche beschrieben wird und einem einfachen Change Detection Ansatz zur Ableitung der gesuchten Größen.

Die Methode, die über ausgewählten Gebieten entwickelt wurde, konnte erfolgreich global angewendet werden. Charakteristische Auswirkungen der einzelnen Klimate auf das Rückstreuverhalten wurden nachgewiesen. Die zur Beschreibung der Rückstreueigenschaften abgeleiteten Parameter zeigen eine klare Korrelation mit charakteristischen Klima und Vegetationszonen. Basierend auf einer detaillierten Analyse der Rückstreueigenschaften, konnten problematische Konzepte in der Formulierung des zugrundeliegenden physikalische Modells aufgezeigt werden. Aufgrund dieser Studien ist eine Verbesserung der Methoden möglich.

Die Validierung der abgeleiteten Bodenfeuchte ergab eine hohe Genauigkeit, der mittlere Fehler liegt im Bereich 5-7 vol%. Die Daten eignen sich daher für eine Reihe von hydrosphärischen biosphärischen und atmosphärischen Anwendungen.

ACKNOWLEDGEMENTS

This research was carried out on the Institute of Photogrammetry and Remote Sensing of Vienna University of Technology. Funding was made available by the Austrian Science Fund under the research grant P14002.

I would like to thank all those who have contributed time and effort to make this research a reality. In the first place, I would like to thank Wolfgang Wagner and Karl Kraus without their enthusiasm and interest this work would not have been possible. Further, I am especially grateful to my co-advisor Christiane Schmullius.

For providing satellite and reference data, I thank Niels Ringelmann, Alan Robock and Zheng Yuling. Special thanks for providing assistance and support whenever I needed go to Marco Trommler, Kathleen Naumann and Richard Kidd.

Finally, I wish to thank my parents, my wife Margot and my children Johanna, Ferdinand and Otto for their unwavering support and encouragement.

CONTENTS

1 INTRODUCTION

1.1 Motivation

Soil moisture exerts a prominent control on the interactions between the hydrosphere, biosphere and atmosphere. Being basic to all surface bio-geophysical processes an accurate assessment of the spatial and temporal variation of soil moisture is important for numerous applications and for answering diverse research questions.

Most generally, soil moisture is defined as the volume fraction of water held in the soil (Hillel, 1982). However, the actual concept of this variable is elusive because specialists from various disciplines perceive soil moisture differently. A farmer's concept of soil moisture is different from that of a water resource manager or a weather forecaster. Nevertheless, broad agreement about the importance of soil moisture prevails. Soil moisture is regarded to be a key state variable of the global energy, water and carbon cycles and is such of crosscutting importance for a wide range of applications, from climate monitoring and ecological applications to the quantification of bio-geophysical fluxes (e.g. Cramer et al., 1999). Soil moisture is the switch that controls the proportion of rainfall that percolates, runs off, or evaporates from the land. It is the life-giving substance for vegetation. Soil moisture integrates precipitation and evaporation over periods of days to weeks and in this way introduces a significant element of memory in the atmosphere/land system. Through its dominant influence on key physical processes, soil moisture is a variable that has always been required in many interdisciplinary scientific and operational applications. These include: (a) agriculture, where knowledge of root zone soil moisture leads to efficient irrigation management, increased production, crop yield forecast, and pest detection and control; (b) forest ecology, where soil moisture information can lead to better harvesting management and yields; (c) civil engineering, where soil moisture can be an important structural consideration or can help to identify geologic hazards; (d) water resources, where water-balance studies, hydrologic process studies, flood forecasting, drought assessment, and precipitation pattern analysis depend on knowledge of soil moisture stores; (e) climate studies, where changes in long-term soil moisture stores have been identified as an indicator of climate change, and soil moisture information can calibrate and validate global climate models; (f) ecosystem modelling, where biogeochemical cycles are dependent on soil moisture states; and (g) soil science, where soil moisture plays a key role in erosion, mass movement, ecology, and land potential.

1.2 Soil Moisture Monitoring

Given the crucial role that soil moisture plays in land-surface processes, it is desirable to monitor soil moisture with the same accuracy and frequency as other important environmental variables such as temperature, precipitation or wind. There are many well-established methodologies for *in-situ*, point measurement of soil moisture. However, area representative precise *in-situ* measurements are in general expensive and tedious to collect (Hollinger and Isard, 1994; Rombach and Mauser, 1997). The great spatial variability of soil moisture at scales from millimetres to hundreds of meters and the associated question how reliable spatial soil wetness values can be derived is one of the major problems of traditional measurement techniques (Schulin et al., 1992). With the exception of a few large-scale measurement networks, providing widespread information on soil moisture (Georgakakos and Baumer, 1996; Robock et al., 2000), continuous information is all but nonexistent. Beside the large-scale soil moisture networks with low frequency sampling (generally every 10 days), and coarse spatial resolution, several experimental small-area measurement sites have been established, such as HAPEX Sahel (Goutorbe et al.) or Little Washita (Jackson et al., 1995). Although these sites have a fine spatial coverage, monitoring generally spans only a short time period, typically only a few weeks.

Wei (1995) considered the lack of a convincing approach to global soil moisture monitoring as a serious problem of current research with far reaching significance to human society. Missing information on soil moisture variability is felt as pressing deficiency in related research disciplines (e.g. Jackson, 2002; Grassl and Bengtsson, 2001; Blöschl and Sivapalan 1995; Dirnmeyer 1995). The problem has also been addressed in global scale studies. For example, within the Global Energy and Water Cycle Experiment GEWEX a Global Soil Wetness Project GSWP was implemented. The goal of GSWP is to produce global soil moisture data, based on meteorological observations from 1987 to 1988, using ten different land surface models. Entin et al. (1999) validated the results and concluded that none of the models did a good job of producing the actual soil moisture data.

Remote sensing of soil moisture from the vantage point of space might bypass the limitations of traditional methods by naturally providing a spatial measure at relative low cost. Research in soil moisture remote sensing began in the mid 1970's shortly after the surge in satellite development. Subsequent research has occurred along many diverse paths. Today it is commonly agreed that among the various sensors, microwave technology has the highest potential to measure soil moisture under a variety of environmental conditions so that it could be extended to a routine measurements system (Engman, 1990). But still soil moisture remote sensing is fraught with

challenges. Only the moisture in the top few centimetres of soil can be detected and the need for surface roughness and vegetation corrections complicates algorithm development.

1.3 Scope of the Work and Structure of the Thesis

Since 1994 the Institute of Photogrammetry and Remote Sensing of Vienna University of Technology, in collaboration with other partners, has been working on a method to retrieve soil moisture from low-resolution active microwave data collected by the ERS scatterometer. The method has been developed systematically over selected study areas. Over the Canadian Prairies the problem of varying incidence angles of the ERS Scatterometer measurements was addressed (Wagner et al., 1999a). Over the Iberian Peninsula the effect of vegetation was studied in detail (Wagner et al., 1999b). To estimate the water content in the soil profile from topsoil moisture as provided by the ERS Scatterometer a method was developed over Ukraine and Russia (Wagner et al., 1999c). The positive experience collected in these studies motivated the next steps and to continue research and development. The scope of this study is twofold: 1) Apply the method on a global basis, collect an extensive reference data set, validate the retrieved soil moisture data over regions with reliable reference data, and finally improve the method based on the findings of the validation effort. 2) Advance our knowledge of the backscattering behaviour over land surfaces in C-band by studying the dependence of backscatter characteristics on vegetation, soil, and climate on a global scale.

The thesis is structured as follows: Chapter 2 reviews developments in active microwave remote sensing, followed by a brief introduction of ERS scatterometer data in Chapter 3. All relevant auxiliary data used are described in Chapter 4. Chapter 5 provides a specification of the applied method and of basic products. Chapter 6 and Chapter 7 are concerned with elementary data validation of derived soil moisture data using spectral analysis tools and *in-situ* data. Finally, Chapter 8 summarizes experiences gained during this study and comments on future directions.

2 STATE OF THE ART

2.1 Progress in Microwave Remote Sensing

The scientific community widely agrees that only microwave remote sensing (active and passive) offers the possibility to collect truly quantitative soil moisture information (Engman, 1990). Investigations into the potential of radars in geosciences began in the 1960s and gained momentum with the launch of the SEASAT satellite in 1978. In the 1980s and early 1990s, given the impending launch of a number of satellite systems, a variety of aircraft and NASA space shuttle missions were conducted in support of radar applications in land, sea and ice monitoring. Radar satellite systems were launched by Europe (ERS-1 and ERS-2), Japan (JERS-1) and Canada (RADARSAT) in the early 1990s and three more satellites are scheduled for launch in the next two years.

There are two broad types of side looking radar sensors, synthetic aperture radar (SAR) and scatterometer, which provide data on different spatial and temporal scales. In general SAR systems provide higher spatial but poorer temporal resolution data than scatterometer systems. For example, the ERS-1 and ERS-2 SAR system provides 25 m spatial resolution data over an area of 100 x 100 km^2 with a 35 day repeat cycle. The ERS-1 and ERS-2 scatterometer provides 50 x 50 km^2 spatial resolution data over an area of 500 x 500 km^2 with global coverage achieved in 3 to 4 days. In the case of RADARSAT, the SAR can be configured in a number of modes with differing spatial and temporal resolution. The ScanSAR mode provides information over a 500-km swath at 100 m spatial and 3-4 day temporal resolution compared to the fine or standard mode that provides information over a 50 to 100-km swath at high spatial (9-25 m) but low temporal (24-day) resolution.

Independent of the sensor type, interpretation of radar data is said to be fraught with challenges. Potential techniques must account for the confounding effects of the processes involved in the scattering of electromagnetic waves. Both the radar configuration (frequency, polarization, viewing geometry) as well as target characteristics (dielectric properties, soil texture, surface roughness, vegetation, topography) influence backscatter from natural surfaces. The complex interaction of these parameters requires a thorough understanding of the underlying physical concepts. In fact, developing methods that properly account for the scattering mechanism has proven to be a major scientific challenge. Despite the existence of numerous radar sensor systems in the 1990s, progress in the use of radar in environmental monitoring, particularly with respect to land surface hydrology, has been slower than anticipated. Even worse, a decline in

innovative research has been noticed. Ulaby (1998) thinks that most of the recently published techniques are adaptions of formerly proposed methods, still of scientific character and lacking of widespread operational application. Taking on a different perspective one may encounter that our understanding of radar capabilities has improved considerably, which allows a more intuitive application of data. Experience has shown that essential elements to improve retrieval capabilities are to use multi-dimensional data such as offered by the new radar systems (multi-polarisation, multi-incidence, multi-temporal) and to constrain the problem to reduce the number of influencing parameters. For example, Quesney et al. (2000) showed that it is possible to estimate a watershed soil moisture index from SAR data by selecting "soil moisture sensitive" targets, over which the impact of vegetation and surface roughness is minimized. Overall, exciting developments in the 1980s and early 1990s have indicated the potential of radars for soil moisture monitoring.

2.2 Retrieval Methods

Since the late 1970s numerous techniques to retrieve geophysical parameters from radar data have been developed. Theoretical, empirical and semi-empirical models have been the topic of considerable research. More recently, approaches involving change detection and neural networks have gained attention.

2.2.1 Theoretical Models

Theoretical models are useful in understanding and interpreting remote sensing data. They can be valuable in predicting the scattering behaviour of natural surfaces under different environmental conditions. Studies of canopy backscatter used the Michigan Microwave Canopy Scattering Model MIMICS (Ulaby et al. 1990) and more recently the radiative transfer model RT2 (Cookmartin et al. 2000). Both models incorporate mechanisms for evaluating the role of soil and plant components in attenuating and scattering the radar signal. Simple geometric forms together with dielectric properties depict the plant components in both instances. Surface roughness and dielectric properties define the soil component.

Simulation results from the MIMICS model involving L- and C-band radar in both wheat and canola showed a good relationship to ground-based scatterometer data throughout the season and effectively estimated soil moisture under the canopy (Touré et al. 1994). The MIMICS model incorporates three different models for geophysical parameter retrieval, the small perturbation and two variations on the Kirchhoff model. The small perturbation model is more appropriate for smooth surfaces and the Kirchhoff models for intermediate or rough surfaces. The validity of the

newer Integral Equation Model IEM (Fung et al. 1992; Fung and Pan, 1987) and Michigan Empirical Model (Oh et al. 1992) over a wider range of natural conditions and radar frequencies overcomes the limitations of the small perturbation and Kirchhoff models (Dubois et al. 1995).

The disadvantage of theoretical models is that their inversion is difficult due to the complex equations involved in describing the scattering process of natural targets (Engman et al. 1995, Shi et al. 1997, Bindlish and Barros, 2000). The use of multifrequency or multipolarized data or the addition of ancillary data (e.g. surface roughness) can overcome the inversion problems by providing additional constraints to the model. Bindlish and Barros (2000) used multifrequency, multipolarization data from SIR-C/X-SAR to derive soil moisture in the Little Washita Watershed in Oklahoma using the IEM model in a direct inversion mode. In another study Narayanan and Hirsave (2001) using data from the same sensor over a different area, applied the simplified Kirchhoff, the physical optics and the geometric optics model, as they found the IEM model to be highly complex and computational too intensive. Both studies obtained reliable soil moisture estimates.

2.2.2 Semi-Empirical Models

Intermediate in complexity between the theoretical and empirical models are the semi-empirical models, sometimes referred to as physically based models. These models, which have fewer parameters and variables, require in general *in-situ* data sets to permit fitting of model coefficients.

For example, Shi et al. (1997) adapted the IEM to handle additional empirical surface roughness parameters. To facilitate inversion of the algorithm, multiple scattering was ignored and replaced by a single term to describe surface roughness, derived from experimental data. The adapted model was successfully applied to L-band multipolarized SAR data.

In terms of vegetation, the Cloud Model proposed by Attema and Ulaby (1978) has been used extensively. This model is based upon the vegetation being represented by a homogenous horizontal “cloud” of identical water spheres distributed uniformly throughout the depth of the canopy. The height and volumetric moisture of the canopy are the only important factors. Unlike the theoretical models, only single scattering is considered and radar backscatter is a function of that from the vegetation component and that from the soil, the latter being attenuated through the vegetation. In particular, the amount of water in the vegetation canopy and the volumetric moisture content in the topsoil are important.

Several authors used variations of the water-cloud model to estimate surface soil moisture and vegetation parameters including canopy moisture and green leaf area index GLAI (Prevot et al. 1993a, Prevot et al. 1993b, Taconet et al. 1994, Xu et al. 1996, Clevers and van Leeuwen 1996, Moran et al. 1998). Studies suggest that dual frequency radars are potentially more suited than single band radars to derive canopy and soil information using the Cloud Model. Moran et al. (1998) found that up to a GLAI value of 4, high frequency K_u (VV) radar was sensitive to increases in GLAI while the lower frequency C-band (VV) was sensitive to soil moisture. Above a GLAI value of four, the Ku band saturated and the sensitivity of C-band to soil moisture decreased due to attenuation of the signal by the vegetation. Similarly, Prevot et al. (1993a) found that the simultaneous of X-band (VV) adapted to biomass estimation and C-band (HH) adapted to soil moisture estimation, enabled both soil moisture and LAI estimation of wheat canopies. Unfortunately, there are no satellite systems providing dual frequency data.

Frison and Mougin (1996) suggested that ERS scatterometer data are useful for monitoring global vegetation since they observed a substantial agreement between backscatter and global vegetation index maps. Consequently, several researchers (Magagi and Kerr, 1997; Frison et al., 1998; Woodhouse and Hoekman, 2000a) developed models capable of dynamically retrieving vegetation parameters from ERS scatterometer data, predominantly applied over semi-arid environments in Africa. In these environments, where seasonal soil moisture and vegetation patterns closely correlate, the models depicted year-to-year differences. However, an application of the model by Woodhouse and Hoekman (2000b) over a Mediterranean region (Spain) did not properly recover the seasonal vegetation signal, but provided soil surface reflectivity values in agreement with monthly precipitation records.

2.2.3 Empirical Models

Empirical models involve the development of a relationship using an existing experimental data set. Examples exist in the literature involving simple linear and non-linear relationships between radar backscatter and target parameters or involving multi-variate regression analysis techniques. For example on the short grass prairie in western Canada where vegetative production is low, a simple linear relationship existed between radar backscatter and both soil and plant moisture content (Major et al. 1994). In situations, with higher vegetative productivity, plant height in combination with canopy water content proved to have a stronger relationship with radar backscatter than either parameter alone (McNairn et al. 1998). Champion (1996) formulated a simple model based upon the assumption that for bare soil surfaces, roughness does not change over time and that the entire variability in the backscatter measurements attributes to changes in

the soil moisture content. In contrast, Oh et al. (1992) and Dubois and Van Zyl (1994) developed empirical models using the fit between ground-based scatterometer data and the root mean square height and dielectric constant of the soil. Both, the Oh and Dubois model, require more than one polarization of radar. Until the launches of the next generation of radar satellites (ENVISAT, RADARSAT-2, ALOS) multipolarized data is not available. Magagi and Kerr (2001), using a modification of the Oh model, retrieved soil moisture over a Sahelian biome using ERS scatterometer data. Soil roughness was estimated during the dry season, and overlying vegetation was estimated separately using first order radiative transfer theory. Using an empirical approach appeared superior to that involving the theoretical models, requiring exact knowledge of the surface physical properties. As at the low spatial resolution of ERS scatterometer data, multiple surface and vegetation types were believed to influence the performance of the theoretical models.

Empirical models are easy to handle and have found wide spread acceptance within the scientific community (Engman et al. 1995). However, empirical models, by definition, are generally restricted to conditions similar to those under which they were developed and care must be taken when the models are migrated to new areas or applications.

2.2.4 Change Detection

Several studies illustrate the use of a temporal series of images and change detection to derive information (Ulaby et al. 1996; Engman et al. 1995; Dobson et al. 1986, Kunch et al. 2000, Yanasse et al. 1992). Rather than using complex methods describing the full range of parameters influencing the scattering process, change detection methods primarily take advantage of seasonal variation or variation over time to derive information.

Moran et al. (2000) used multitemporal SAR data over a semiarid rangeland to retrieve soil moisture. While the correlation between the backscattering coefficient and soil moisture measured at three test sites was low (r^2=0.27), the correlation was r^2=0.93 when a SAR image from the dry season was subtracted from all other images to correct for surface roughness and standing brown biomass.

Wagner et al. (1999a, 1999b, 1999c) developed a method to retrieve the moisture content of the remotely sensed surface layer. The technique is as change detection approach based on ERS scatterometer data, taking full advantage of the multi-viewing capabilities of the sensor, the availability of several years of backscatter data and the high temporal sampling rate. At the core of the method is an empirical backscatter model, describing the scattering behaviour of each point on the Earth's surface. Parameters are estimated from long backscatter series. Soil moisture is

retrieved by means of a change detection method, considering seasonal vegetation cover effects. The separation of temporal soil moisture and vegetation effects on the scatterometer signal is possible thanks to the multi-viewing capabilities of the ERS Scatterometer. The method has proven to yield consistent results for various climatic and vegetation zones that compare favourably with rainfall and in-situ soil moisture data (Wagner and Scipal, 2000).

2.2.5 Neural Networks

Neural networks take a different approach to problem solving than conventional models. Information processing is similar to the human brain. A large number of highly interconnected processing elements working in parallel to solve a specific problem compose the network. Unlike theoretical or semi-empirical models, neural networks do not need to know the mapping function between input and output parameters in its explicit forms. Thus, neural networks can be an appropriate tool in solving non-linear mapping problems encountered in the retrieval of geophysical parameters from radar data. The quality of the output parameters is directly dependent upon the quality of the data used to train the processor. The learning patterns must therefore be selected carefully otherwise the network might not function correctly.

The most direct way to train a neural network is by using ground observations. However, the scarcity of appropriate data led to a more pragmatic approach based on synthetically generated data using empirical or theoretical surface scattering models. Dawson et al. (1997) retrieved soil moisture by applying a statistical based estimator, which in its concept is similar to neural networks. Results are comparable to those retrieved with empirical models of Oh and Dubois, with the major advantage that the applicability of the method is not dependent on any specific set of field data. The question on what can be achieved using neural networks on global real world data remains to be evaluated.

2.3 Statement of the Problem and Way Forward

2.3.1 Description of Surface Roughness and Vegetation

Various approaches to retrieve geo-physical parameters from radar data have been discussed, ranging from simple regression models to elaborated theoretical models. Most of these models have an experimental character, not suited for widespread routine application.

Still a major problem is the statistical description of roughness of non-artificial surfaces and the limited range of validity of currently available bare soil backscatter models. As a result, a given model performs well over one area or given data set, while errors are high over other areas

respectively data sets. This applies to both semi-empirical models, like the model from Oh et al. (1992), and theoretical models like the geometrical optics model (Ulaby et al., 1986) and the Integral Equation Method IEM developed by Fung (1994).

Roughness of natural soil surfaces is generally described by an autocorrelation function and the associated variables r.m.s. height and correlation length. Only recently, several scientists questioned the accuracy of this characterization (e.g. Davidson et al. 2000). Dobson and Ulaby (1998) found that the inadequate representation of surface roughness variations of real surfaces is partly responsible for the relatively poor agreement between modelled and experimentally observed radar responses. Similarly, Davidson et al. (2000) state that the weak point in the development of model based soil moisture retrieval algorithms appears to be due to an inadequate description and measurement of natural surfaces. Often, a superposition of many scales describes soil roughness better. For example, by using a 25-m long laser profiler Davidson et al. (2000) could show for five agricultural fields that the roughness characteristics are well described by the superposition of a single scale process related to tillage stage with a multi-scale random fractal process related to field topography.

Another challenge yet is to account for vegetation cover. In principle, models capable of comprehensively describing backscatter from vegetated surfaces are available (Ulaby et al., 1990) but the problem is that these models require a detailed description of the vegetation layer. Consequently, these models can yield insight into the backscattering behaviour of vegetation, but inversion is either impossible or at least very tedious (Oevelen and Hoekman, 1999). Therefore, simpler models requiring less input parameters, such as the Cloud Model developed by Attema and Ulaby (1978), have generally been preferred.

2.3.2 Approaches in Scatterometry

In scatterometry, research has focused on the use of semi-empirical and empirical models for retrieving geophysical parameters such as soil moisture, snow/soil thawing, vegetation, and snow accumulation. Wismann (2000) investigated the capability of the ERS Scatterometer for detecting thawing of soil and vegetation in Siberia. A simple change detection method produced results that were consistent with air temperature observations and SSM/I derived snow cover maps. Scipal (1999) investigated methods to detect freezing and thawing in Northern Canada obtaining results that compared well with synoptic weather records.

Vegetation distributions were studied by Frison and Mougin (1996), using data from the ERS Scatterometer. Distibution of derived radar parameters revealed many similarities to global vegetation maps. The first quantitative studies comparing results with reference data showed for

example a good correlation of derived radar parameters to canopy density and phytomass over Siberia (Schmullius, 1997).

A number of research teams investigated the use of semi-empirical models for retrieving soil moisture from ERS Scatterometer data. So far, semi-empirical models have been developed by Pulliainen et al. (1998) for boreal forests, by Magagi and Kerr (1997) and Frison et al. (1998) for arid to semi-arid environments, and by Woodhouse and Hoekman (2000a) for Africa and Spain. All models are based on the first-order solution of the radiative transfer equation, also known as Cloud Model if the vegetation-soil interaction term is neglected. In addition, these models generally use mixed target models to explain overall backscatter of one pixel. Nevertheless, they show significant differences. For example, Woodhouse and Hoekman (2000a) have decided to use the geometrical optics model for describing backscatter from bare soil surfaces, while Frison et al. (1998) use the model from Oh et al. (1992), and Magagi and Kerr (1997) used an empirical bare soil scattering model obtained by fitting the model to data. Therefore, these models can vary by several decibels for a given soil roughness and soil permittivity. To date these models have neither been compared to each other nor have been applied globally. Hence, their relative performance is not known and it is uncertain if they provide consistent information over a wide range of environmental conditions.

Several authors addressed that shifting from the spatial domain to the time domain by applying simple change detection methods might be superior to traditional methods. In the time domain, the parameters influencing the scattering process act on very different scales. Therefore variable processes can be discerned more readily and invariant processes can be ignored. The interpretation of the backscattered signal reduces to the problem of separating the highly variable soil moisture process and seasonal vegetation patterns. However, a main constraint of this approach is that a frequent observation cycle is required. Change detection is therefore often not practical with SAR systems but works well for scatterometers. Following these principal idea Wagner et al. (1999a, 1999b, 1999c) successfully developed a method to retrieve soil moisture from ERS scatterometer data, which is regarded as the most mature method for soil moisture retrieval currently available (Wismann and Woodhouse, 2001).

3 ERS SCATTEROMETER

3.1 The ERS Scatterometer

The ERS scatterometer is an active low-resolution microwave sensor flown on board of the ERS-1 and ERS-2 satellites (ESA, 1992). ERS-1 was launched in July 1991 followed by the identical ERS-2 in April 1995. Despite technical problems in the calibration and validation phase of ERS-2 (Lecomte and Wagner, 1998), both instruments generated an uninterrupted stream of high quality data since 1991. ERS-1 completed its operation in 1999, overlapping with the new ERS-2 launched in 1995. ERS satellites have a sun-synchronous, near polar, near circular orbit at a mean altitude of 785 km and an inclination of 98.5 degrees. During the initial three months of the commissioning phase, the satellite had a 3-day repeat cycle at an altitude of 785 km, known as the reference orbit. Subsequent satellite heights adjustments have provided two multi-disciplinary phases with a 35-day repeat cycle, two ice phases with 3-day repeat cycles and two geodetic phases with 168-day cycles. The majority of the mission was performed in the 35-day repeat cycle. ERS-1 and ERS-2 are considered a major success providing information about ocean and land surfaces previously not available, hence contributing substantially to the scientific study of the ocean and land surface.

One of the instruments onboard is the Active Microwave Instrument AMI. AMI combines two instruments, the scatterometer and the Synthetic Aperture Radar SAR. The scatterometer shares with the SAR some hardware aspects. The SAR and the Scatterometer mode are therefore mutually exclusive. Hence, over regions with frequent SAR operations, e.g. Europe, the temporal sampling rate of the ERS Scatterometer is low.

The ERS scatterometer operates at 5.3 GHz (C-band) vertical polarization, collecting backscatter measurements over an incidence angle range from 18° to 57°. The scatterometer uses three sideways looking antennae (beams), one pointing normal to the satellite flight path, one pointing 45° forward and one pointing 45° backward. The antenna beams continuously illuminate a 500 km wide swath as the satellite advances along its orbit achieving global coverage within 3 to 4 days. Each beam provides measurements of radar backscatter from the sea and land surface for overlapping 50 km resolution cells with a 25-km grid spacing (Figure 3-1). The results are three independent backscatter measurements relating to cell centre nodes, using the three different viewing directions separated by only by a very short time delay. Given the orbit and viewing parameters, the satellite crosses the equator with the descending node at about 10:30 am local

time and with the descending node at about 10:30 pm. Depending on latitude observation time can vary up to a few minutes.

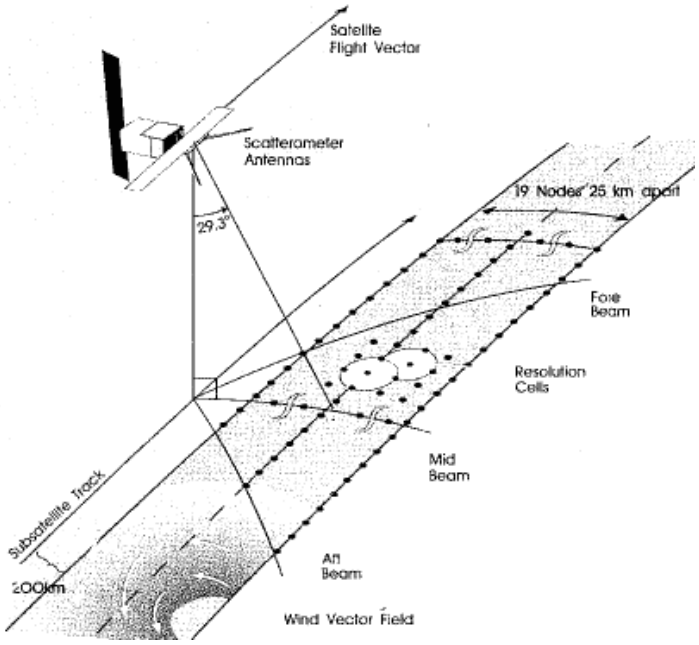

Figure 3-1: ERS wind scatterometer geometry (Courtesy ESA)

3.2 Data

The soil moisture database is derived from historical ERS Scatterometer observations covering the period January 1992 to January 2001. Data was delivered on CDROMs by the Institute Francais de Recherche pour l'Exploitation de la mer (IFREMER). Each CDROM contains approximately three weeks of data. An ERS scatterometer product consists of 19 x 19 pixels corresponding to a 500 x 500 km² large area on the ground. For each pixel, the geographic location (longitude, latitude) and the backscattering coefficient for all three antennas are given together with the respective incidence angles and azimuth angles (Quilfen, 1995).

3.3 Analysis Grid

The method to retrieve geophysical parameters from scatterometer data applied in this study is a combination of an empirical backscattering model describing principal scattering properties of the earth surface and a change detection method allowing the retrieval of relative soil moisture information. The empirical backscattering model is characterised by a number of parameters, extracted from long-term backscatter series. This principal concept necessitates the regridding of scatterometer data delivered in an image format to a time series format for each point of the land

surface. Equation (3.1) defines a grid with a grid spacing of approximately 28 km (Figure 3-2) for the entire globe, required by the processing method. In equation (3.1) φ defines the longitude and λ the latitude of each grid point i, j, where I ranges from 0 to 360 and j from 0 to 1440*cosλ. Constant spacing involves that the number of points in longitude direction decreases with increasing latitude. In this way, more than 180000 single points define the land surface of the globe. Coastal zones and inland water bodies where ERS Scatterometer measurements are influenced by water are excluded from the analysis.

$$\lambda_j = -90 + 0.25 \cdot (j - 0.5) \qquad 0 \le j < 4 \cdot 90$$
$$\varphi_{i,j} = -180 + 0.25 \cdot \frac{(i - 0.5)}{\cos\lambda} \qquad 0 \le i < 4 \cdot 360 \cdot \cos\lambda \qquad (3.1)$$
$$i, j \ \forall \ N$$

To facilitate data processing , the globe is structured in 10° x 10° cells, where each grid point is associated with a cell. Subsequent analysis is completed for each cell based on the defined grid. Raw data, all parameters (meta information) and retrieved time series are stored in the grid structure, i.e. for each grid point a number of meta and data files exist. Consequently, backscatter measurements of the IFREMER scatterometer data archive are redistributed to the defined grid. For each grid point, ERS scatterometer measurements collected within 36 km distance are extracted and stored in a time oriented structure spanning the entire analysis period (Figure 3-2).

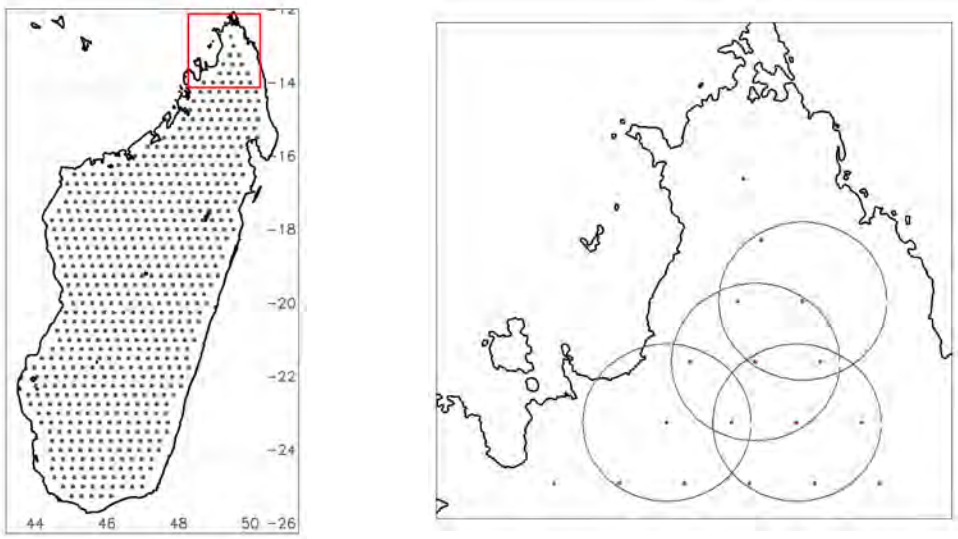

Figure 3-2: Left: Defined Scatterometer Analysis Grid for Madagascar. Right: Grid point resolution for selected points.

4 DATA

To process, analyse and validate scatterometer data an extensive global database has been set up. In large-scale studies, it is often a challenge to find adequate high-quality reference data. Metadata is therefore critical for correctly interpreting the data or derived results. Careful review of the applied methods is necessary to identify the most appropriate data sets and to avoid possible pitfalls. Unfortunately, metadata is often unavailable or difficult to obtain. The following section will summarize characteristics of data used in this study.

Currently, the reference data base encompasses global meteorological data, global interpolated precipitation data, *in-situ* soil moisture data for selected countries and global gridded data on climate, soil physical properties and land cover. Additionally, to ease data interpretation, basic geographical data supplied with the Digital Chart of the World (ESRI, 1993) is used.

4.1 Meteorological Data

The Climate Prediction Centre CPC of the US National Centres for Environmental Prediction NCEP maintains a global archive of surface synoptic weather observations. The CPC extracts surface synoptic weather observations, exchanged on the Global Telecommunications System GTS, performs limited automated validation of the parameters, and summarises the data for all reporting stations on a daily basis. Data records contain: maximum and minimum temperature, precipitation, evapotranspiration, maximum and minimum relative humidity, vapour pressure, sea level pressure, snowfall, descriptive weather, cloud cover, wind direction and wind speed for the years 1992-2000. The archive contains data of more than 12000 synoptic weather stations. The spatial distribution of stations over the mid-latitudes of the northern hemisphere is uneven but adequate for analysis of large-scale phenomena. Over much of the tropics, the southern hemisphere and the high north the number of stations is far fewer (Figure 4-1). Additionally it is emphasized that the number and the spatial distribution of stations has varied considerably over time. Thus, there are large spatial and temporal gaps in the surface station coverage.

Meteorological synoptic surface observations have been used extensively throughout the retrieval for verification of derived time series. Of special interest are temperature, precipitation and snow cover records.

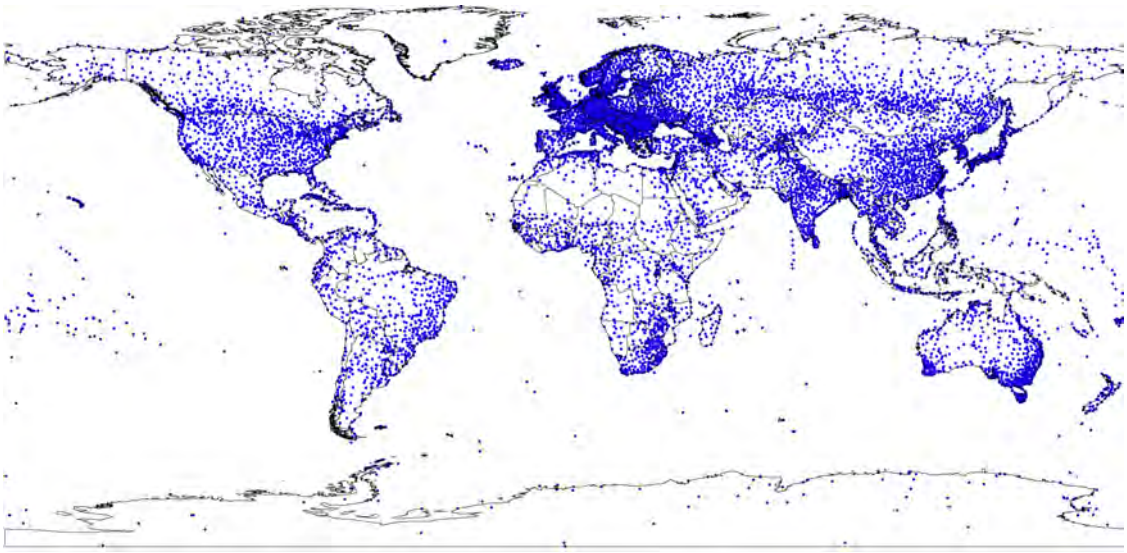

Figure 4-1: Spatial distribution of surface synoptic weather stations.

4.2 Global Gridded Precipitation Data

The Global Precipitation and Climatology Centre GPCC of the German Weather Service, maintains monthly total precipitation, derived from observed data, interpolated to a 1° by 1° grid. The GPCC products are derived from quality-controlled data, measured by rain gauges, covering the earth's land surface (GPCC, 1998).

Conventionally measured data from rain gauge networks are considered to be the most reliable information to obtain area-averaged precipitation of the land surface. Nevertheless, the accuracy and usefulness of the gridded products strongly depend on the availability and quality of the observed gauge data. Hence, data should be treated with care especially in data poor regions (Rudolf et al., 1994). The entire GPCC database includes monthly precipitation totals of approximately 50000 stations. Since the late 1980's, a gradual decrease in the number of stations from 38000 in 1986-89 down to 7000 stations in 2001 has been observed. The spatial distribution of the station network is similar to the station network plotted in Figure 4-1. The distribution indicates that especially in the tropics and in the high latitudes interpolated data has to be used with care.

Gridded precipitation data are used to evaluate derived soil moisture maps. Although precipitation and soil moisture are different geophysical processes, climatic anomalies are expected to be reflected in both parameters.

4.3 In-Situ Soil Moisture Data

Extensive *in-situ* soil moisture data for five different countries, Russia, Ukraine, China, India and Illinois were available in this study. Taken together they encompass a wide range of soil types and climatic regions. Data for Illinois and India were extracted from the Global Soil Moisture Archive maintained by the University of Maryland (Robock et al., 1995). Data for Russia and the Ukraine was available from previous projects (Wagner, 1998). The Chinese Meteorological Administration provided soil moisture data from the Chinese agrometeorological network. To facilitate data analysis, soil moisture samples of the 1m soil profile layer have been used. If data for the respective layers has not been available (such is the case for the Indian data, only reaching to a depth of 60 cm) the nearest soil moisture sample was used.

Primarily originating from agrometeorological networks, data generally represents grasslands or agricultural areas. Soil moisture samples are taken using different methods, at different layers at different times, depending on the data set. Additionally data quality varies significantly. Only the Russian and Ukraine soil moisture data are known to be thoroughly checked. Unfortunately, no literature exists providing a comparison between the different data sets. For the Indian and Chinese data sets, literature in English is even unavailable because the methods of data collection are published in local journals. Therefore, data are used separately in the analysis (Chapter7). Table 4-1 summarizes the principal properties of the different soil moisture data sets; Figure 4-2 shows the spatial distribution of the networks.

TABLE 4-1: Summary of in-situ soil moisture dataset used in this study

Dataset	**No. of stations**	**Years**	**Frequency**	**Soil Properties**	**Method**
Russia	160	1992-1996	3 per month	Yes	Gravimetric
Russia	52	1992-1996	3 per month	No	Gravimetric
Ukraine	99	1991-1996	3 per month	Yes	Gravimetric
China	101	1992-2000	3 per month	Yes	Gravimetric
China	52	1992-2000	3 per month	No	Gravimetric
Illinois	19	1991-1996	1-4 per month	Yes	Neutron Probe
India	10	1991-1998	1 per week	Yes	Gravimetric

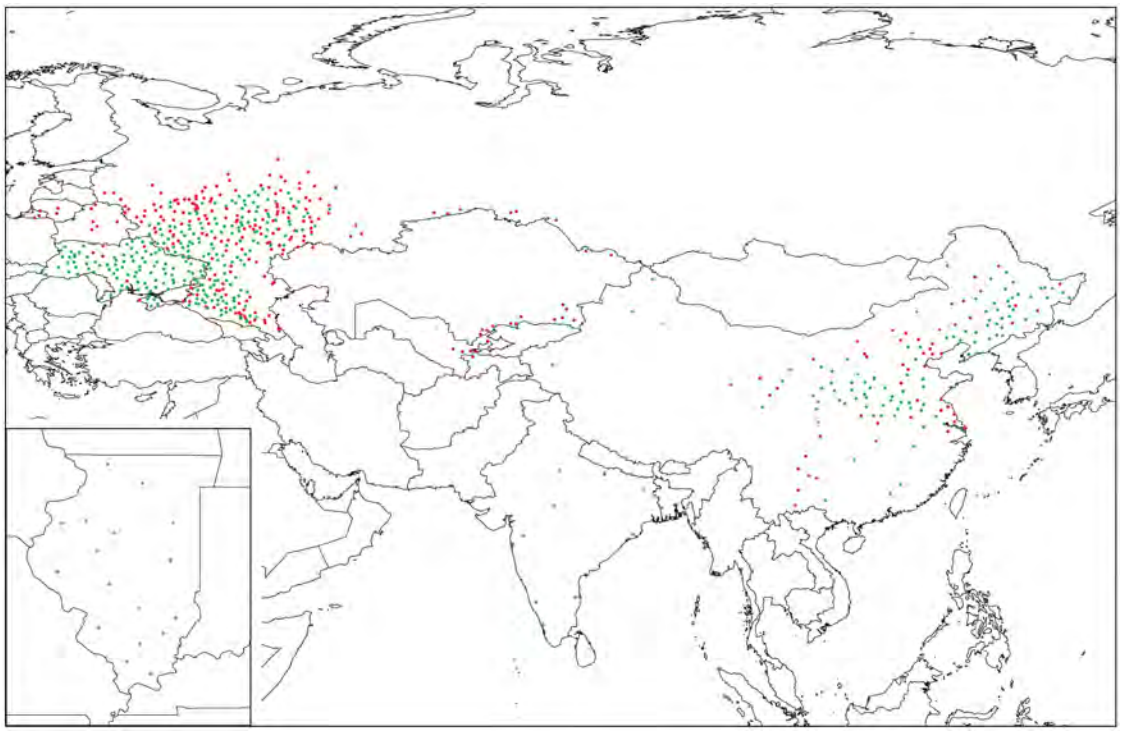

Figure 4-2: Spatial distribution of the soil moisture network used for validation. Green colour indicates that soil constants (wilting level and field capacity) are available, red colour indicates that soil constants are unavailable or incomplete.

4.3.1 Russia & Ukraine

Agro-meteorological stations of the former Soviet Union have an elaborate observational program (Vinnikov and Iserkepova, 1991). Soil moisture content is measured by gravimetric method during the warm season, from the beginning of the field work (as a rule in April) until harvest time. The results of this monitoring are prepared three times per month (on the 8th, 18th, 28th of each month). For each site soil moisture samples are taken for four major crops over Russia (maize, winter wheat, spring wheat, and barley), and for three major crops over the Ukraine (maize, winter wheat and spring wheat). In Russia measurements are made at depths of 0-5 cm, 0-10 cm, 0-20 cm, 0-50 cm, and 0-100 cm. In the Ukraine measurements are made for two layers, 0-20 cm and 0-100 cm. Each soil moisture measurement is an average of measurements taken at four points of the same field. While the gravimetric method allows to measure the total water content of the soil level, the agronomists are actually interested in plant-available soil moisture. Therefore, non-productive soil moisture was subtracted from each soil moisture sample to provided plant-available soil moisture. Non-productive soil moisture is defined as soil moisture at the wilting level.

Additionally the archive includes soil physical properties. Soil type encompasses data on field capacity, volumetric density, and wilting level, which are periodically evaluated for most of these fields. When a field is spatially inhomogeneous, several cross-sections are made to get a reliable estimate of these quantities. Out of 99 Ukrainian agro-meteorological stations 93, and 160 out of 374 stations for Russian agro-meteorological stations have information on soil physical properties on file.

4.3.2 Illinois

This data set consists of total soil moisture measured at 19 stations in the state of Illinois, USA, from 1981 to August 1996 (Hollinger et al. 1994). The temporal resolution of measurement is about one to two weeks during the growing season and once per month during the rest of the year. Soil moisture is measured with the neutron probe technique, calibrated with gravimetric observations. The data are collected for the top 10 cm of soil, and then for 20 cm layers (e.g., 10-30 cm, 30-50 cm, ...) down to a depth of 2 m. The vegetation at all stations is grass, except for one station with bare soil measurements, at the same location as a grass-covered station. Ancillary information about field capacity and wilting level completes the data set.

4.3.3 China

Soil moisture data of China is available for 153 agrometeorological stations throughout the entire country. Soil moisture samples are taken predominantly from agricultural fields, using the gravimetric method on the 8^{th}, 18^{th} and 28^{th} day of each month for the entire year. For some stations, no measurements were taken in the cold season due to the frozen surface. The vegetation types include wheat, corn, oats, maize, sorghum etc. For each measurement, four samples in the same field are taken and the soil moisture value is the average of these four samples. For 101 stations information on wilting level, field capacity and bulk density is available.

4.3.4 India

The India data set contains total soil moisture data of 10 stations for 1987-1995. Soil moisture samples were taken using the gravimetric method in regions with predominantly grass vegetation once per week at six layers down to a depth of 60 cm. Unfortunately each sample is only accompanied with the week number the sample was taken. Precise measurement dates for each soil sample are not included in the archive, and could not be determined (Srinivasan, 2001). The archive only contains the week number. To facilitate data comparison the date has been fixed to

Thursday each week, which might introduce a bias. Soil physical properties are available on wilting level, field capacity and bulk density for all stations.

4.4 Global Climate Data

The Food and Agriculture Organisation of the UN provide global climate estimates, used in this study for qualitative cross-checking of the results. Climate estimates are based on mean monthly values of temperature, precipitation and cloudiness, published by the International Institute for Applied Systems Analysis IIASA (Leemans and Cramer, 1991). The IIASA data correspond to an imaginary net covering the Earth's surface with a mesh size of 0.5 degrees. Monthly climatic data for each cell in the net are provided by weather stations and consist of an average value of monthly climate elements. Using spatial extrapolation, a value is computed for each cell based on the neighbouring station values. The IIASA database includes three key climatic elements: average monthly rainfall totals, average monthly temperature, and average monthly sunshine. For each of the stations used in the gridding exercise, data have been assembled over a long period - usually between 1961 and 1990 - and then averaged. Annual totals for rainfall, and the averages for temperature and sunshine, were derived from the monthly values. FAO's Agrometeorology Group converted the IIASA tables into grids and derived two further parameters, a climate classification according to Koeppen (1936), and potential biomass according to Lieth (1972).

4.4.1 Climate Classification

The most widely used system of climate classification is that of the German climatologist Koeppen (1936). Generally, more recent classifications are refinements or variants of the Koeppen system. The classification assigns codes to the main climates, based on monthly rainfall and temperatures (Figure 4-3). Each of the main climate classes is divided into sub-classes based mainly on the distribution of rainfall and temperature over the year. Koeppens Climate Classification was used to separate principal climatic biomes in support of data analysis.

4.4.2 Potential Biomass

Potential biomass is the amount of plant biomass that can be accumulated in one year under the assumption of ideal conditions prevailing for photosynthesis, i.e. absorption of solar energy by plants and storage of the energy as plant material. The unit of measurement is grams of dry matter per square meter per year. The method applied to estimate potential biomass was developed by Lieth (1972). Although methods that are more complex largely superseded Lieths approach, the method seems appropriate to get an initial estimate of large-scale potential biomass

(Figure 4-4). Potential biomass was used for qualitative discussion of scattering properties over the land surface and to evaluate retrieved parameters.

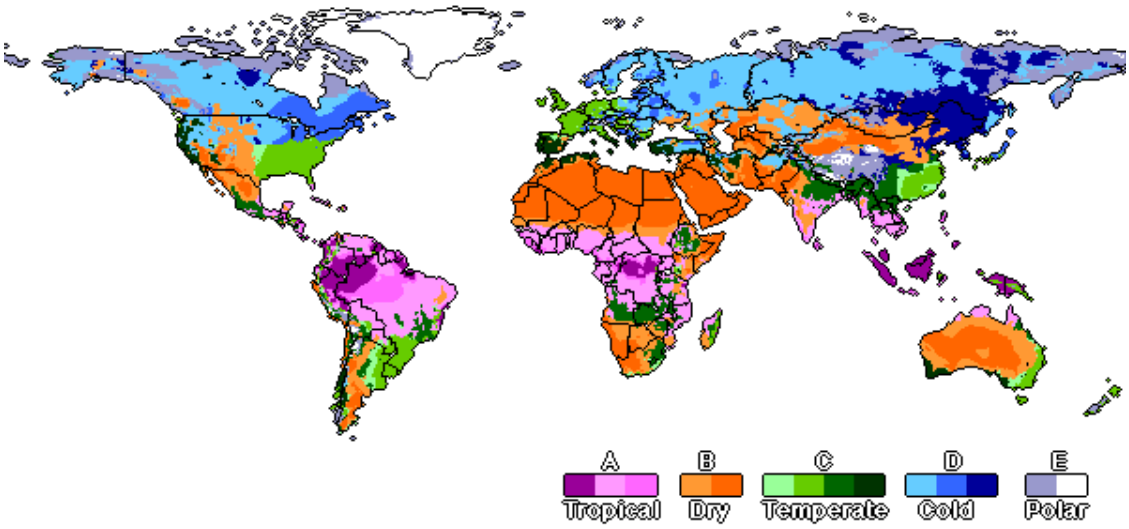

Figure 4-3: Koeppens Climate Classification. (Courtesy: FAO – SDRN - Agrometeorological Group – 1997)

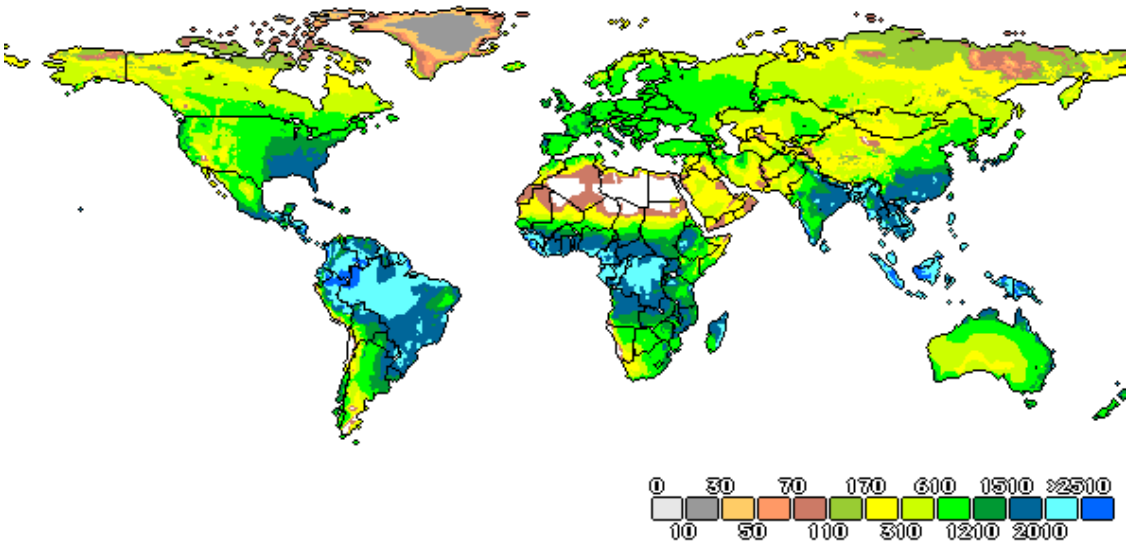

Figure 4-4: Biomass potential in grams of dry matter per square meter per year derived from 1961-1990 climate normals according to Lieth (1972). (Courtesy: FAO – SDRN - Agrometeorological Group – 1997)

4.5 Soil Physical Properties

The International Geosphere Biosphere Program provides global data on soil physical properties within their Global Soil Data Task program. The Global Soil Data Task was an international collaborative project with the objective of making accurate and appropriate data relating to soil properties accessible to the global change research community (Global Soil Data Task, 2000).

The Global Gridded Surfaces of Selected Soil Characteristics data set contains seven parameters of the 0-100 cm soil layer: soil-carbon density, total nitrogen density, field capacity, wilting point, profile available water capacity, thermal capacity, and bulk density. According to the Global Soil Data Task (2000), derived parameters of selected soil characteristics are suitable for modelling and inventory purposes. Data on wilting level and field capacity are required to transform scatterometer based relative soil moisture records to volumetric soil moisture.

Figure 4-5: Global distribution of wilting level for the0-100 cm soil layer in mm derived from the Global Soil Data Task of the International Geosphere Biosphere Program. (Courtesy Oak Ridge National Laboratory, Distributed Active Archive Center)

Figure 4-6: Global distribution of field capacity for the0-100 cm soil layer in mm derived from the Global Soil Data Task of the International Geosphere Biosphere Program. (Courtesy Oak Ridge National Laboratory, Distributed Active Archive Center)

To facilitate data processing, soil physical properties available at a resolution of 5x5 arc minutes were resampled to the scatterometer grid taking the weighted mean of all soil samples within 30 km distance of each scatterometer grid point.

4.6 Land Cover Data

The U.S. Geological Survey USGS, the University of Nebraska-Lincoln UNL and the European Commission's Joint Research Centre JRC have generated a 1-km resolution global land cover characteristics database for use in a wide range of environmental research and modelling applications (Loveland et al., 2000). The global land cover characteristics database was developed on a continent-by-continent basis. All continental databases have 1-km nominal spatial resolution, and are based on 1-km Advanced Very High Resolution Radiometer (AVHRR) data spanning April 1992 through March 1993. Each database contains unique elements based on the geographic aspects of the specific continent. In order to provide flexibility for a variety of applications, a core set of derived thematic maps produced through the aggregation of seasonal land cover regions are included in each continental database. The continental databases are combined to make seven global data sets, each representing a different landscape based on a particular classification legend. The global data set used in this study was generated applying the USGS classification schema resulting in 22 different land cover classes.

To facilitate data processing the cover percentage for each land cover class for each scatterometer cell has been derived by summarizing all land cover grid points within a 30 km distance of each scatterometer grid point.

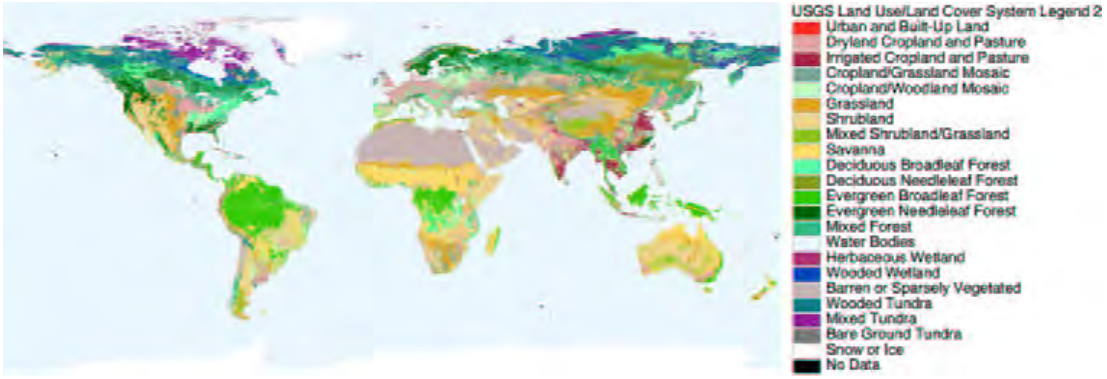

Figure 4-7: Global Land Cover according to the USGS classification schema.

5 SOIL MOISTURE RETRIEVAL

Chapter 2 introduced the fundamental concept of the method to retrieve soil moisture information from scatterometer data. The following section presents a brief review of the physical and mathematical model involved. Wagner et al. (1998, 1999a, 1999b, 1999c) used very specific biomes, the African Sahel, the Canadian Prairies and mid-latitude ecosystems (Spain and Ukraine) for the methodological development. From a climatic viewpoint, these areas range from tropical to cold (Koeppen, 1936), including major climate zones of the world. Nevertheless the study areas were limited in their spatial extent, raising the question if the developed methods are applicable on a global scale. Hence, global distribution of basic backscattering properties is discussed subsequent to the model specification. Weak points will be addressed based on model simulations and empirical evidence. The third part of this Chapter, discusses the properties of the retrieved geophysical parameters. These encompass relative topsoil moisture m_S and the soil water index *SWI*, representing the degree of wetness of the respective layer, volumetric soil moisture and freeze/thaw information.

5.1 Physical Concept

To describe backscatter from land surfaces (bare and vegetated) an empirical model that uses about a dozen parameters was developed. The parameters fully characterise the backscattering behaviour for land surfaces under the paradigm of certain physical assumptions. Model estimates of these parameters are extracted from long-time backscatter series. Hence, for a given point on earth, excluding open water and wet snow surfaces, a scattering knowledgebase describing various scattering effects is extracted. The formulated model rests on certain empirically observed evidences, which have found theoretical justification. Formally, these can be summarized as follows:

1. The backscattering coefficient σ^0 of natural targets depends strongly on the incidence angle.
2. The incidence angle dependency is a function of vegetation and roughness. Soil moisture variations do not or only minimally effect the incidence angle dependency.
3. When vegetation grows, backscatter may decrease or increase, depending on whether the attenuation of the soil contribution is more important than the enhanced contribution from the vegetation canopy, or vice versa.
4. Because the relative magnitude of the effects described above depend on the incidence angle θ, the curve $\sigma^0(\theta)$ chances with vegetation phenology over the year.

5. Vegetation phenology influences σ^0 on an annual scale. The measurement process, due to the low resolution of the sensor, suppresses local short-term fluctuations.
6. At the resolution of the scatterometer, roughness is temporal invariant.
7. Dielectric variations caused by changing soil moisture content or freezing and thawing, influence σ^0 more or less constantly over all incidence angles in the logarithmic range meaning that in the natural range the behaviour is approximately exponential.
8. There exist distinct incidence angles θ_{dry} and θ_{wet}, where the backscattering coefficient σ^0 is relatively stable despite seasonal changes in above ground vegetation biomass for dry and wet conditions.
9. The relationship between soil moisture variability and σ^0 is linear.
10. Backscatter depends only weakly on the azimuth viewing direction.

Using a simple model based on radiative transfer theory, the principal trends stated above are illustrated. Wagner (1998) developed the model by postulating its general form and by identifying the possible range of model parameters based on a literature review and on a comparison of model simulations with ERS Scatterometer data acquired under known conditions in the Canadian Prairies and over tropical rain forest. A final set of vegetation and surface parameters was selected to achieve an agreement of model simulations and ERS Scatterometer measurements over the Iberian Peninsula. In the model, backscatter is modelled as a mixture of non-transparent (forests, bushes, shrubs) and translucent (grassland, agricultural land) vegetation, assuming a linear relationship between σ^0 in decibels and θ. A perfectly rough surface is assumed for describing the soil vegetation interaction. Table 5-1 summarizes the mathematical formulations involved and give an overview of the range of parameters used. Figure 5-1 shows how $\sigma^0(\theta)$ varies according to the model from grassland to densely forested areas (increase of A_{nt}), from dry to wet soil conditions (increase of soil moisture), and from winter to summer (decrease of the optical depth of translucent vegetation types).

TABLE 5-1: Backscattering model for ERS Scatterometer data over vegetated land surfaces from Wagner (1998). The forth column shows the estimated range of possible values based on a literature review and a comparison with ERS Scatterometer measurements over the Canadian Prairies, the Iberian Peninsula, and tropical rain forest. The last column shows the values used in simulation.

$$\sigma^0 = (1 - A_{nt}) \cdot \sigma^0_{tr} + A_{nt} \cdot \sigma^0_{nt}$$

$$\sigma^0_{nt} = \frac{\omega_{nt} \cos\theta}{2}$$

$$\sigma^0_{tr} = \frac{\omega_{tr} \cos\theta}{2}(1 - e^{-\frac{2\tau_{tr}}{\cos\theta}}) + \sigma^0_s(\theta) e^{-\frac{2\tau_{tr}}{\cos\theta}} + 2\chi\Gamma_0\omega_{tr}\tau_{tr}e^{-\frac{2\tau_{tr}}{\cos\theta}}$$

$$\sigma^0_s = \sigma^0_{s,dry}(40) + \sigma'_s \cdot (\theta - 40) + S_s m_s \quad \text{in dB}$$

Symbol	Name	Unit	Range of Values	Value used in Simulation
σ^0	ERS Scatterometer backscattering coefficient	m^2m^{-2}		
σ^0_{nt}	σ^0 of non-transparent vegetation	m^2m^{-2}		
σ^0_{tr}	σ^0 of translucent vegetation	m^2m^{-2}		
A_{nt}	*Percentage area* of non-transparent vegetation	-	0 – 1 (0 – 100 %)	0 – 1 (0 – 100 %)
θ	Incidence angle	deg	18 – 59	18 – 59
ω_{nt}	Single scattering albedo of non-transparent vegetation	-	0.38 – 0.48	0.45
ω_{tr}	Single scattering albedo of translucent vegetation: *Winter* (dormant vegetation) *Summer* (fully grown vegetation canopy)	-	 0.05 – 0.1 0.05 – 0.3	 0.06 0.1
τ_{tr}	Optical depth of translucent vegetation: *Winter* (dormant vegetation) *Summer* (fully grown vegetation canopy)	Np	 0.05 – 0.15 0.05 – 2	 0.1 0.3
χ	Empirical multiplier	-		3
Γ_0	Fresnel power reflectivity at nadir	-	0.05 – 0.5	0.05 – 0.5
σ^0_s	σ^0 of soil surface	dB		
$\sigma^0_{s,dry}(40)$	σ^0_s of a dry soil surface at $\theta = 40°$	dB	-18 – -16	-16
σ'_s	Slope of $\sigma^0_s(\theta)$ at $\theta = 40°$	dB/deg	-0.3 – -0.4	-0.36
S_s	Sensitivity of σ^0_s to changes in the surface soil moisture content	dB	7 – 8	7
m_s	Degree of saturation of soil surface layer *Dry* conditions *Wet* conditions	-	0 – 1	 0 1

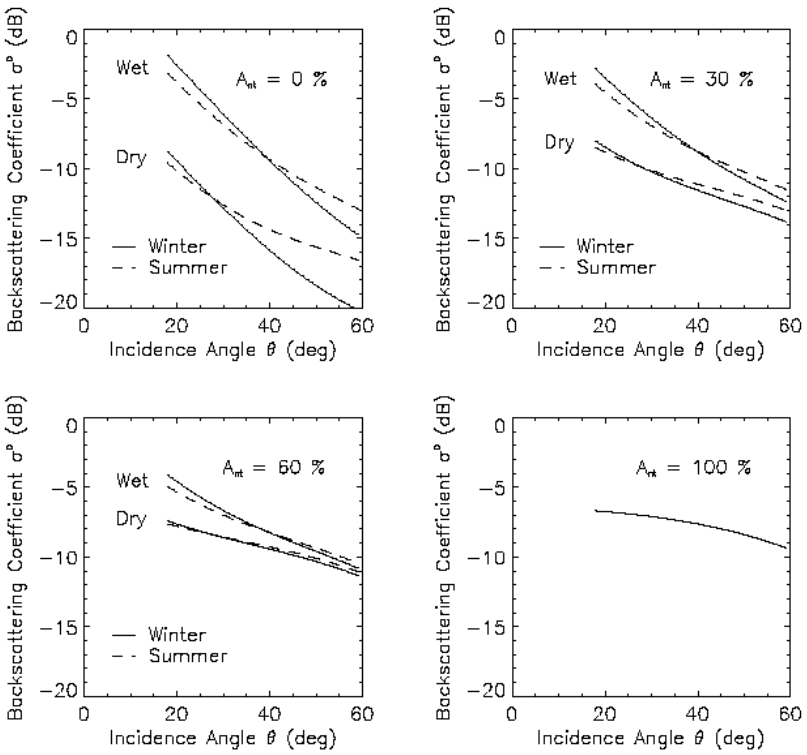

Figure 5-1: Illustration of the dependency of the backscattering function $\sigma^0(\theta)$ on vegetation and soil state simulated using a simple backscatter model.

Model simulations (Figure 5-1) and experience (Wagner 1999a, 1999b, 1999c) suggests that the physical concept used to retrieve soil moisture is a well-balanced simplification of reality. Although the concept is very strict with far reaching impacts, it offers a proper, physically sound working hypothesis.

Key parameters describing scattering properties of the land surface, included in the scattering knowledge base are the estimated standard deviation of $\sigma^0(\theta)$, the incidence angle dependency of σ^0 and the associated variability over the course of the year, and values of the backscattering coefficient for dry and wet conditions, C^0_{dry} and C^0_{wet} which depend on vegetation and soil type. Subsequent to model parameter estimation and normalisation of $\sigma^0(\theta)$, soil moisture information of the topsoil layer can be retrieved by applying a simple change detection algorithm, were the instantaneous backscattering coefficient is compared to the lowest and highest measurements ever recorded. Assuming a linear relationship between σ^0 and the soil moisture content a relative measure of soil wetness in the surface layer, m_S, is obtained. The mathematical formulations of the model, the change detection approach and equations to retrieve a profile soil moisture index and volumetric soil moisture estimates are summarized in Table 5-2.

TABLE 5-2: Mathematical model of the applied soil moisture retrieval method

Quantity	Mathematical Formulation	Comments
Estimated standard deviation of σ^0	$ESD(\sigma^0) = \frac{SD(\vartheta)}{\sqrt{2}}$	ϑ is the difference between σ^0 measured by the fore and aft beam
Incidence Angle Dependency	$\sigma^0(\theta,t) = \sigma^0(40,t) + \sigma'(40,t)(\theta-40) + \frac{1}{2}\sigma''(40,t)(\theta-40)^2$	σ' is defined as the first derivative of $\sigma^0(\theta)$ σ'' as the second derivative of $\sigma^0(\theta)$
Seasonal Variation of the slope	$\sigma'(40,t) = C' + D' \cdot \Psi'(t)$	C' is the annual minimum slope value D' is the annual dynamic range of σ' $\Psi'(t)$ is an empirical periodic function describing the annual variation of σ'
Seasonal Variation of the curvature	$\sigma''(40,t) = C'' + D'' \cdot \Psi''(t)$	C'' is the annual minimum slope value D'' is the annual dynamic range of σ' $\Psi''(t)$ is an empirical periodic function describing the annual variation of σ''
Normalized backscatter coefficient	$\sigma^0(40) = \frac{1}{3}\sum_{i=1}^{3}\sigma_i^0(\theta,t) - \sigma'(40,t)(\theta-40) - \frac{1}{2}\sigma''(40,t)(\theta-40)^2$	$\sigma^0(40)$ is the average backscatter recorded by the three antenna, extrapolated to 40°
Backscatter under dry and wet conditions	$\sigma^0_{DRY}(40,t) = C^0_{DRY} - D'\Psi'(t)(\theta_{DRY}-40) - \frac{1}{2}D''\Psi''(t)(\theta_{DRY}-40)^2$ $\sigma^0_{WET}(40,t) = C^0_{WET} - D'\Psi'(t)(\theta_{WET}-40) - \frac{1}{2}D''\Psi''(t)(\theta_{WET}-40)^2$	$\sigma^0_{dry}, \sigma^0_{wet}$ are backscatter from dry and saturated canopy θ_{dry}, θ_{wet} are the crossover angle for dry and wet soil conditions (at this angle vegetation has no influence) C^0_{dry}, C^0_{wet} are the annual minimum and maximum backscatter $D'\Psi(t)$ describe the annual variation of σ^0 due to the influence of vegetation

Top Soil Moisture	$m_s = \frac{\sigma^0(40,t) - \sigma^0_{dry}(40,t)}{\sigma^0_{wet}(40) - \sigma^0_{dry}(40,t)}$	m_S is defined as the degree of saturation ranging from 0 –100%
Soil Water Index	$SWI(t) = \frac{\sum_i m_s(t_i) e^{\frac{t-t_i}{T}}}{\sum_i e^{\frac{t-t_i}{T}}}$	*SWI* is a trend indicator of the profile moisture content ranging between 0-100%
Volumetric Soil Moisture	$W(t) = WL + SWI(t) \cdot \left(\frac{FC + TWC}{2} - WL \right)$	*WL* is the Wilting Level *FC* is the Field capacity *TWC* is the total water holding Capacity This empirical relationship was developed over the Ukraine

5.2 Implementation

To process, analyse and archive scatterometer data the software package WARP[1] has been developed. The implementation of WARP is based on the programming environment IDL (Interactive Data Language) of Research Systems Inc. During the previous 5 years a package encompassing more than 540 sub routines and 35000 lines of code has been established and is continuously upgraded based on ongoing research and on experience collected in pilot projects. WARP comprises two main packages, an analysis package used to set up the scattering knowledge base and a processing package to retrieve soil moisture information. Data processing is completed systematically (Figure 5-2). In a first step, data is regridded to the regular grid defined in Chapter 3. Raw data series are used to estimate the variance of $\sigma^0(\theta)$ and to retrieve parameters describing the incidence angle dependence of σ^0. Once these parameters have been derived, $\sigma^0(\theta)$ can be extrapolated to the reference incidence angle of 40°. Backscatter at 40°, the crossover angles θ_{dry} and θ_{wet} and information on the angular dependency of $\sigma^0(\theta)$ are used to retrieve the relative time dependent contribution of volume scattering from the vegetation canopy and in consequence to determine backscatter under dry and wet conditions. To derive surface soil moisture, m_S, the instantaneous backscattering values are then compared to these extremes. To estimate the profile soil moisture, the soil water index *SWI* is calculated applying a simple two-layer water balance model. Finally, volumetric soil moisture is calculated using soil hydrologic parameters.

[1] Soil **WA**ter **R**etrieval **P**ackage, Version 4.

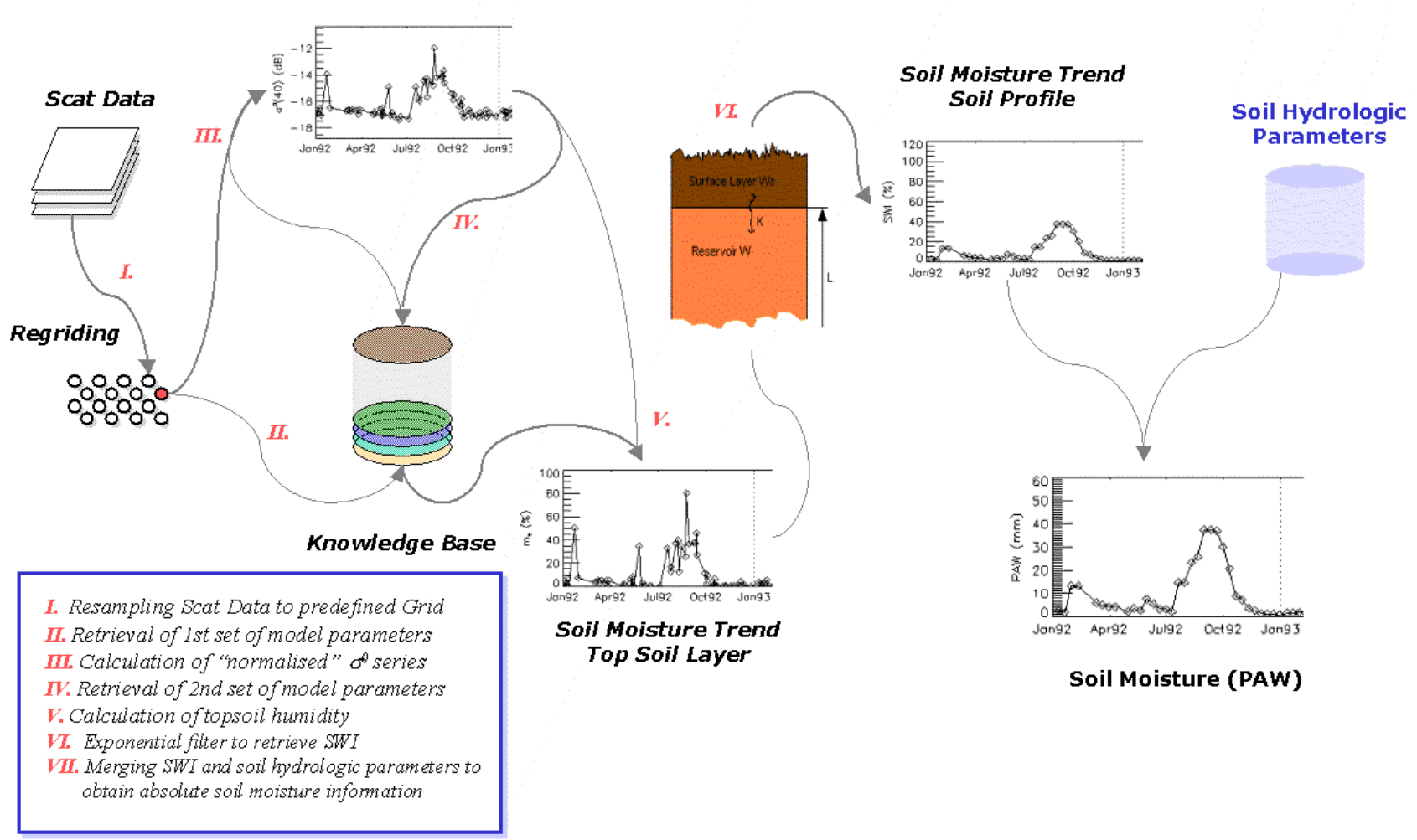

Figure 5-2: Flowchart of WARP, a software package to process, analyse and archive scatterometer data.

5.3 Global Scattering Properties

5.3.1 Azimuthal Effects

The ERS scatterometer measures $\sigma^0(\theta)$ at different azimuth angles raising the question about the influence of azimuthal effects. Generally it has been observed that land surfaces are azimuthal anisotrope, i.e. $\sigma^0(\theta)$ is largely independent of the viewing direction (Wisman and Boehnke, 1994; Frison et al. 1996). It has been argued that only large-scale topographic features, i.e. mountain ranges, have significant effect on the azimuth viewing direction. However, there is evidence that also small-scale terrain features can have significant systematic impact on $\sigma^0(\theta)$. For example, Long et al. (2000) and Rott et al. (1995) found that backscatter of Antarctic Firn, measured with different scatterometers, depends on the azimuth viewing direction. The observed dependence is determined by sastrugies[2]. It is therefore of relevance to verify if similar effect can also be observed over land surfaces. Two aspects have to be considered:

1. The terrain topography determines the incidence angle. The sensor can only record the look angle. For natural land surfaces, characterised by a local slope or systematic roughness patterns, the look angle is not necessarily equal the incidence angle.
2. The topography of a landscape influences microclimate and vegetation. Hence, the sensor might observe different vegetation patterns and different dielectric properties.

We can use the simple backscatter model discussed in Chapter 5.1 to illustrate the influence of azimuthal effects. Figure 5-3 shows backscatter calculated for three artificial surface types using different vegetation conditions under the assumption of (a) 5° surface inclination; (b) horizontal surface with superimposed ripples (c) both effects. Backscatter is calculated for a look angle of 40° and the azimuth angle range 0°-360°. Generally, the effect of relief features is significant and can reach values up to 4 dB for bare soil surfaces. The effect decreases for an increasing percentage of non-transparent vegetation. Azimuthal patterns in Figure 5-3 are similar to those reported in literature (Long et al. 2000) and can be used to estimate the worst case.

[2] Sastrugies are very hard snow slabs that have been eroded by wind to form sharp ridges and anvil-shaped protrusions that point toward the wind.

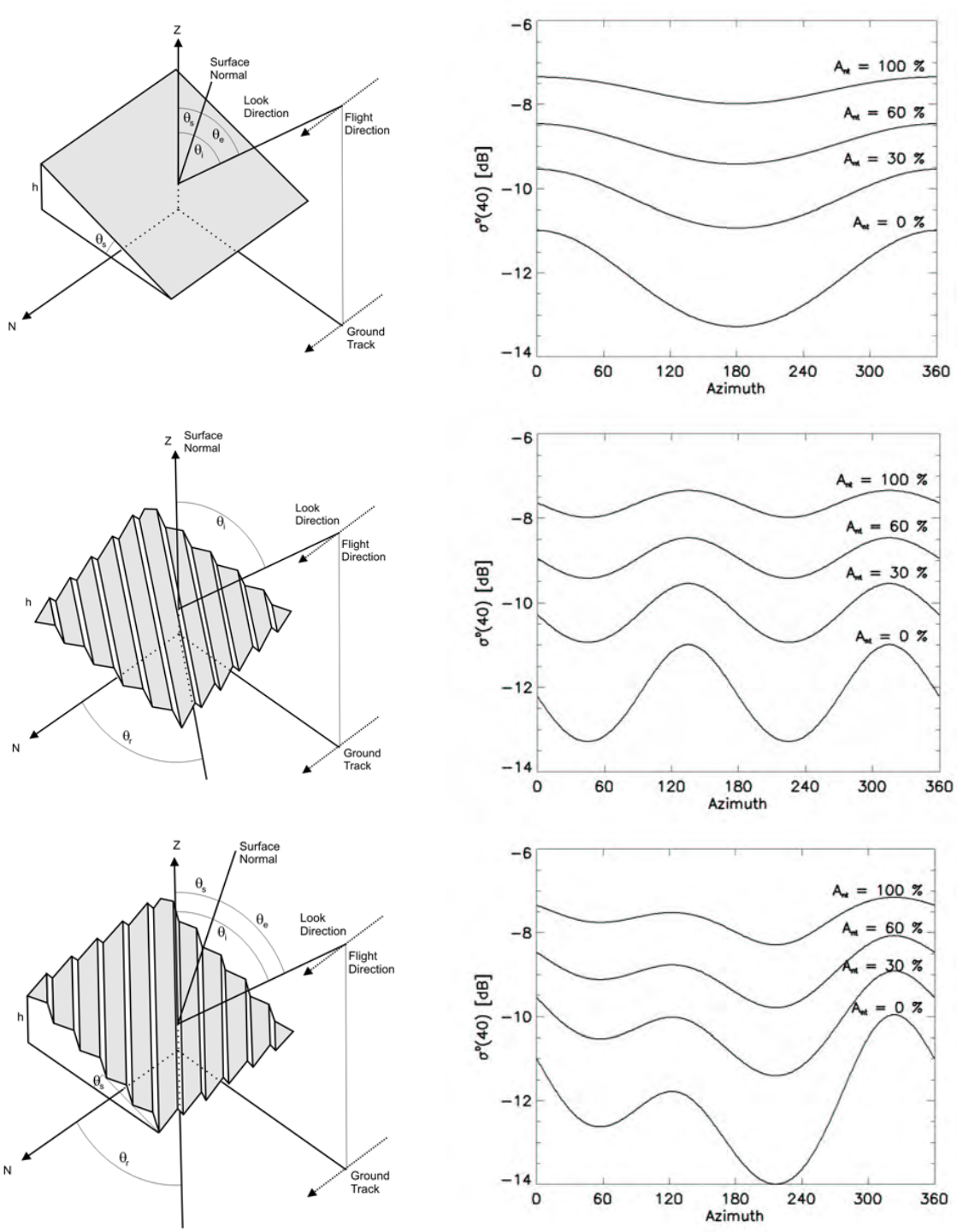

Figure 5-3: Simulated backscatter for different surface types based on a simple backscatter model (Table 5-1). The look angle was set to 40°. Backscatter was calculated for different percentages of non-transparent vegetation (0%, 30%, 60%, 100%) for the azimuth angle range 0°-360°.

Given the low resolution of the ERS scatterometer, it is more realistic to assume random distribution of surface slopes. Hence, azimuthal variations are likely an order smaller than estimated in Figure 5-3.

A measure for the magnitude of azimuthal effects on $\sigma^0(\theta)$ data is the difference between $\sigma^0(\theta)$ measured with the fore and aft beam antenna. The fore and aft beam antenna measure the backscattering coefficient at the same incidence angle almost at the same time. In case of a flat horizontal surface σ^0_{fore} and σ^0_{aft} are identical, only differing due to instrument noise, interbeam calibration inaccuracies and speckle. As discussed, azimuthal effects are lowest when the percentage of non-transparent vegetation is highest. We can therefore use the tropical forests as a reference target to get an estimate of the perpetual noise. The average difference over tropical forest is in the range –0.1 dB - 0.1 dB. Over a wide range, the observed difference is as low as this reference value, indicating that land surfaces at the scale of the scatterometer are generally isotropic. High values are observed over mountain ranges, over regions characterised by low vegetation such as the Kasachien Steppe in Central Asia or the Great Plains in North America. Maximum values above 1dB are found over sandy deserts such as the Sahara, Gobi desert and Rub al Khali desert on the Arabian Peninsula and permanent ice covered regions such as Greenland. It seems therefore appropriate to integrate azimuthal variations as additional error source until techniques exist to correct σ^0. Nevertheless, it is important to identify areas with high azimuthal noise and if necessary exclude them from subsequent processing.

Based on the difference of σ^0_{fore} and σ^0_{aft} a statistical model to estimate the standard deviation of σ^0, $ESD(\sigma^0)$, is formulated. $ESD(\sigma^0)$, integrating errors due to instrument noise, speckle and azimuthal effects, is useful to explain site-to-site differences and to estimate the worst-case error for any parameters. Figure 5-6 shows that azimuthal effects increase the standard deviation of σ^0 from about 0.2 over the tropics to about 0.5 over the Great Plains, the Pampas and the Kasachien Steppe to high values above 1 dB for the Sahara, Gobi desert and Rub al Khali desert on the Arabian Peninsula. Nevertheless, $ESD(\sigma^0)$ is generally low with 81% of the values below 0.3 dB. Only 4% of the values are in the high range above 0.5 dB. Figure 5-7 depicts the influence of above ground biomass on $ESD(\sigma^0)$. With increasing biomass, $ESD(\sigma^0)$ approaches a value of 0.2 dB. Plotting the histograms of $ESD(\sigma^0)$ indicates that for all climates the bulk of values are in the low range of 0.1-0.3 dB. Only Polar and Dry regions as defined by Koeppen are characterised by high values. As high values of $ESD(\sigma^0)$ effect the retrieval accuracy, regions where $ESD(\sigma^0)$ is above 1dB are masked out by strict quality control procedures. Regions not so

heavily affected might pass quality control and influence subsequent parameter retrieval. Azimuthal effects on retrieved geophysical parameters will be discussed in detail in Chapter 5.5.

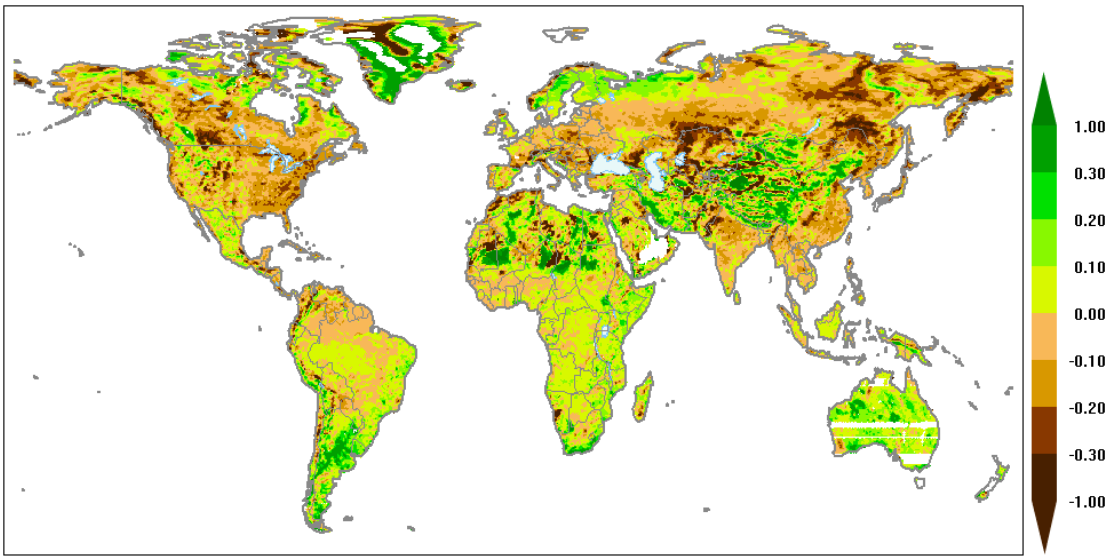

Figure 5-4: Average difference of σ^0_{fore} and σ^0_{aft} in dB for ascending passes.[3]

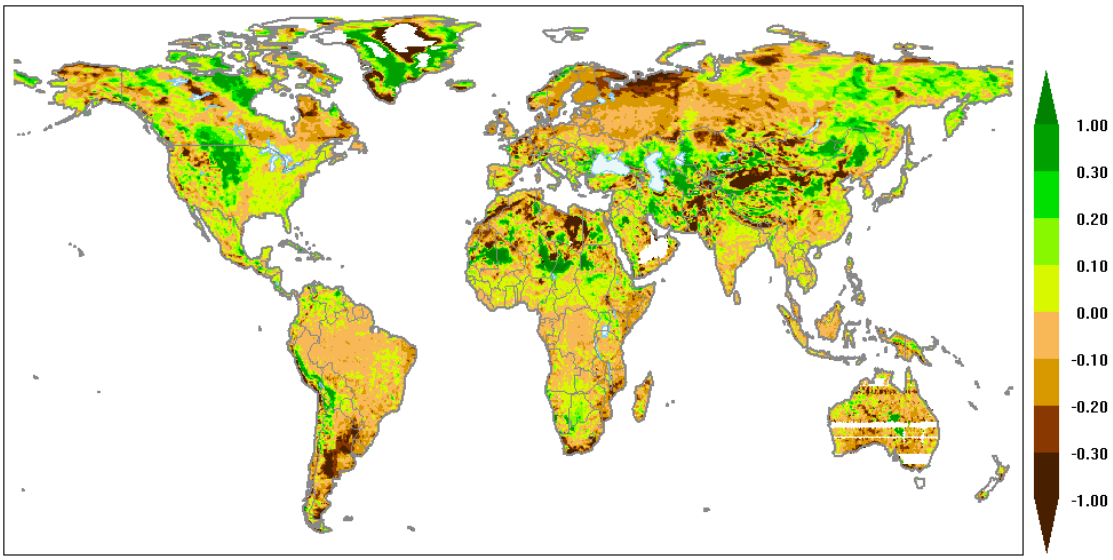

Figure 5-5: Average difference of σ^0_{fore} and σ^0_{aft} in dB for descending passes.

[3] Over Australia $\sigma^0(\theta)$ is largely missing for descending passes resulting in "white stripes" in the plot. Currently the reason responsible for the missing data is not evident.

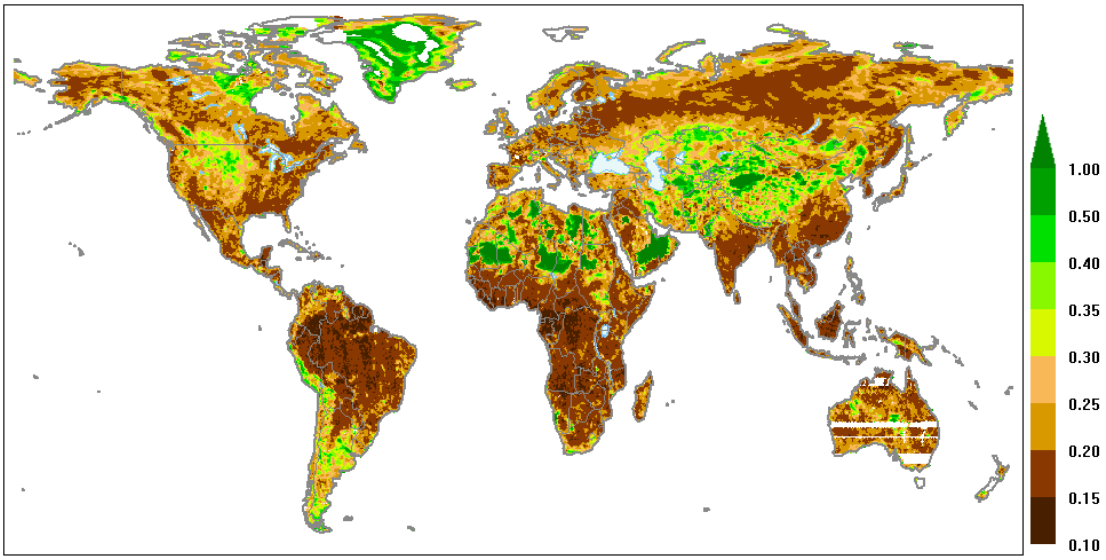

Figure 5-6: Estimated Standard Deviation of $\sigma^0(\theta)$ in dB. High values are generally found over large mountain ranges such as the Himalayas, deserts such as the Sahara or Gobi desert and regions with predominantly low vegetation such as the Great Plains in North America, the Pampas in South America or the Kasachian steppe in Central Asia.

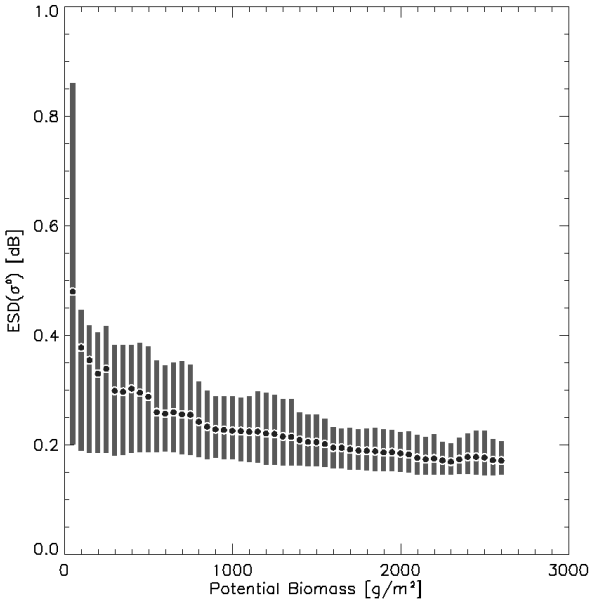

Figure 5-7: Comparison between modelled annual potential biomass and the Estimated Standard Deviation of $\sigma^0(\theta)$. The dark dot represents the average, 75% of all values are within the range given by the grey bars. With increasing above ground biomass ESD(σ^0) approaches a value of 0.2dB, which can be regarded as an estimate of interbeam calibration error, speckle and noise. Only over bare soil surfaces with potential biomass below 300 g/m², ESD(σ^0) reaches higher values.

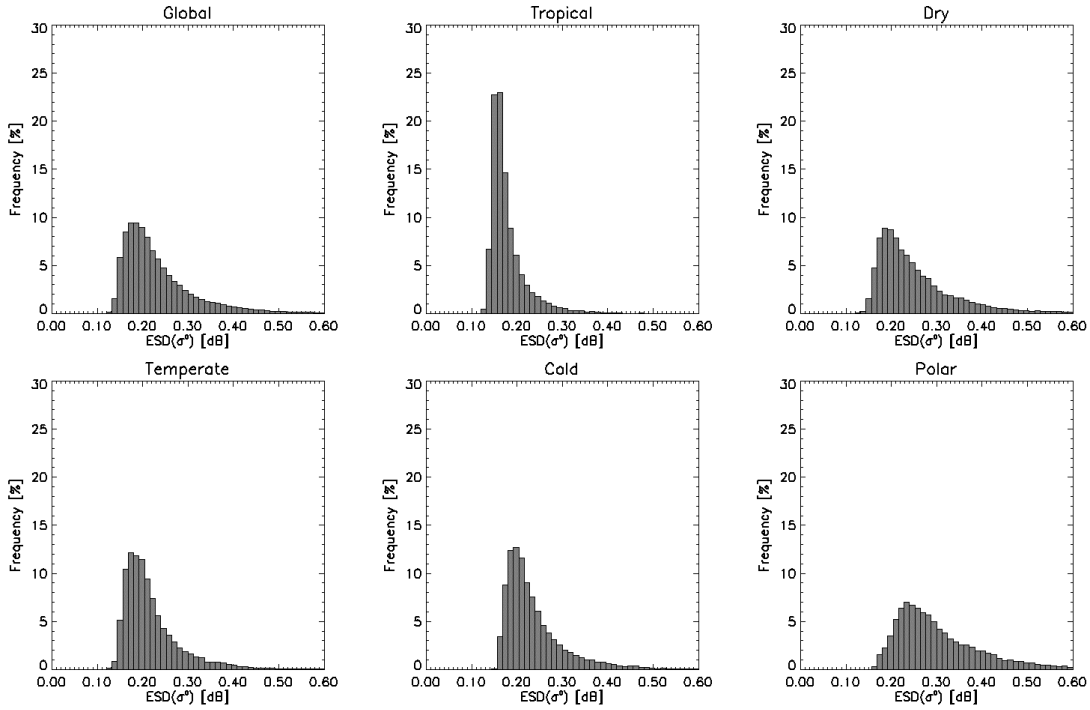

Figure 5-8 Histogram of ESD(σ^0) for different climatic regimes defined by Koeppen

5.3.2 Incidence Angle Dependency

The ERS scatterometer acquires backscatter data over a wide range of incidence angles θ from 18° to 57°. Typically, backscatter of the Earth's surface decreases with incidence angle, where the roughness of the observed surface and the amount of biomass determines the dependence of σ^0 on the incidence angle. Hence, the steepness of $\sigma^0(\theta)$ is an indicator for the dominating scattering mechanism. A second order polynomial is sufficient to describe backscatter of land surfaces:

$$\sigma^0(\theta,t) = \sigma^0(40,t) + \sigma'(40,t)(\theta - 40) + \tfrac{1}{2}\sigma''(40,t)(\theta - 40)^2 \qquad (5.1)$$

Figure 5-9 illustrates how the second order polynomial fits to backscatter data from different biomes: the steppe, a midlatitude temperate zone and the tropical forest. In the examples, surface scattering conditions are stable (constant soil moisture conditions, frozen soil, dense tropical forest), which is why consecutive measurements line up on a well-determined curve.

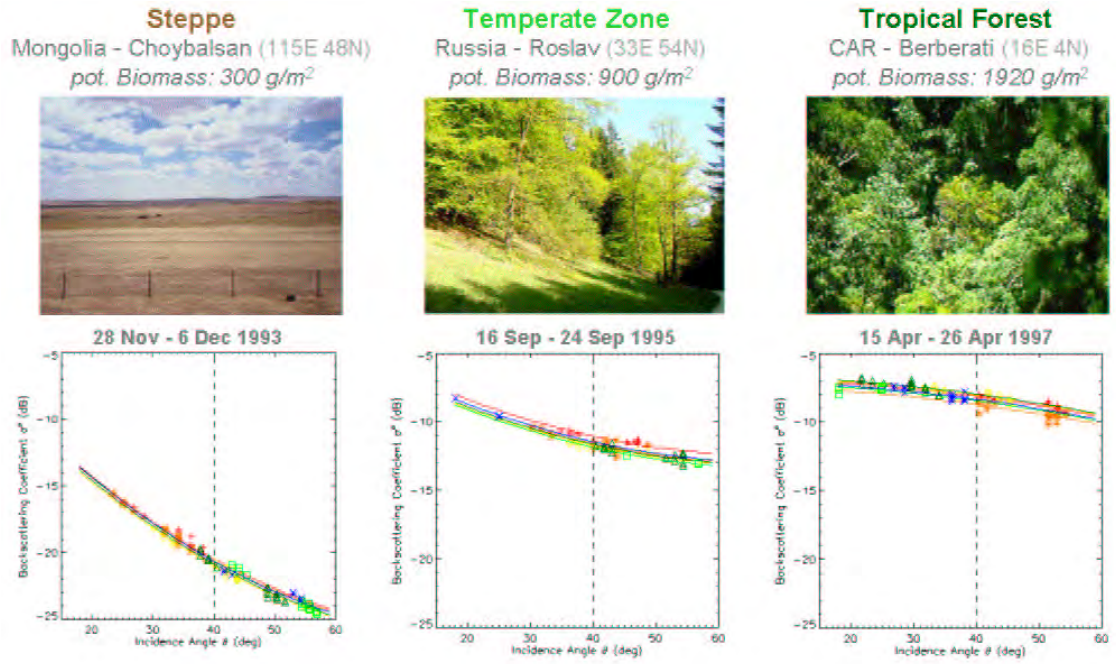

Figure 5-9: Backscatter recorded over three different biomes under stable meteorological conditions. Data was acquired over the synoptic weather stations of Choybalsan – Mongolia, Roslav – Russia and Berberati – Central African Republic. Additional modelled annual potential biomass is specified.

Key parameters in this model are the slope σ' and the curvature σ''. The slope σ' is defined through a constant value C' relating to the steepest slope possible over a certain surface, and a dynamic component, defined by $D\Psi'(t)$ reflecting the influence of the annual vegetation phenology on $\sigma^0(\theta)$. $\Psi'(t)$ is described by an empirical periodic function ranging from 0 to 1. Given that physiography remains constant over the year, $\Psi'(t)$ depends principally on vegetation phenology induced by climate variability or by changing snow cover conditions. Parameters describing the annual phenology of the curvature σ'' are defined similarly (Table 5-2).

When vegetation grows, backscattering may decrease or increase, depending on whether the attenuation of the soil contribution is more important than the enhanced contribution from the vegetation canopy, or vice versa. The slope is observed to be lowest over most vegetated biomes during winter. During winter, biomass is generally lowest resulting in higher transmissivity of vegetation and strong surface scattering. Under these conditions, σ^0 shows a strong incidence angle dependency (high gradient) with higher values in the near range and lower values in the far range. With increasing biomass the transmissivity of vegetation decreases, volume scattering enhances with respect to surface scattering and the slope becomes less steep. Therefore, the slope is generally highest in summer (low gradient) when vegetation has reached a maximum in wet biomass. Figure 5-10 shows plots of the annual phenology of the slope together with climographs

for the synoptic weather stations specified in Figure 5-9. The slope generally follows the climatic conditions. Highest dynamics are observed over the steppe, over the tropical forest the dynamic range of the slope is lowest. Generally, variations in the slope estimated empirically from scatterometer data (indicated by diamond symbols) are smooth, and the model describing the temporal phenology of the slope fits well.

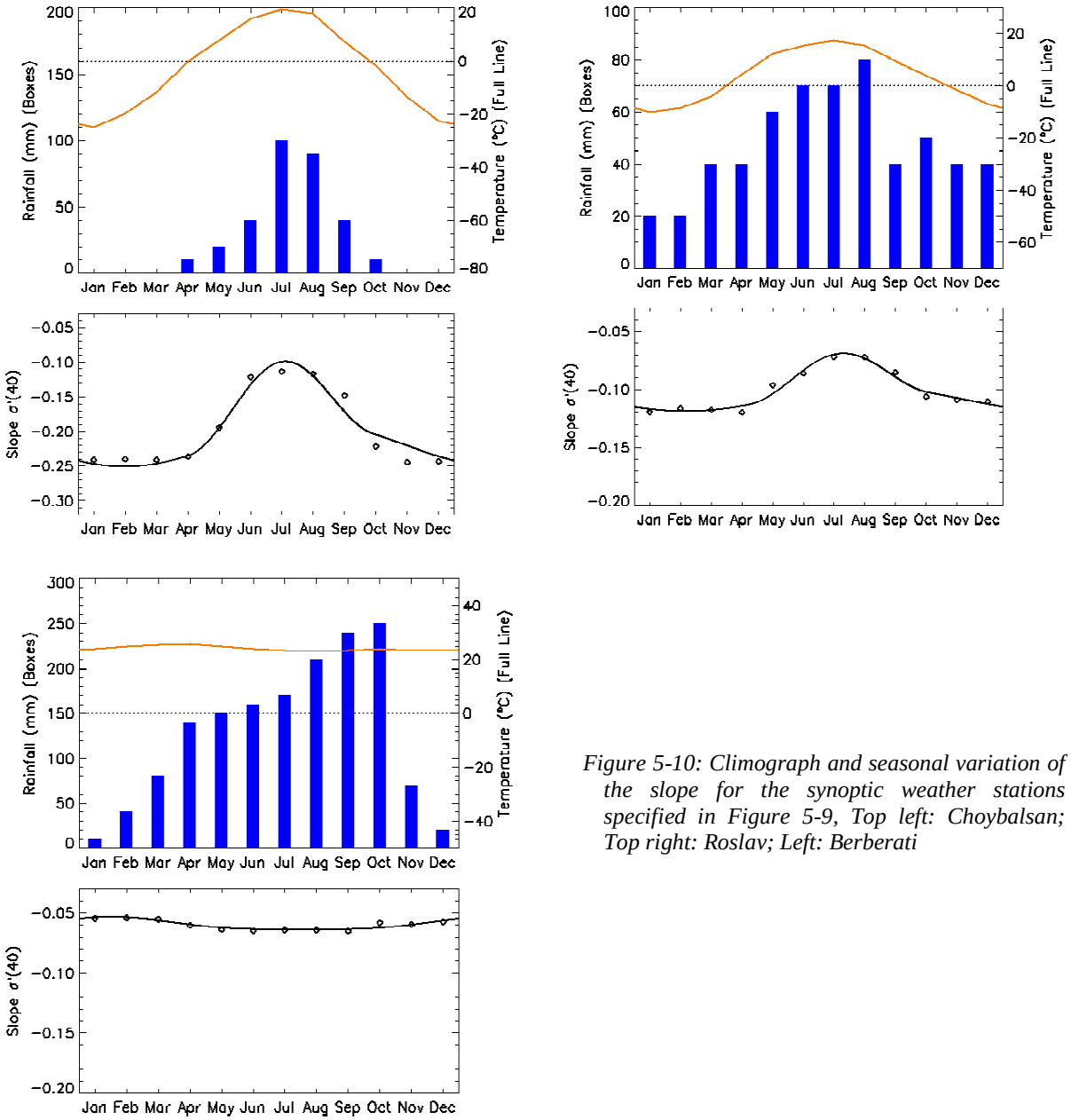

Figure 5-10: Climograph and seasonal variation of the slope for the synoptic weather stations specified in Figure 5-9, Top left: Choybalsan; Top right: Roslav; Left: Berberati

As discussed the maximum slope value should be expected when above ground biomass is highest. Figure 5-11 shows the time during the year where the maximum slope value is observed. The spatial distribution of the slope maximum is consistent and correlates well with climatic conditions. For example in the northern Hemisphere, characterised by cold winters, the maximum is observed in the 3rd quarter of the year when vegetation reaches a maximum during the warm season. Only small regions do not follow the general trend. For example in Africa, north of the Equator the maximum slope should be observed during the 3rd quarter of the year when the Intertropical Convergence Zone crosses the region. However maximum slope values are observed as late as December. These regions are characterised by a marked seasonal cycle in vegetation phenology with distinct dry and wet seasons. The slope $\sigma'(40)$ is consistently lower during the rainy season than during the dry season (Figure 5-12). A possible explanation of this phenomenon is that the ground surface is extremely rough leading to high $\sigma'(40)$ in absence of vegetation. With the growth of vegetation, the slope might under these special conditions even decrease. Given the prerequisitions, these effects are limited to Steppe like biomes. Until reliable surface roughness information and detailed information on vegetation phenology is available, quantification of these effects is difficult.

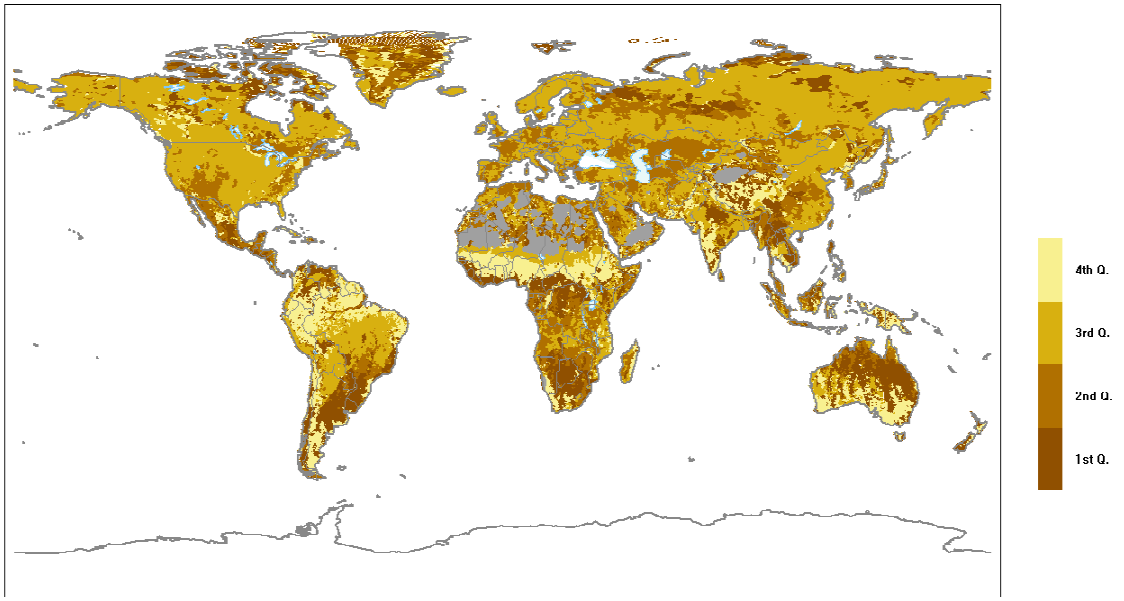

Figure 5-11: Quarter of the year where the maximum of the slope is observed. Grey indicates regions of high azimuthal anisotropy.

Also in the Cold to Polar Regions, a specific seasonal cycle of σ' is observed deviating from the general trend. In regions with a pronounced cold season the slope increases during fall, decreases in spring and increases again during summer (Figure 5-12). This phenomenon is more or less pronounced. A possible explanation for the increase of σ' during winter is the formation of ice lenses, pipes and grain clusters in the snow layer resulting in enhanced volume scattering. These features can be efficient scatterers at C-Band, when the snow cover is dry, resulting in high cross- and copolarization with reduced dependencies on the incidence angle and therefore a less steep slope (Mätzler 1987, Mätzler et al. 1997).

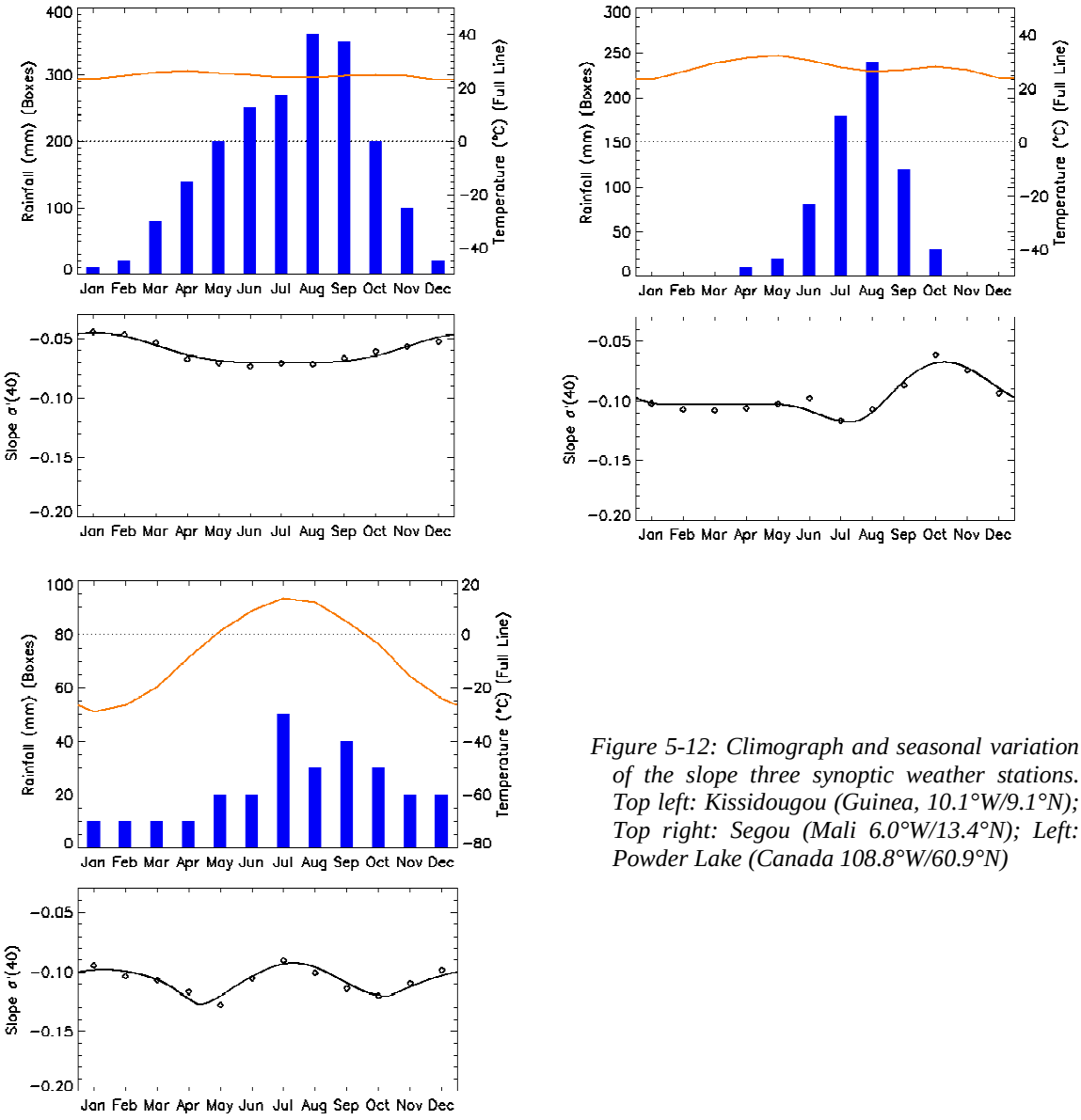

Figure 5-12: Climograph and seasonal variation of the slope three synoptic weather stations. Top left: Kissidougou (Guinea, 10.1°W/9.1°N); Top right: Segou (Mali 6.0°W/13.4°N); Left: Powder Lake (Canada 108.8°W/60.9°N)

Table 5-3 gives an overview of the empirical periodic functions $\Psi'(t)$, describing the phenology of σ', used in this study. A total of 65 models has been formulated. Based on a simple sine function or a combination of sine functions with specific weighting terms, the models are grouped in four broad types.

1. A constant function for areas, were the scattering mechanisms influencing the slope are stable throughout the year, such as tropical forest or deserts.
2. Sine functions for regions with distinct vegetation phenology and pronounced maximum.
3. A sine function with a second maximum for regions with a second growing season, such as the Horn of Africa.
4. A sine function with a second maximum for regions with a marked cold season.

Each model is determined by the time t and by a phase term δ. The phase term δ is used for dynamically setting the maximum of the sine function to the observed maximum. For each model type a number of sub models has been defined (Table 5-3). These sub models principally include weighting terms enhancing or damping the model behaviour during a distinct period of the year, for example equation (5.3) defines as simple sine function with enhanced slopes.

$$\Psi'(t) = \left(\frac{\sin\left(\frac{\pi}{6} \cdot (t - \delta) \right) + 1}{2} \right)^2 \tag{5.2}$$

Figure 5-13 gives an overview of the spatial distribution of the applied model types. Model type I is only found over the tropical forests of Africa, showing that σ' is highly sensitive to variations in surface and volume scattering resulting in a distinct seasonal phenology of the slope. Model type II applies over most regions. Model type III and IV are found in areas with a second growing season and in areas with a marked cold season. Separation between type III and IV is difficult because they are very similar in their temporal appearance, which is why they are not plotted separately. Generally, regions experiencing two distinct rainfall seasons are located near the equator, influenced by the movement of the Inter Tropical Convergence Zone. These areas are characterised by tropical climates with high precipitation and incoming radiation rates throughout the year. Vegetation growth is therefore independent of the climatic cycles. Only in dry climates such as the Horn of Africa with a distinct separation of the rainfall seasons and a marked dry period in-between, type III/IV applies. Beside the Horn of Africa, the North East of the India subcontinent and eastern China are characterised by a second maximum of the slope during the year. Neither vegetation cover effects nor accumulated snow cover can explain this

phenology. A detailed explanation of the effects has to remain open until detailed vegetation cover and surface roughness data is available for the respective regions. Nevertheless, the dynamic range of the second maximum is generally small and the effect is only significant for a limited number of points.

TABLE 5-3: Overview of applied slope models

Model	Type	Percent Area	No. of sub models	Examples
Constant	I	1.3	--	--
Distinct vegetation cycle	II	71.2	27	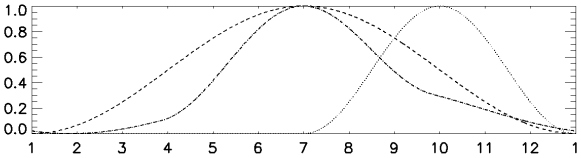
Distinct vegetation cycle with an increase during winter	III	27.4	37	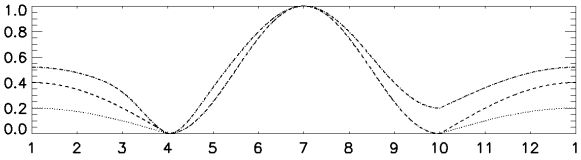
Distinct vegetation cycle with a second growing season	IV			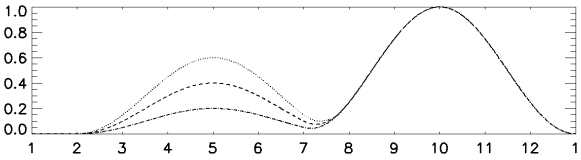

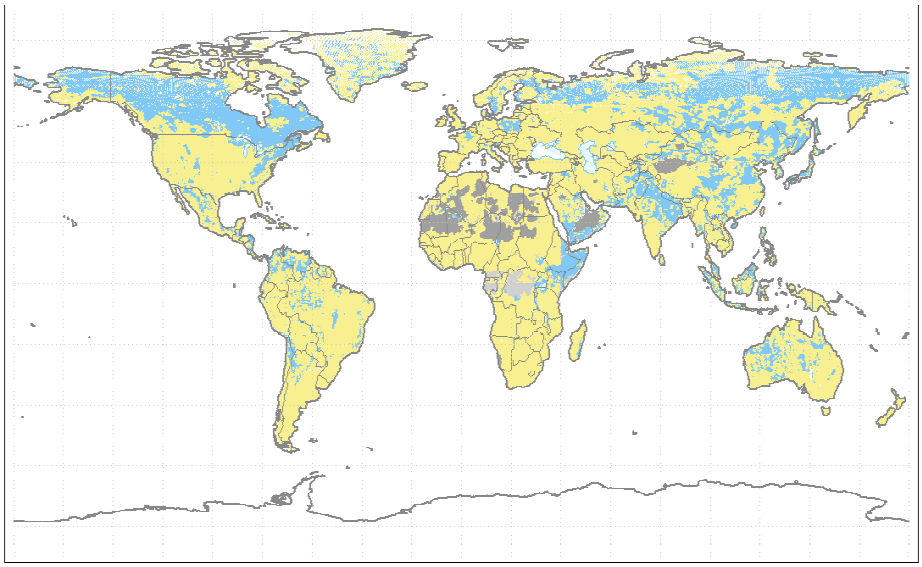

Figure 5-13: Distribution of model types specified in Table 5-3. Light grey indicates model type I, yellow colour indicates model type II and blue colour indicates model type III and IV. For a definition of model types see text.

Figure 5-14 and Figure 5-15 show global maps of the constant slope parameter C' and the dynamic range D'. Both parameters reflect vegetation patterns and climatic conditions quite well. High values of C' and low values of D' generally occur in the tropics, low values of C' and high values of D' in regions with distinct seasonal vegetation dynamics such as the Kasachien and Mongolian Steppe, or the North American Great Plains. Over wide ranges, C' is higher than -0.15 dB/deg. The dynamic range D' is generally lower than 0.05 dB/deg, higher values above 0.1 dB/deg indicate a distinct differences in vegetation abundance during the dry and the rain season.

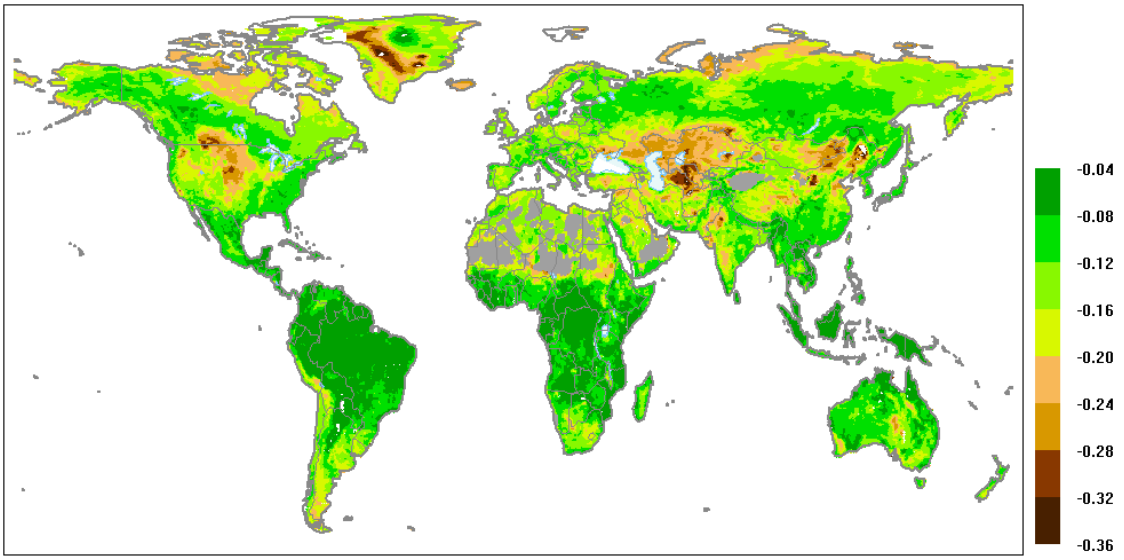

Figure 5-14: Global distribution of the constant slope parameter C′ dB/deg. *Grey color indicates regions of high azimuthal anisotropy.*

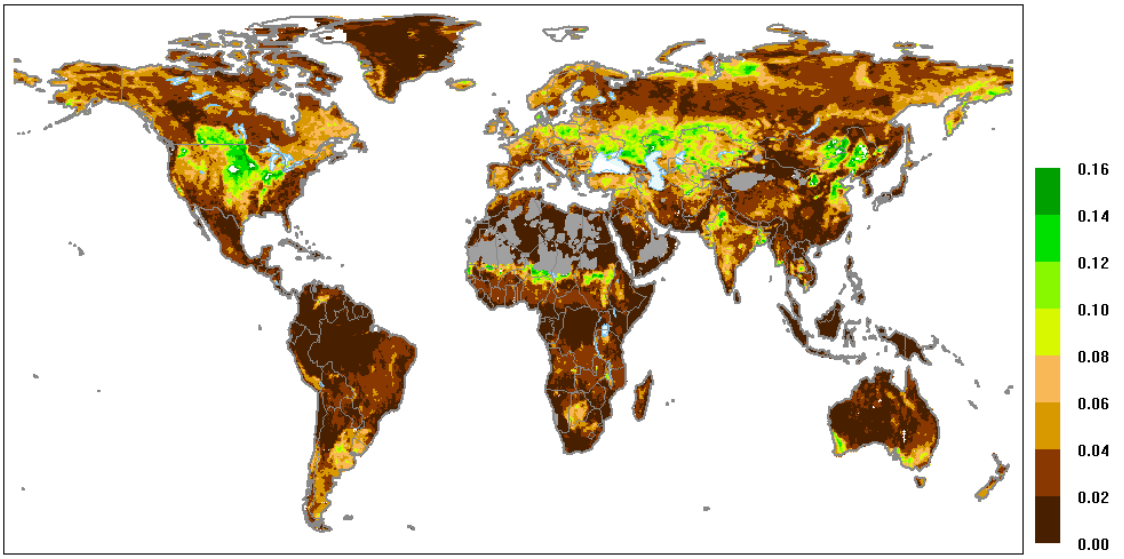

Figure 5-15: Global distribution of the dynamic slope parameter D´ in dB/deg. Grey colour indicates regions of high azimuthal anisotropy.

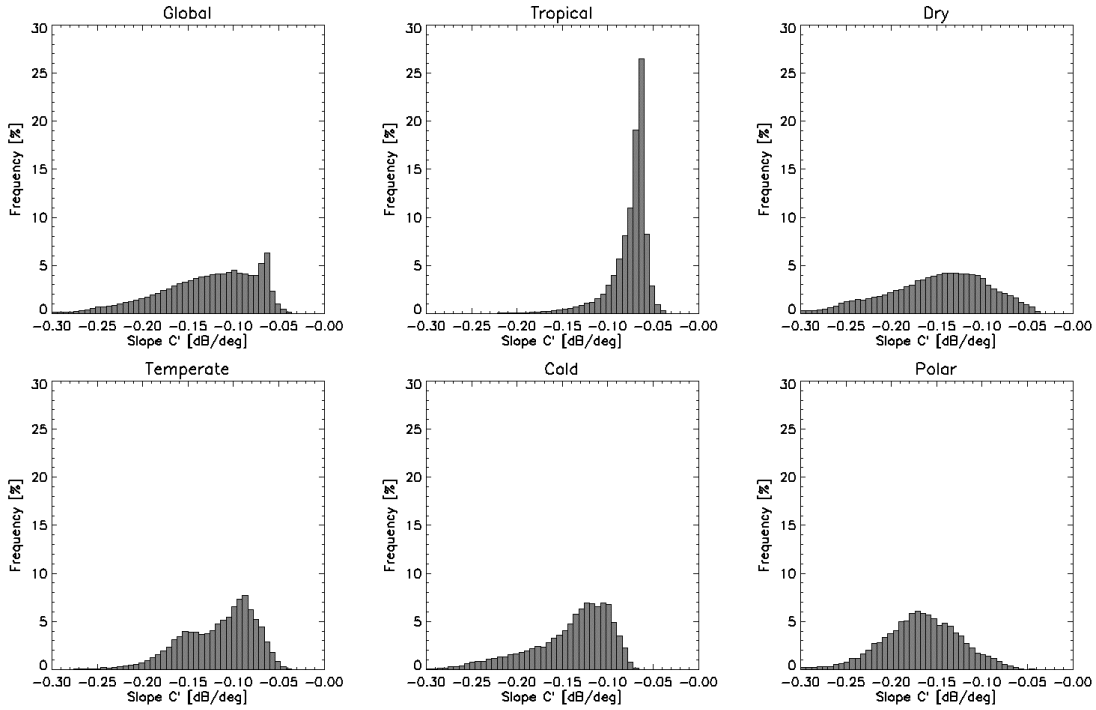

Figure 5-16 Histogram of the constant slope parameter C′ for different climatic regimes defined according to Koeppen.

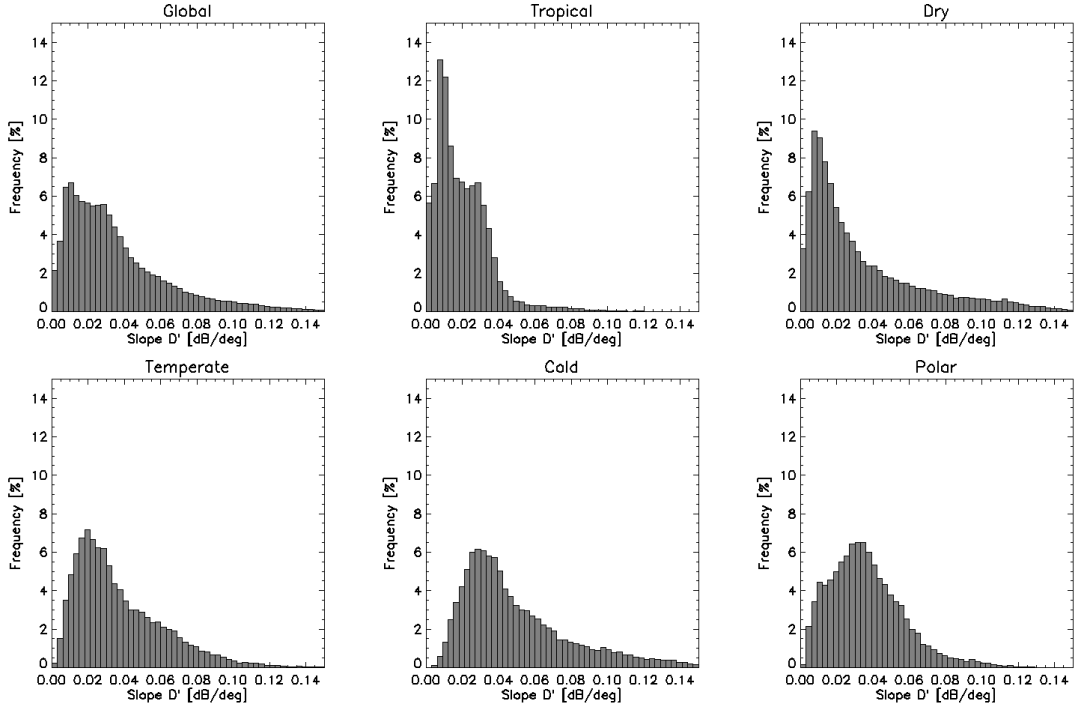

Figure 5-17 Histogram of the dynamic slope parameter D′ for different climatic regimes defined according to Koeppen

Comparing simulated potential biomass with the slope parameters C' and D' indicates a significant correlation between the parameters (Figure 5-18). According to the Figure 5-18 up to 500 g/m^2 biomass has no distinct influence on C'. Between 500-2000 g/m^2 sensitivity is significant. Above 2000 g/m^2 C' saturates. The dynamic range D' increases with increasing biomass up to a value of 1000 g/m². Above this value, D' decreases. It is argued that below 1000 g/m² potential biomass, the biome is characterised by a distinct seasonal cycle leading to an increase in D' with increasing biomass. Values above 1000 g/m² are indicative for forested vegetation biomes. These are not subject of distinct differences of vegetation abundance over the course of a year leading to a general decrease of D' if potential biomass increases. Although Figure 5-18 confirms that scatterometer derived parameters are capable to describe broad vegetation types a definitive statement is tentative. A problem in the interpretation is the spatial variability of surface roughness (Wagner et al., 1999a, Woodhouse and Hoekman, 2000b). If vegetation cover is sparse, soil roughness effects become important and can lead to values as high as observed over forest biomes. Spatial patterns of C' and D' are therefore explained by a complex interaction of vegetation and soil surface morphology. This is most likely a problem in relatively dry climatic regions with sparse vegetation cover leading to high variance of the observed correlation (Figure 5-18). However, Figure 5-18 shows a general trend and with more reliable reference data on vegetation and roughness conditions a clearer picture of the phenology of the slope might be received.

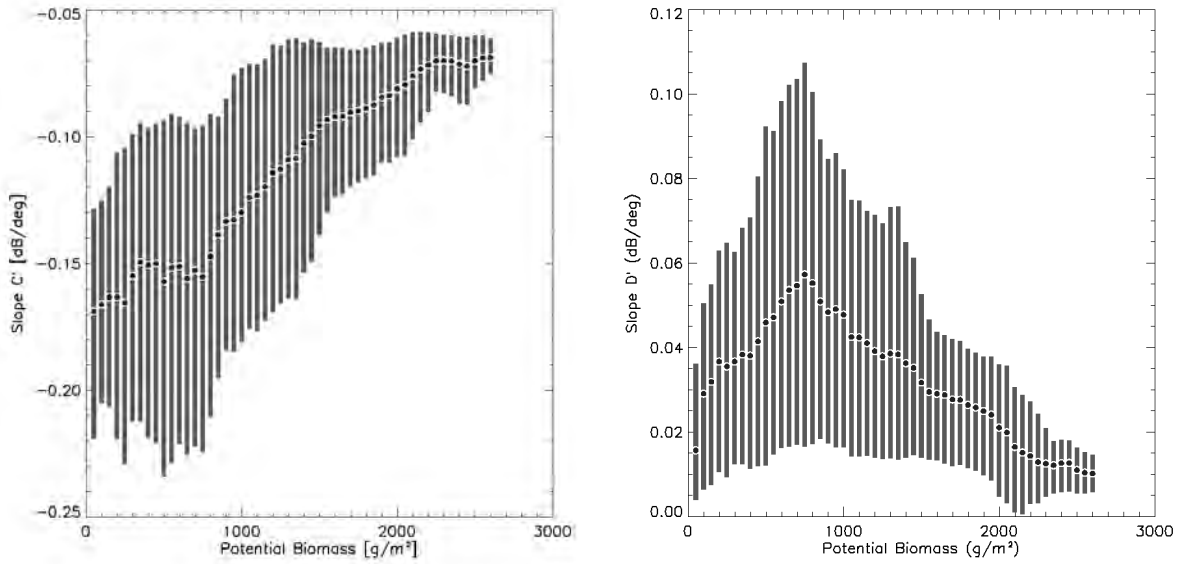

Figure 5-18: Scatter plot of the slope parameters C´ (dB/deg), D´ (dB/deg) and modelled annual potential biomass. The dark dots indicate the mean value, 75% of the values are within the grey bars.

Compared to the slope σ' the curvature σ'' exhibits an inverse behaviour. The constant parameter C'' is lowest over areas with a high amount of above ground biomass and high over sparsely vegetated areas. D'' is lowest for regions with distinct difference in vegetation abundance. However, the influence of the curvature on $\sigma^0(\theta)$ is small. Given the similar trends in both σ' and σ'' a detailed discussion on the spatial patterns of σ'' seem redundant.

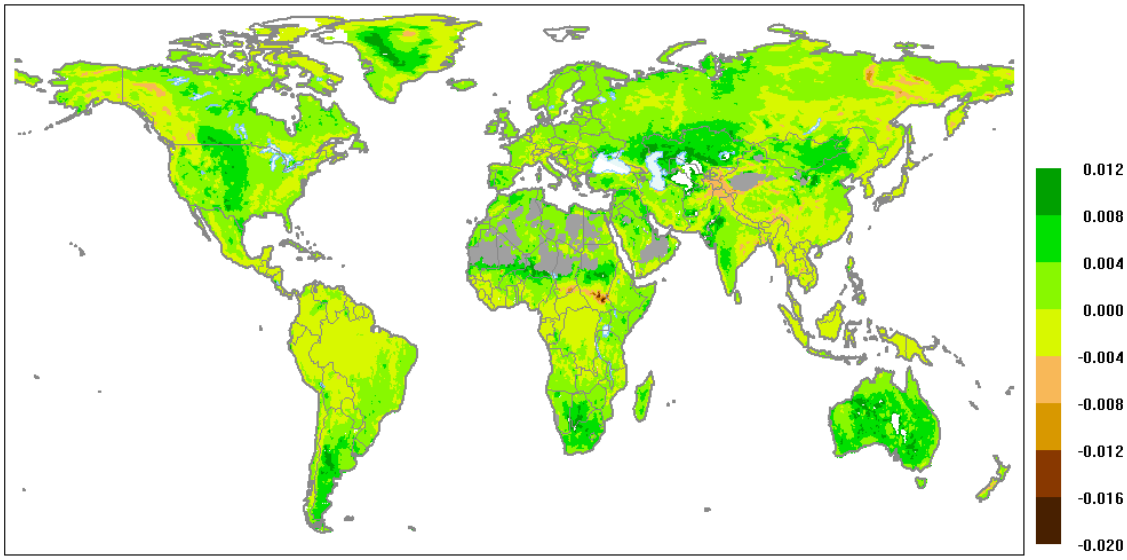

Figure 5-19 Global distribution of the constant curvature parameter C'' in dB/deg^2 Grey colour indicates regions of high azimuthal anisotropy.

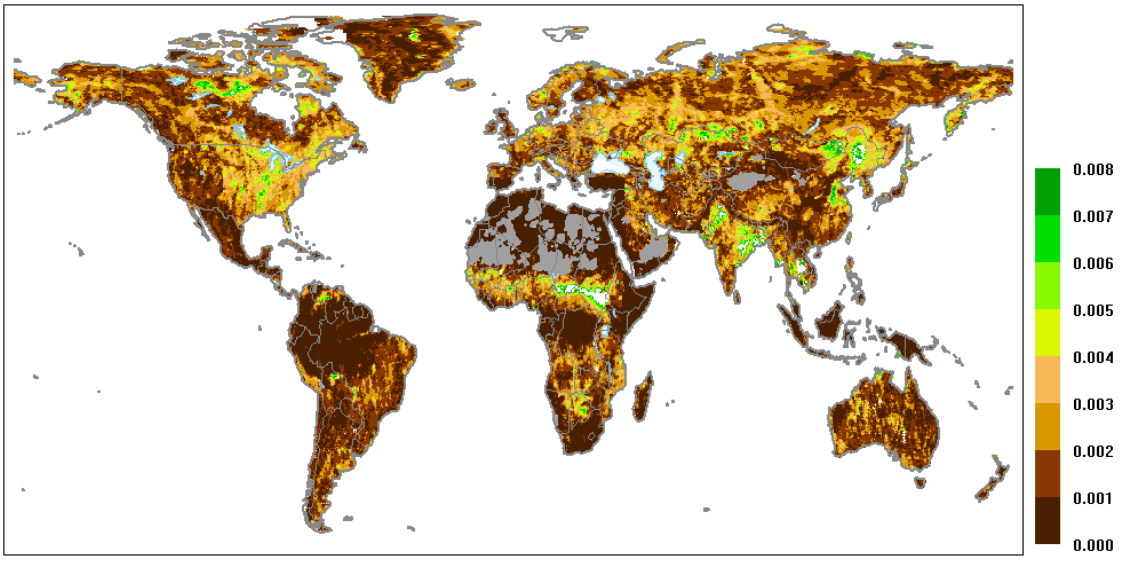

Figure 5-20: Global distribution of the constant curvature parameter D'' dB/deg^2. Grey colour indicates regions of high azimuthal anisotropy.

5.3.3 Backscatter under Dry and Wet Conditions

Temporal variations of $\sigma^0(\theta)$ are induced by vegetation and soil moisture variability. Consistent estimation of soil moisture necessitates correct representation of the influence of vegetation phenology on $\sigma^0(40)$. Vegetation cover effects can be described by linking the temporal variation of $\sigma^0(\theta)$ due to vegetation growth to the temporal variation of the slope $\sigma'(\theta)$ because if the slope changes, $\sigma^0(\theta)$ must necessarily change too. The rate of change depends on the incidence angle. At some incidence angle however, which we call the "crossover angle", $\sigma^0(\theta)$ of dormant vegetation and a fully developed vegetation canopy must cross over (Figure 5-3). If such a "crossover angle" exists then it depends on surface soil moisture, which affects the relative level of the surface and volume scattering contribution. For dry soils, the crossover angle should be found at lower incidence angles than for wet soils. If for given soil wetness conditions the crossover angles are known then the temporal evolution of $\sigma^0(\theta)$ due to vegetation growth is known at any incidence angle. The cross over angles are determined by comparing estimates of $\sigma^0_{dry}(40,t)$ and $\sigma^0_{wet}(40,t)$ to the minimum and maximum values of $\sigma^0(40)$ multi year backscatter time series. Over various climates, setting θ_{dry} equal to 25° and θ_{wet} equal to 40° gives a good fit to the lowest and highest $\sigma^0(40)$ values ever measured. Setting θ_{wet} to 40° means that σ^0_{wet} is a constant independent of vegetation development. Figure 5-21 to Figure 5-24 show examples of $\sigma^0(40)$ time series for the main climatic regimes defined by Koeppen. It can be observed how the minimum and maximum values sit on $\sigma^0_{dry}(40,t)$ and $\sigma^0_{wet}(40,t)$ independent of the season. Minimum values predominately occur during cold periods when soil freezes resulting in low surface water levels or after drought periods. High values are found shortly after strong rain showers or periods of long lasting rainfall.

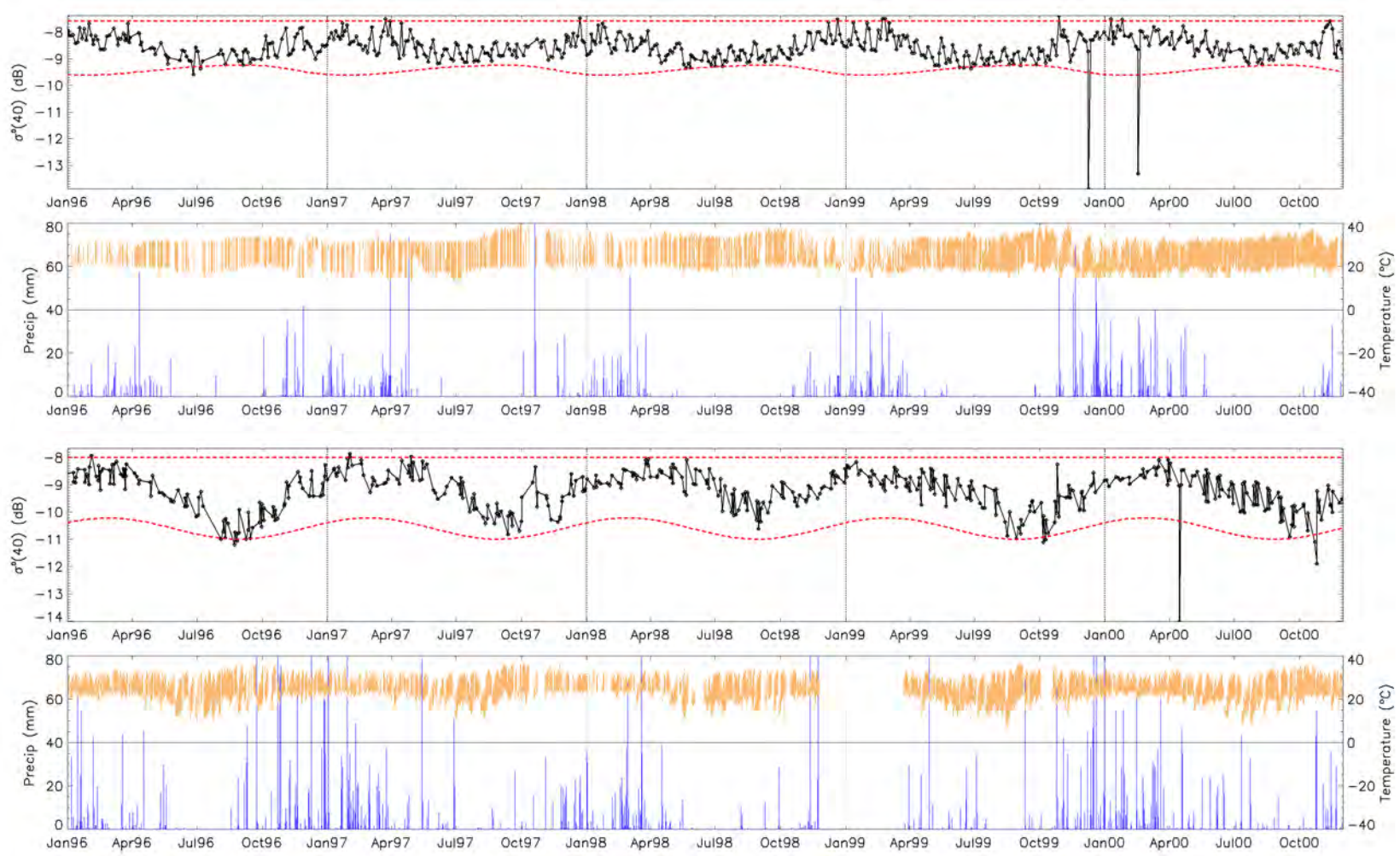

Figure 5-21: Backscatter $\sigma^0(40)$ together with $\sigma^0_{dry}(40)$ and $\sigma^0_{wet}(40)$ and meteorological records for a tropical climate. Top: Bom Jesus – Brazil (44.1°W, 9.1°S); Bottom: Trinidad – Bolivia (65.0°W, 14.9°S)

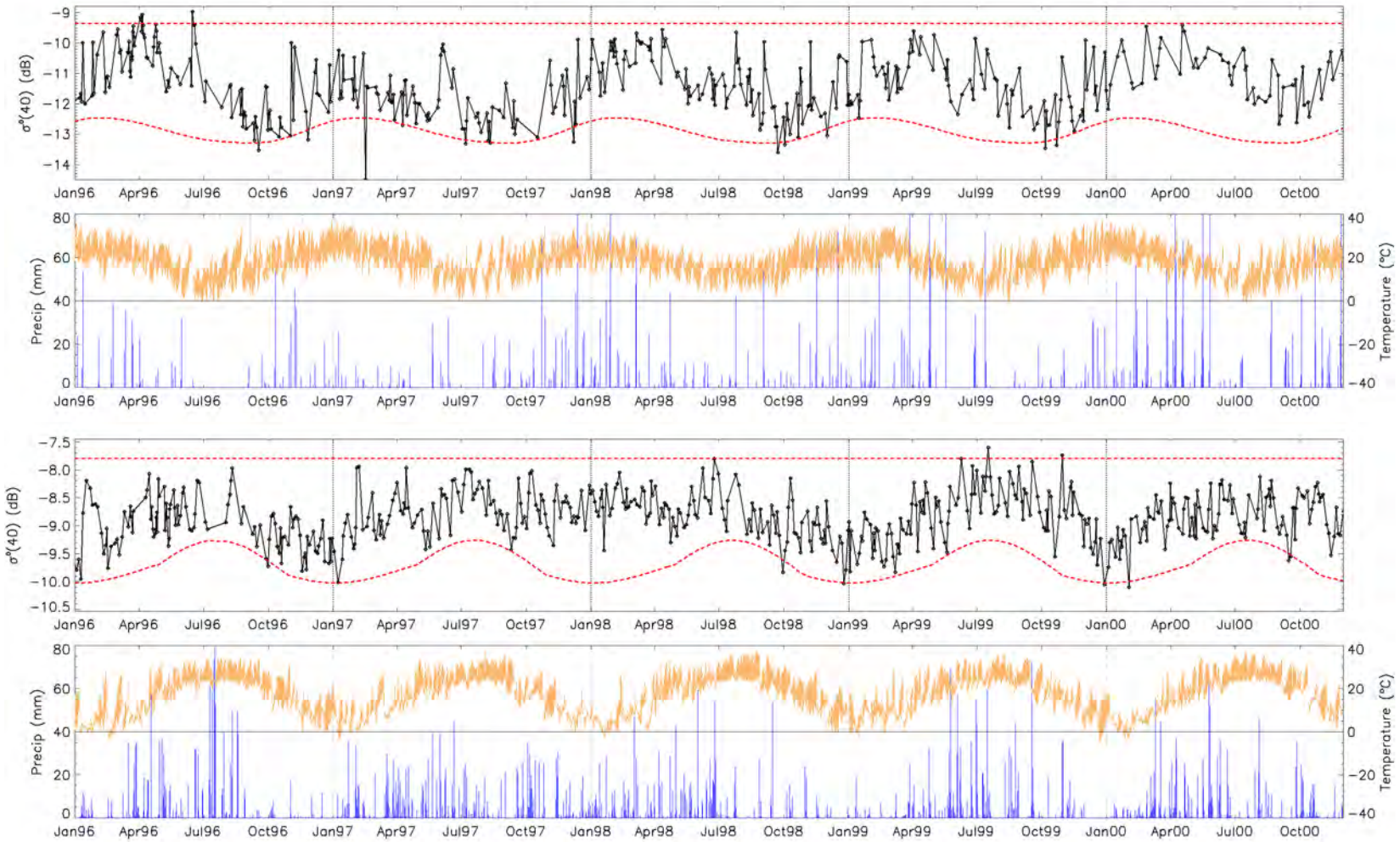

Figure 5-22: Backscatter $\sigma^0(40)$ together with $\sigma^0_{dry}(40)$ and $\sigma^0_{wet}(40)$ and meteorological records for a temperate climate. Top: Parana – Argentina (60.5°W, 31.9°S); Bottom: Wugang – China (110.6°E, 26.9°N)

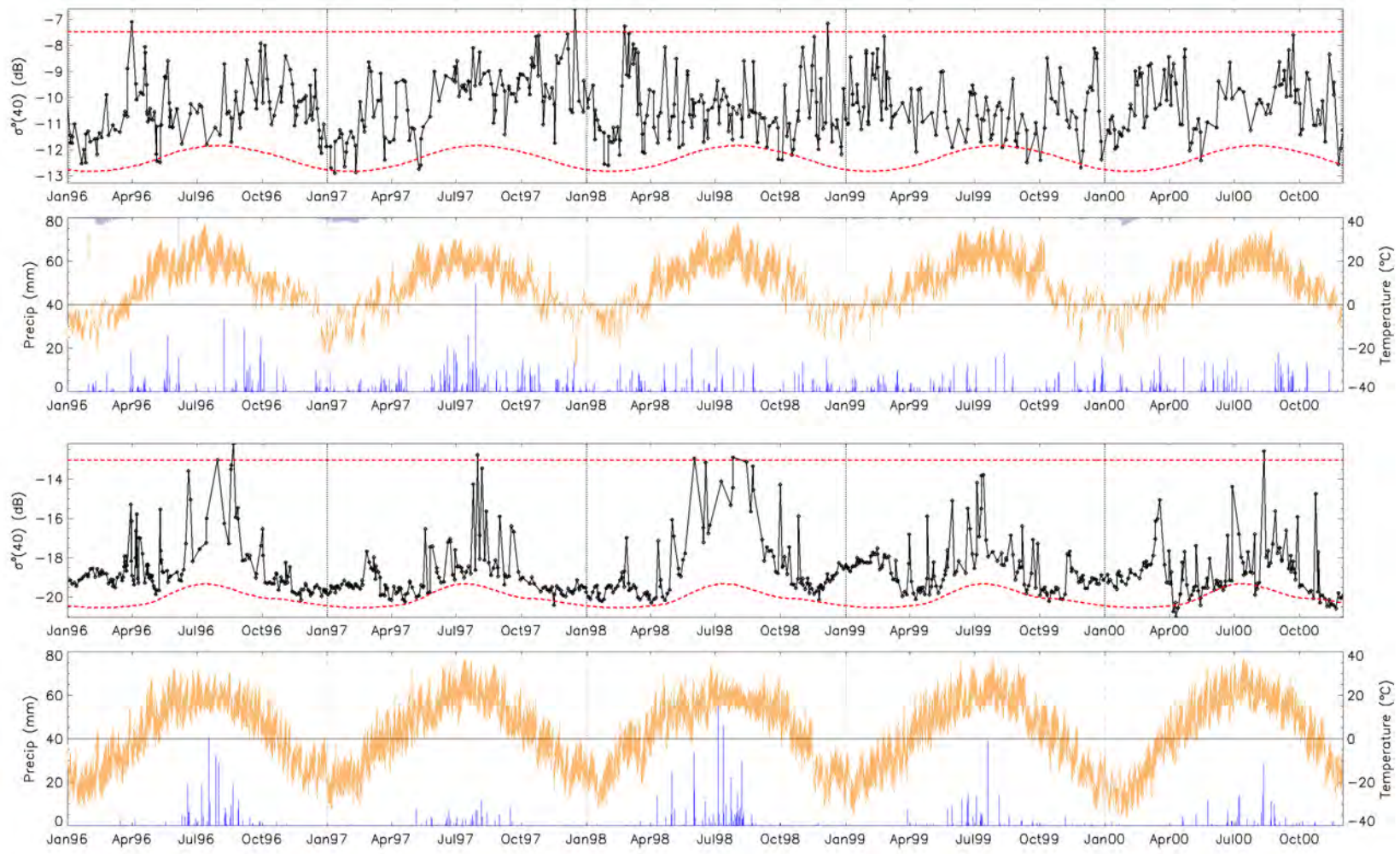

Figure 5-23: Backscatter $\sigma^0(40)$ together with $\sigma^0_{dry}(40)$ and $\sigma^0_{wet}(40)$ and meteorological records for a dry climate. Top: Doneck - Russia (37.8°E, 48.1°N); Bottom: Abag Qi – China (115.6°E, 44.1°N)

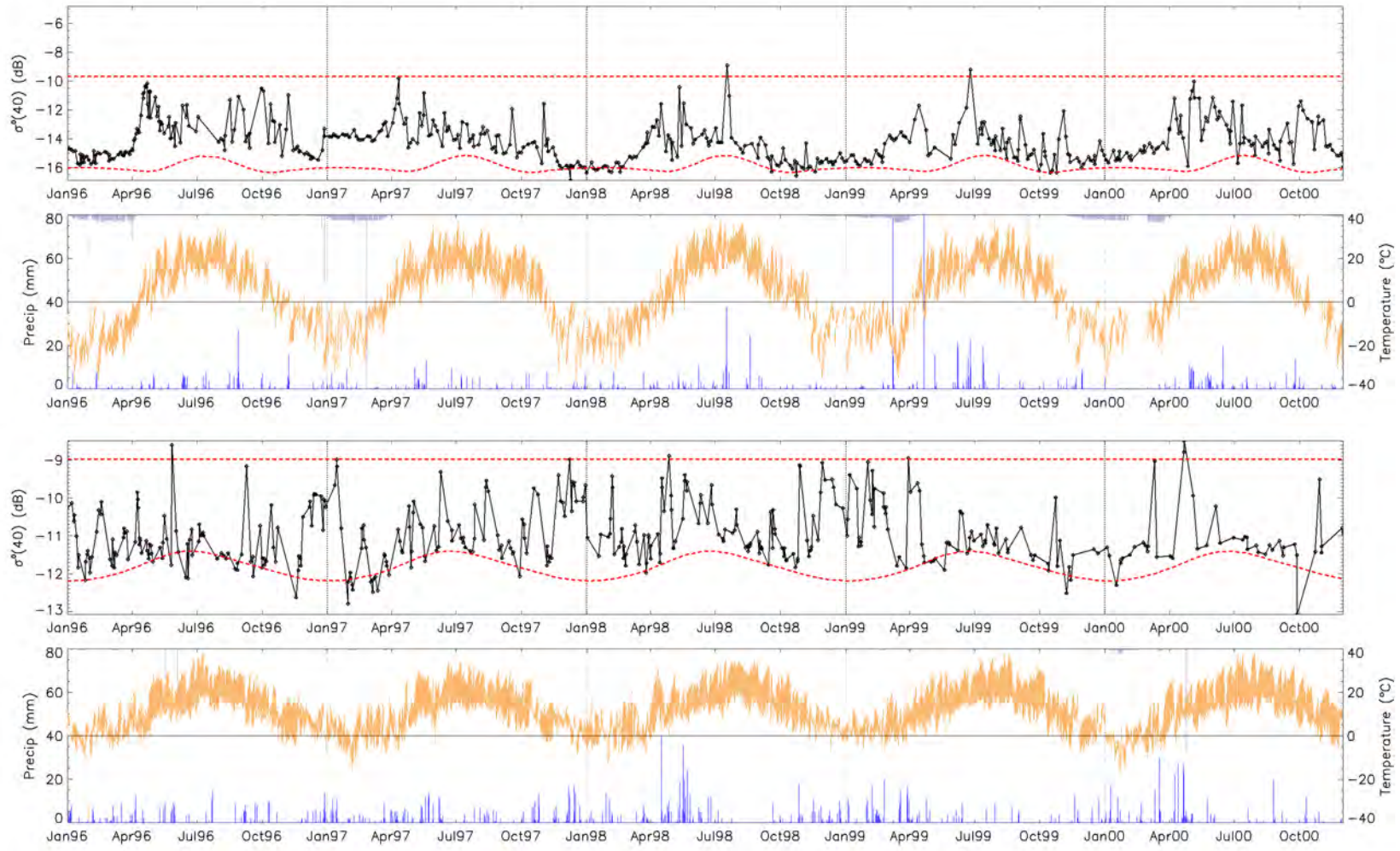

Figure 5-24: Backscatter $\sigma^0(40)$ together with $\sigma^0_{dry}(40)$ and $\sigma^0_{wet}(40)$ and meteorological records for a cold climate. Top: Celinograd - Russia (71.4°E, 51.1°N); Bottom: Ekisehir – Turkey (30.6°E, 39.9°N)

If backscatter was observed over long periods, σ^0_{dry} and σ^0_{wet} will likely represent a completely dry soil surface and a saturated soil surface and the difference between σ^0_{dry} and σ^0_{wet} defines the sensitivity of $\sigma^0(40)$ to soil moisture variations. Given the nine-year period of scatterometer observations it is likely that backscatter has been recorded under dry and saturated conditions for most climates and σ^0_{dry} and σ^0_{wet} generally represent their respective wetness value. However reliable estimation will depend significantly on the climatic regime. The condition of dryness is most easily fulfilled in climates with a dry season and high temperatures or in climates with a distinct cold season as a frozen soil has a backscattering coefficient similar to that of dry soil. On the other hand, the condition of saturation is most easily met in climates where ample precipitation may occur, including all moist and wet-dry climates. For the dry climatic types however, rainfall may not be sufficient to saturate the soil surface, a situation that is aggravated for sandy soils and high potential evaporation such as encountered in deserts. If σ^0_{wet} does not represent saturated conditions, bias is introduced in the soil moisture retrieval, and correction is required. Before an empirical method to correct σ^0_{wet} is defined, it is advisable to discuss the spatial patterns of C^0_{dry} and C^0_{wet}. According to Table 5-1, C^0_{dry} and C^0_{wet} define the minimum and maximum backscatter observed.

It has been demonstrated that most of the spatial variability of backscatter parameters can be explained by the amount of above ground biomass. Depending on the percent area of translucent vegetation and the percent area of non-transparent vegetation within the resolution cell of the ERS Scatterometer backscatter parameters will decrease or increase. Generally, it can be expected that with increasing percentage of non-transparent vegetation C^0_{dry} increase as the attenuation of the signal by the vegetation cover decreases. The sensitivity C^S defined as the difference of C^0_{dry} and C^0_{wet} generally decreases with increasing vegetation. Figure 5-28 and Figure 5-29 confirm this statement. Both parameters compare favourable with climate regimes. Maximum values are observed over the tropics, minimum values over regions with low vegetation. Figure 5-25 and Figure 5-26 indicate that C^0_{dry} varies greatly depending on the land cover indicating a clear relationship with above ground biomass whereas C^0_{wet} is fairly constant for most regions although conditions can range from bare soil surfaces to tropical rainforests. Only over desert regions, C^0_{wet} drops off strongly and reaches lower values. Because C^0_{wet} is generally found to show little dependence on vegetation cover (Figure 5-26), it can be concluded that, although soil effects may also play a role, the decrease of C^0_{wet} in dry climate regimes is associated with the failure to saturate the soil surface leading to an underestimation of σ^0_{wet}.

The same trends are observed in the sensitivity C^S, defined as the difference between σ^0_{dry} and σ^0_{wet}. Generally, the sensitivity towards soil moisture depends on the amount of above ground biomass. High amounts of biomass will lead to low sensitivity towards soil moisture variations.

Figure 5-30 shows the spatial distribution of the estimated maximum sensitivity. The sensitivity is highest over areas with no or sparse vegetation and reduce to a minimum over densely vegetated areas. Over mountainous regions such as the Himalayas, the Rocky Mountains or the Mackenzie mountains this general trend is not confirmed. Although vegetation is low, the sensitivity towards soil moisture is comparably low. Most likely these low values are a result of the rock surface, showing no sensitivity to soil moisture variations. In desert regimes characterised by a dry climate with extreme temperature variations and low rainfall, the sensitivity should be high as vegetation is absent. However sensitivity is observed to be on the low side.

Additionally it is noted that even in regions with high vegetation cover a proper retrieval of soil moisture is possible if some parts of the area are grassland or agricultural fields. Only areas covered by dense tropical forest are not suited for a proper retrieval of soil moisture. These regions are characterised by sensitivity below 2 dB. As proper retrieval of soil moisture is not possible, these regions will be excluded in the subsequent processing.

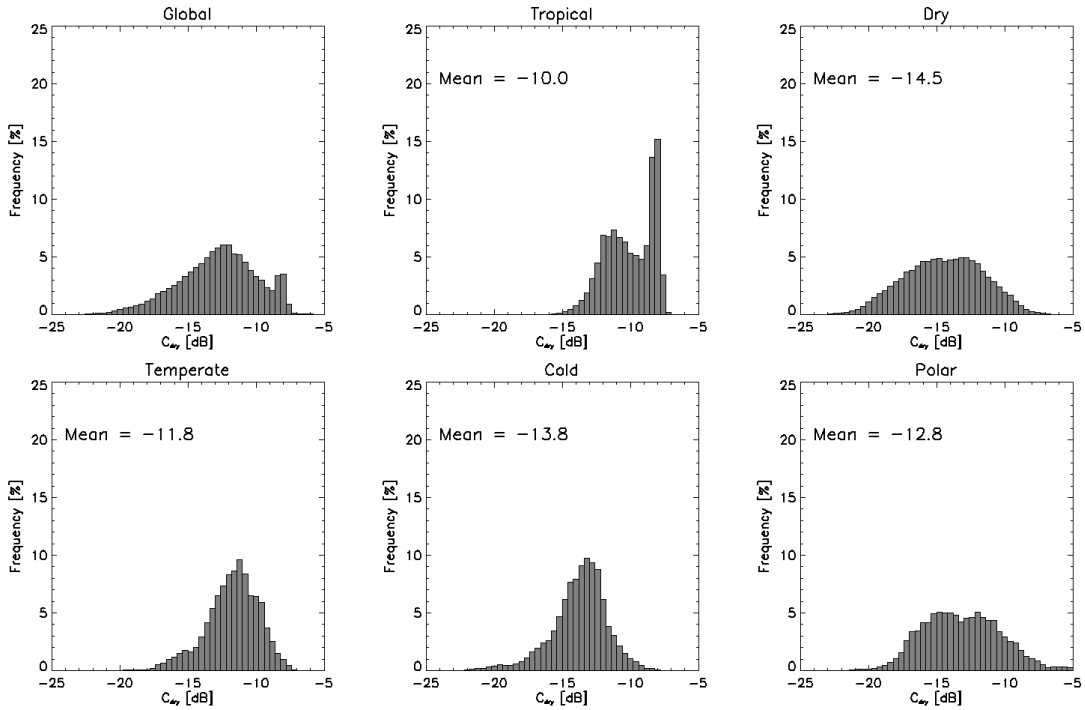

Figure 5-25 Histogram of C^0_{dry} for different climate regimes defined by Koeppen.

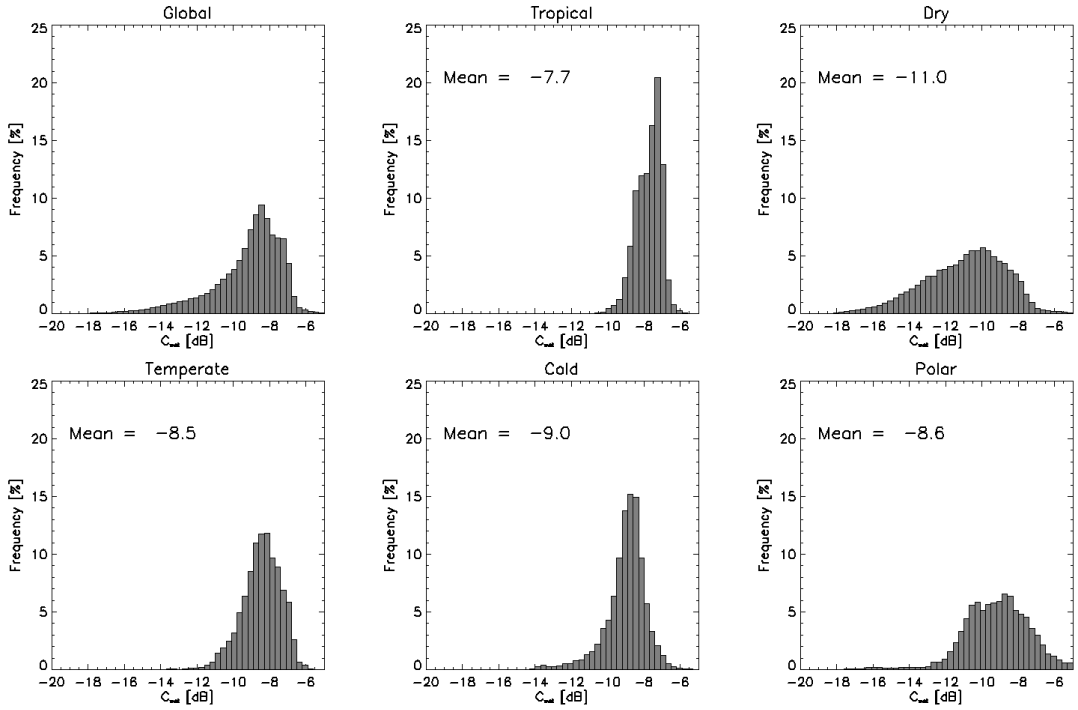

Figure 5-26 Histograms of C^0_{wet} for different climate regimes defined by Koeppen.

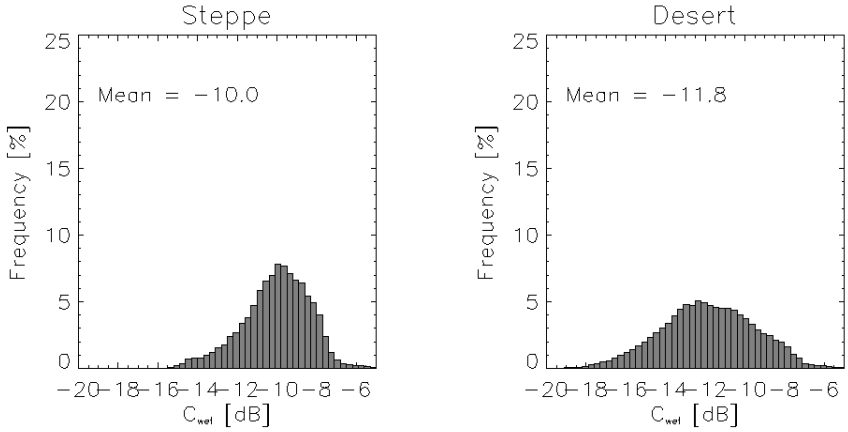

Figure 5-27 Histograms of C^0_{wet} for the two subclasses Steppe and Desert of the dry climate regime defined by Koeppen

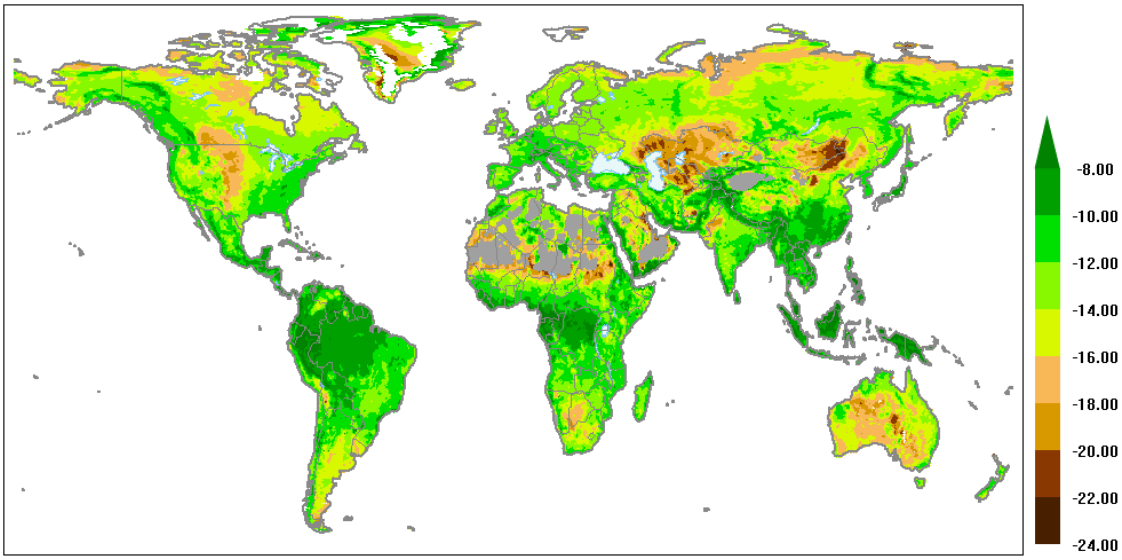

Figure 5-28: Minimum Backscatter C^0_{dry}.in dB.

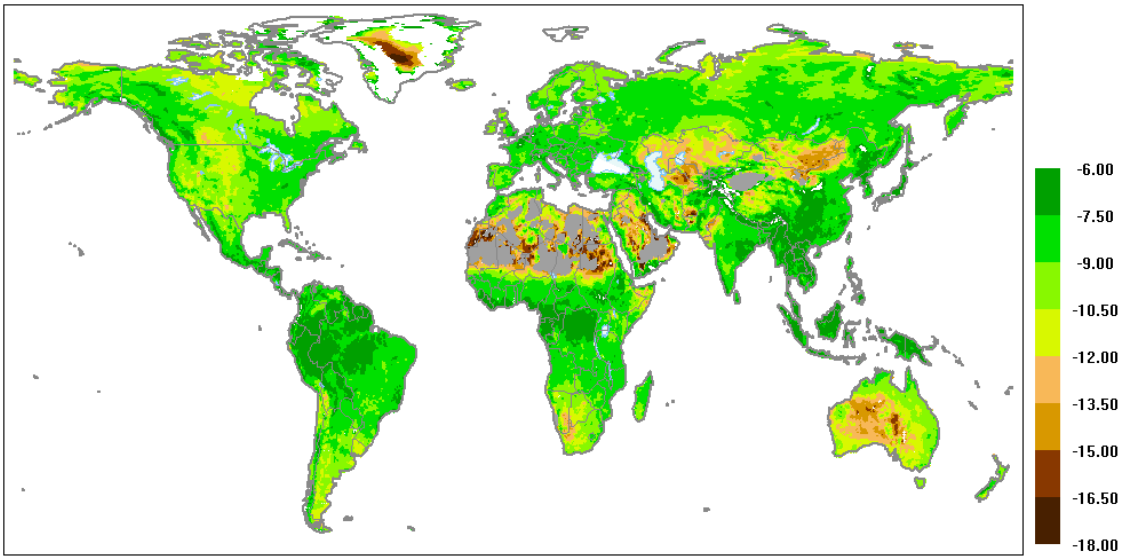

Figure 5-29 Maximum backscatter C^0_{wet} in dB.

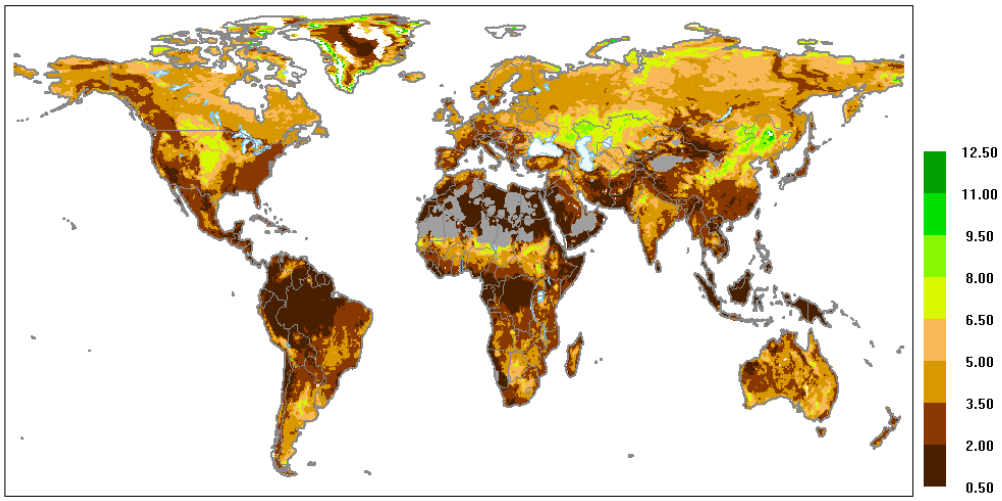

Figure 5-30 Maximum sensitivity C^S towards soil moisture changes.

To correct C^0_{wet} an empirical formulation has been established. The correction is based on the fact that the sensitivity C^S is generally low for a high area percentage of non-transparent vegetation and high for regions with low vegetation. A sensitive indicator for the area percentage of non-transparent vegetation is the constant slope parameter C'. Assuming that surface roughness do not significantly impair the relationship, we can link the sensitivity C^S to C'. In Figure 5-31 the basic relationship between slope C' and the sensitivity C^S is illustrated. Despite high scatter, a linear relationship with high confidence exists over most climates. Dry climates however violate this relationship with a pronounced second histogram peak at low C^S values. This effect becomes even more evident if we consider only the desert subclass of the dry climate regime defined according to Koeppen (Figure 5-32). Generally, Steppe like climates follow the general trend. Even over deserts, certain regions correctly depict the relationship between C^S and C'. However, a bulk of data has constant sensitivity while C' varies over a range of 0.3 dB/deg. To quantify these effects a linear model is fit to the data. Table 5-4 lists the estimated correlation coefficients and parameters of a fitted linear function of the form:

$$C^S = a + b \cdot C' \tag{5.3}$$

Generally *(5.3)* is defined by an offset value *a* ranging between 0.3 and 2.1 and a slope *b* ranging between –13.2 and –24.6. The offset value *a* describes the theoretical sensitivity of soil moisture if vegetation reaches a maximum value (i.e. when C' approaches zero). The slope parameter *b* is a measure of the dependence of C^S on the amount of above ground biomass.

Using this linear relation a corrected estimate of C^0_{wet} can be derived according to

$$C^0_{corrwet} = (a + b \cdot C') + C^0_{dry} \quad (5.4)$$

C^0_{wet} is only corrected if the respective value is lower than the value estimated using equation *(5.4)*. Ad hoc the parameters of *(5.3)* have been set to *a=1* and *b=-30*, by visually defining the best fit of the model to data observed over Africa. Over the Asian continent it was visually observed that this assumption lead to an overestimation of C^0_{wet}, therefore the relationship has been relaxed and parameters were set to *a=-1* and *b=-30*.

Although the slope value of –30 is significantly higher than the slope values estimated empirically during a reanalysis, the setting resulted in a good approximation of the true C^0_{wet} for Africa and Asia. It is noted, that the parameters estimated empirically (Table 5-4) can be biased by data from dry regions. In all plots very low C^S values are evident, damping the estimated slope.

Principally the correction method is only sensitive to dry regions, and should run without specifying the respective regions. However, surface roughness effects can introduce problems. As discussed very rough surfaces can lead to high C' values and thus may impair the relationship between C^S and C'. Therefore, regions where the correction algorithm was applied were selected manually.

TABLE 5-4: Parameters of a linear function fitted to data from Figure 5-31 and Figure 5-32

Climate	R^2	Offset	Slope
Global	0.36	1.06	-19.59
Tropics	0.27	0.34	-24.67
Temperate	0.48	0.97	-19.69
Cold	0.24	1.98	-18.03
Polar	0.23	2.12	-15.38
Dry	0.18	1.53	-13.85
Dry – Steppe	0.26	1.71	-15.81
Dry – Desert	0.15	1.27	-13.26

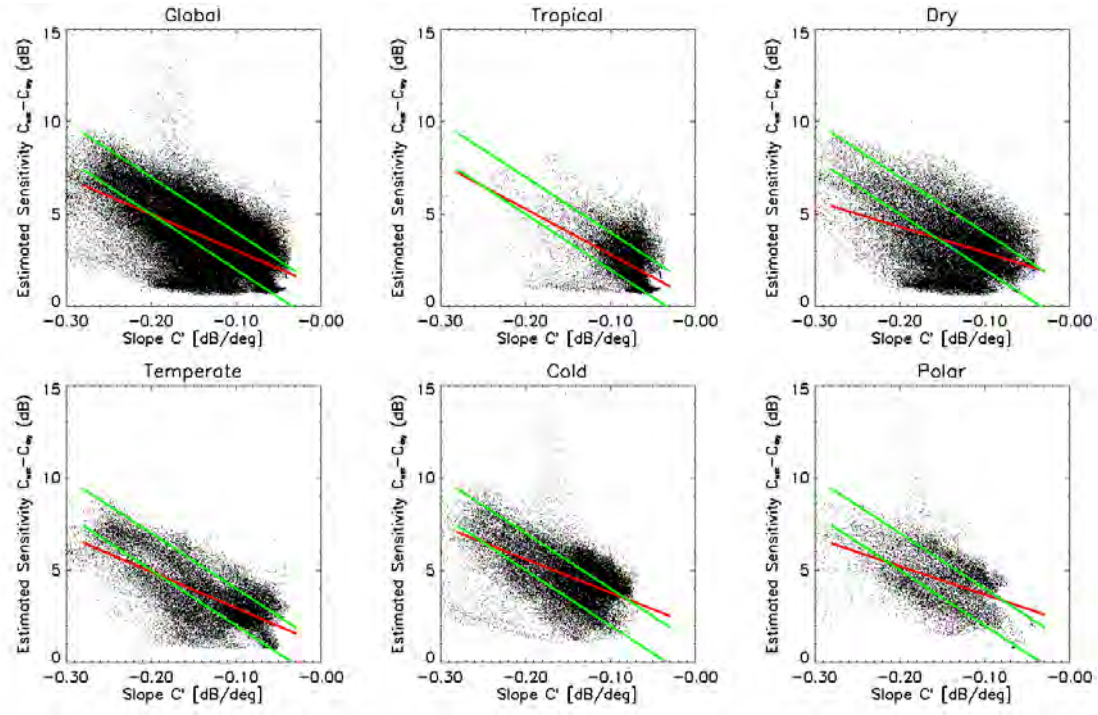

Figure 5-31 Scatter plots of the constant slope value C´ and the estimated sensitivity C^S defined by C^0_{dry}-C^0_{wet} for different climate regimes defined by Koeppen. The red line is a linear least square fit to the data. Green lines are result of a visual fit and are used to correct C^0_{wet}.

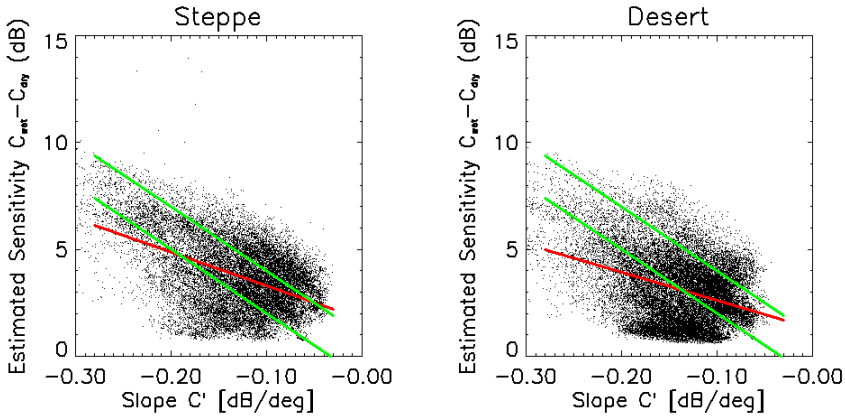

Figure 5-32 Scatter plots of the constant slope value C´ and the estimated sensitivity C^S defined by C^0_{dry}-C^0_{wet} for different climate regimes defined by Koeppen. The red line is a linear least square fit to the data. Green lines are result of a visual fit and are used to correct C^0_{wet}.

Figure 5-35 and Figure 5-33 illustrate the effect of this correction procedure. Figure 5-35 shows a scatter plot of total annual rainfall and the estimated sensitivity C^S. With an increasing amount of rainfall, C^S, generally decreases, which is a result of the higher amount of vegetation found under these conditions. When rainfall is below a certain level, characteristic for desert climates, C^S drops of and reaches minimum levels of below 2 dB. After the correction procedure, this drop

off is no longer evident in the data. Figure 5-33 shows the magnitude of correction. Correction is highest over hot deserts like the Sahara. In the plot, it becomes evident that two different parameter sets have been used in the correction procedure resulting in an undesirable spatial pattern. Based on these findings, a more consistent correction method can be investigated in future studies, which shall be based on a better description of surface roughness.

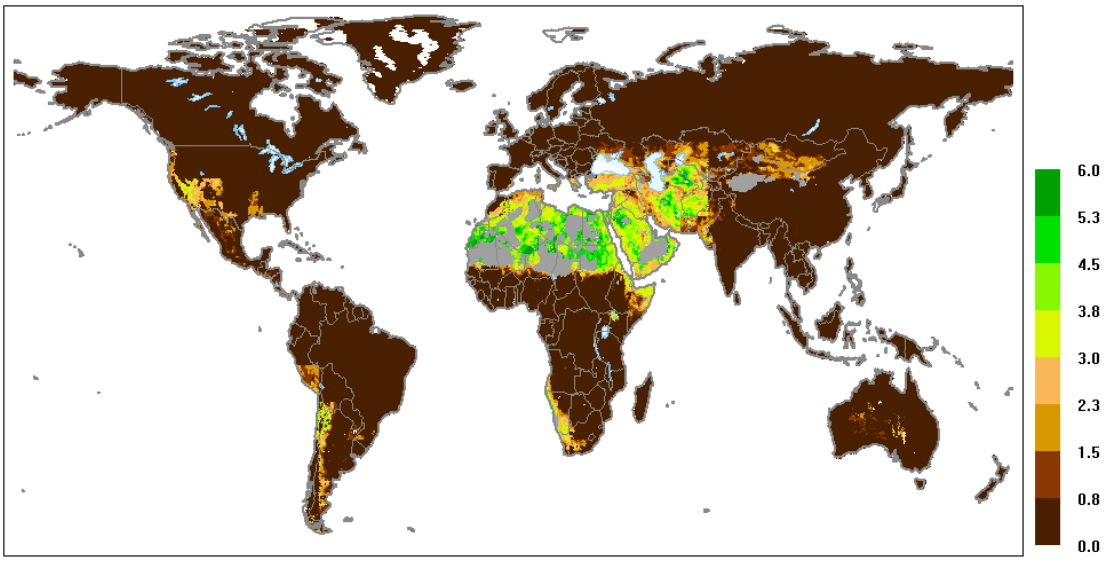

Figure 5-33: Magnitude of correction of C^0_{wet} in dB.

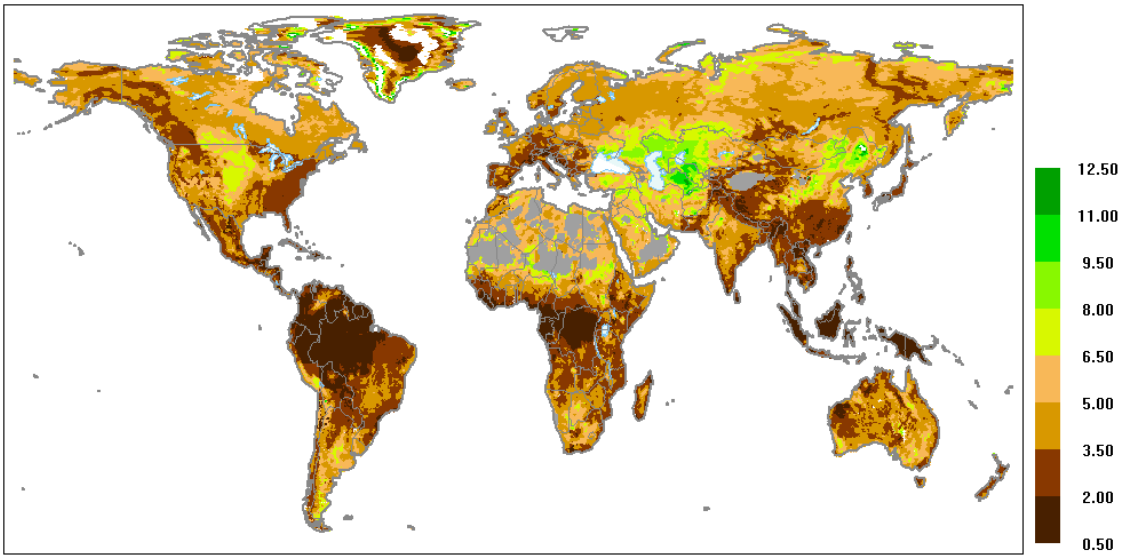

Figure 5-34 Corrected sensitivity estimated sensitivity C^S in dB defined as the difference between C^0_{dry} and C^0_{wet}.

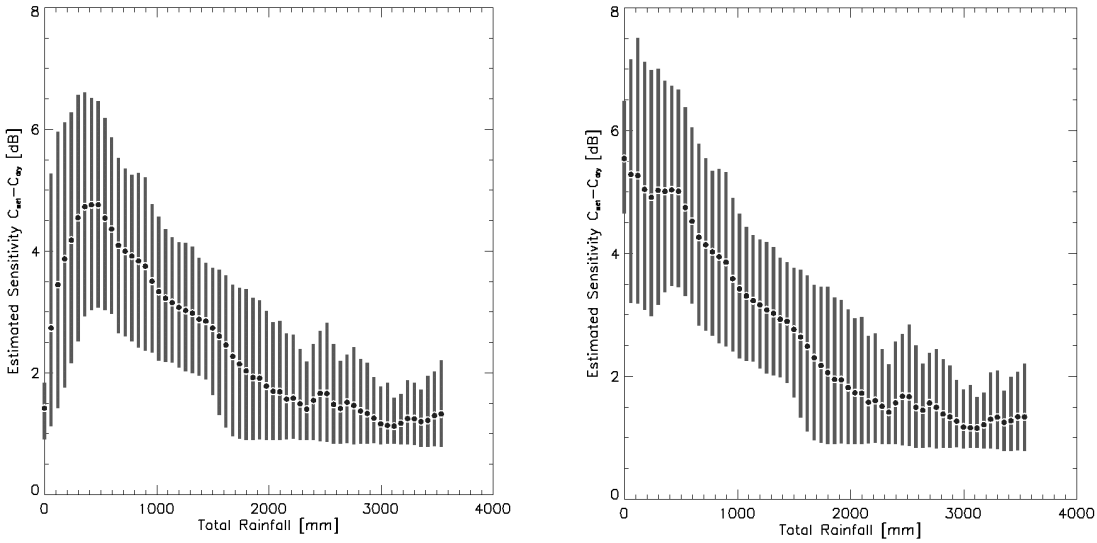

Figure 5-35 Relation between total annual rainfall and the sensitivity estimated sensitivity C^S defined as the difference between C^0_{dry} and $C^0_{wet.}$ 75% of the observed values are within the grey error bars.

5.4 Comparison with Landcover

Finally it is investigated if the scatterometer derived parameters of chapter 5.3 are consistent with theoretical expectations. The influence of the land cover on the backscattering behaviour is analysed by means of a multi-regression analysis between ERS Scatterometer parameters and the percentage area occupied by the land cover types specified in the USGS land cover schema. For the analysis only those land cover types were used occupying more than 2% of the global land surface (Table 5-5). Overall, the elected 15 land cover classes cover 94.32% of the total area. Excluding minor classes was necessary because otherwise the equations involved in multi-regression analysis would have become singular.

To see how each of the land cover types influences ERS Scatterometer parameters, a linear multiple regression analysis was performed:

$$x = X_0 + \sum_{i=1}^{15} A_i x_i \qquad (5.5)$$

where x stands for one ERS Scatterometer parameter (C', D', C^0_{dry} *and* C^S), A_i is the area occupied by one land cover class within a single pixel in percent, x_i is a linear regression coefficient and X_0 is an interception term. The basic assumption is that each of the 15 land cover types can be represented by a unique parameter value x_i. This is a strong simplification because areas assigned to one class can vary significantly in their characteristics (e.g. biomass). To make inference about

the significance of the 10 classes a one tailed *t*-test was performed. Table 5-5, presents the results of the *t*-test. Because D' *and* C^S show opposite trends then C' and C^0_{dry} they are multiplied by –1. This allows identifying land cover classes with common behaviour more easily.

Before reviewing the results, it should be noted that only general trends can be deduced from the obtained statistics. First we have to note that the C', D', C^0_{dry} and C^S are not normally distributed, a basic assumption of multiple regression analysis. Secondly, a simple residual analysis indicated that the linear model used to describe the multiple regression is insufficient to describe all aspects of the observed parameters. Nevertheless, the applied method can be used to study general trends.

TABLE 5-5-: Results of a multiple regression analysis between ERS Scatterometer derived parameters (C', D', C^0_{dry} and C^S), and the percentage area occupied by the dominating land cover types listed in the first column (only land cover types occupying more than 2% of the global land surface were used). A one tailed t-test was performed for each regression coefficient. The symbols + and – indicate that the t-test suggests that the given land cover type is significant for the explanation of the respective parameter at the α=0.01 level. The symbol + signifies positive correlation and the symbol – negative correlation.

Land Cover Type	**Total Area (%)**	C'	$-D'$	C^0_{dry}	$-C^S$
Deciduous Broadleaf Forest	4.3	+	+	+	+
Evergreen Broadleaf Forest	9.5	+	+	+	+
Evergreen Needleleaf Forest	3.7	+	+	+	+
Mixed Forest	5.9	+	+	+	-
Savanna	12.1	+	+	+	+
Shrubland	11.9	-	+	-	-
Cropland/Woodland Mosaic	5.4	+	-	+	+
Irrigated Cropland and Pasture	2.4	-	-	+	+
Dryland Cropland and Pasture	9.2	-	-	-	-
Cropland/Grassland Mosaic	3.4	-	-	-	-
Grassland	8.2	-	-	-	-
Wooded Tundra	4.9	-	-	-	-
Water Bodies	2.2	-	-	-	-
Barren or Sparsely Vegetated	11.3	-	-	-	-

Other than in a previous study (Wagner, 1998) where the impact of vegetation type on ERS Scatterometer derived parameters has been studied over Spain using the CORINE land cover

classification data set, all land cover types reveal a statistically significant trend at the α =0.01 level. Results of this analysis can be summarized as follows:

1. Although inland waters cover only 2.2 percent of the global land surface, they have a pronounced effect on the backscatter behaviour, D' and C^S increases and as expected C' and C^0_{dry} decreases.
2. Open spaces with little or no vegetation specified by land cover type "Barren or Sparsely Vegetated" tend to decrease C' and C^0_{dry}. This means that these surface types are typically smooth for C-band microwaves. As expected D' and C^S increase in the absence of vegetation.
3. Land cover classes that are characterised by translucent vegetation types such as dryland, cropland, grasslands and tundra exhibit a clear tendency to decrease C' and C^0_{dry} and to increase D' and C^S.
4. Non-transparent vegetation as represented by deciduous, evergreen and mixed forests increase C' and C^0_{dry} y and decrease D' and C^S.

Although the assumption that each land cover type can be represented by a single parameter value appeared to be strong between 58.9% and 66.9% of the variability of the backscatter parameters can be explained. The rest of the variability should be mainly due to in-class differences including surface roughness effects.

5.5 Derived Geophysical Parameters

Parameters derived from ERS Scatterometer time series are the degree of saturation, the Profile soil moisture content of the top one meter soil profile, volumetric soil moisture and freeze thaw information. In the following sections the retrieval of the parameters will be described and a few examples will illustrate the quality of the data. Table 5-6 summarizes the retrieved data.

TABLE 7-1: Summary of geophysical parameters derived from ERS scatterometer data.

Parameter	Symbol	Frequency	Resolution	Range	Commets
Degree of saturation	m_S	~ 3-4 days [1]	50 x 50 km²	0 - 100 %	Relative measure of surface soil moisture
Soil Water Index	*SWI*	7 days 10 days 1 month [2]	50 x 50 km²	0 - 100%	Relative measure of profile soil moisture
Volumetric Soil Moisture	*VSM*	7 days 10 days 1 month [2]	50 x 50 km²	0 – 50 Vol % [3]	Absolute measure of profile soil moisture
Freeze Thaw	-	~ 3-4 days [1]	50 x 50 km²	0/1	Indicator if soil is frozen snow covered or thawed

[1] The Frequency depends on the available sattelite data over a respective region. 3-4 days is an average value.

[2] any timestep is possible but 7 days is recommended as minimum time step.

[3] the upper limit is based on experience, higher values are possible.

5.5.1 Surface Soil Moisture

The retrieval algorithm is in principle a simple change detection method where the instantaneous backscattering coefficient is compared to the lowest and highest measurements recorded. Assuming a linear relationship between $\sigma^0(40)$ and the soil moisture content a relative measure of soil wetness in the surface layer, m_s, is obtained, ranging between 0 and 1 (0 % to 100 %). It represents an average value over all bare ground surfaces and areas covered by translucent vegetation types such as grassland or agricultural land within the resolution cell. The retrieved information has a physical meaning if σ^0_{dry} and σ^0_{wet} represent their respective wetness values. If σ^0_{dry} represents a completely dry soil surface and σ^0_{wet} a saturated soil surface then m_s is equal to the degree of saturation which is the soil moisture content expressed in percent of porosity (also called total water holding capacity). Qualitative comparison with rainfall and temperature data indicates a good quality of the remotely sensed surface soil moisture estimates. Unfortunately, quantitative validation using field measurements appear hardly feasible because of the high degree of the land-surface related variability of the surface soil moisture content over small

distances and because of the high costs of field surveys. Figure 5-36 to Figure 5-39 show m_S time series for the main climatic regimes defined by Koeppen together with basic meteorological variables and are summarized in the following paragraphs.

Generally, the qualitative comparison with meteorological observations and auxiliary information indicates a good quality of the remotely sensed surface wetness values. The degree of saturation as observed with the scatterometer correlates well with precipitation records. High m_S values are associated with rainfall events and low m_S values occur after some time without rain or during frost periods. Unfortunately, the temporal sampling rate of the ERS Scatterometer is not high enough to detect every rainfall event especially in dry climates when evaporation rates are high and precipitation is low. Rainfall followed by a dry period, results in a quasi-exponential decrease. This behaviour can be explained by the redistribution of the water in the wetted surface layer into the relatively dry deeper layers (Hillel, 1980) and is characteristic for soil moisture records of the topsoil layer.

5.5.1.1 Tropical Climate

Tropical moist climates extend northward and southward from the equator to about 15 to 25 degrees of latitude. In these climates, all months have average temperatures greater than 18 degrees Celsius and annual precipitation is greater than 1500 mm. Figure 5-36 shows time series of the synoptic stations Boa Vista in Guyana and Jagdalpur in India. According to Koeppen, both stations are within the tropical wet and dry (savanna) subclass. This class is characterised by an extended dry season during winter. Precipitation during the wet season is usually less than 1000 millimetres, during winter precipitation records are rare. The degree of saturation generally follows the climatic trends with high values during the wet season and low values during winter. Single rainfall events are evident in the data independent of the season. However, for both stations higher soil moisture values persist into the dry season. Possible explanation are shadowing effects of vegetation that keeps the surface moist, or an improper representation of vegetation cover. Nevertheless the latter effect is deemed moderate, and it can be concluded that the applied method correctly capture soil moisture conditions.

5.5.1.2 Temperate Climate

This climate generally has warm and humid summers with mild winters. Its extent is from 30 to 50 degrees of latitude mainly on the eastern and western borders of most continents. During the winter, the main weather feature is the mid-latitude cyclone. Convective thunderstorms dominate summer months. Figure 5-37 shows data of the synoptic stations Bethal in South Africa

belonging to the meditaraneen subclass. These regions receive rain primarily during winter season from the mid-latitude cyclone. Extreme summer aridity is caused by the sinking air of the subtropical highs and may exist for up to 5 months. In the m_S series the extreme summer aridity is well reflected with values below 10%. The degree of saturation reaches maximum values only during winter when enough rain falls. The synoptic station of Raileigh-Durham in the US belongs to the humid subtropical subclass with hot muggy summers and frequent thunderstorms. Winters are mild and precipitation during this season comes from mid-latitude cyclones. Because of frequent rainfall consistently observed over the year the degree of staturation seldomly reaches minimum values as evident for the Bethal series. Nevertheless, a clear seasonal trend is evident in the series with higher soil moisture conditions during summer than during winter

5.5.1.3 Dry Climate

Figure 5-38 shows data for the Dry climate regime. The most obvious climatic feature of this climate is that potential evaporation and transpiration exceed precipitation. This climate type extends from 20 - 35 degrees North and South of the equator and is in large continental regions of the mid-latitudes often surrounded by mountains. Series of the station Yelimane in Mali are representative for a dry semiarid steppe climate characterised by grassland, receiving precipitation from the intertropical convergence zone. During the dry season the ERS Scatterometer retrieved soil moisture values correctly depict the dry soil conditions. A remarkable feature during the dry season 19996/97 is the rainfall event in May evident in both the m_S and the rainfall series. The ERS Scatterometer does not observe some of the initial rainfall events at the beginning of the wet season because the sampling interval is longer than the persistence of these localised and singular showers at the soil surface. Only when rainfall becomes more frequent a lasting increase of the m_S values can be observed.

The synoptic station of Burdylak represents dry arid conditions as encountered in cold deserts. Rainfall never reaches values high enough to cause a lasting increase in soil moisture. Nevertheless, single rainfall events are evident in both m_S and precipitation series. It can be argued that the magnitude of these events observed in the m_S series is to high compared to other climates. Nevertheless, the trend is well reflected and if adequate soil moisture information is available these values can be better calibrated.

5.5.1.4 Cold Climate

Figure 5-39 shows data for cold climates characterised by warm to cool summers and cold winters. The location of these climates is pole ward of the temperate climates. The average

temperature of the warmest month is greater than 10 degrees Celsius, while the coldest month is less than -30 degrees Celsius. Winters are severe with snowstorms and strong cold winds from Continental Polar or Arctic air masses. For the station Karymskaya in Russia the typical phenology of m_S for these climates can be observed. During winter when soil freezes often for a few decimetres the scatterometer observes dry conditions. This is consistent with theory as in frozen soils the open water content is reduced to a minimum value. During spring when snow melts soils become wet. For Karymskaya this results in intermediate soil moisture conditions. Only when the first rainfalls are recorded during summer maximum values are observed in the m_S series. A similar phenology is observed in the data of the synoptic station of Norman Wells in Canada. However contrary to the general conditions represented by the Russian series and increase in backscatter is observed during winter. Scipal (1998) argued that this increase can be caused by special strartigraphic feature of lake ice. However an exact assessment of the reason has to remain open.

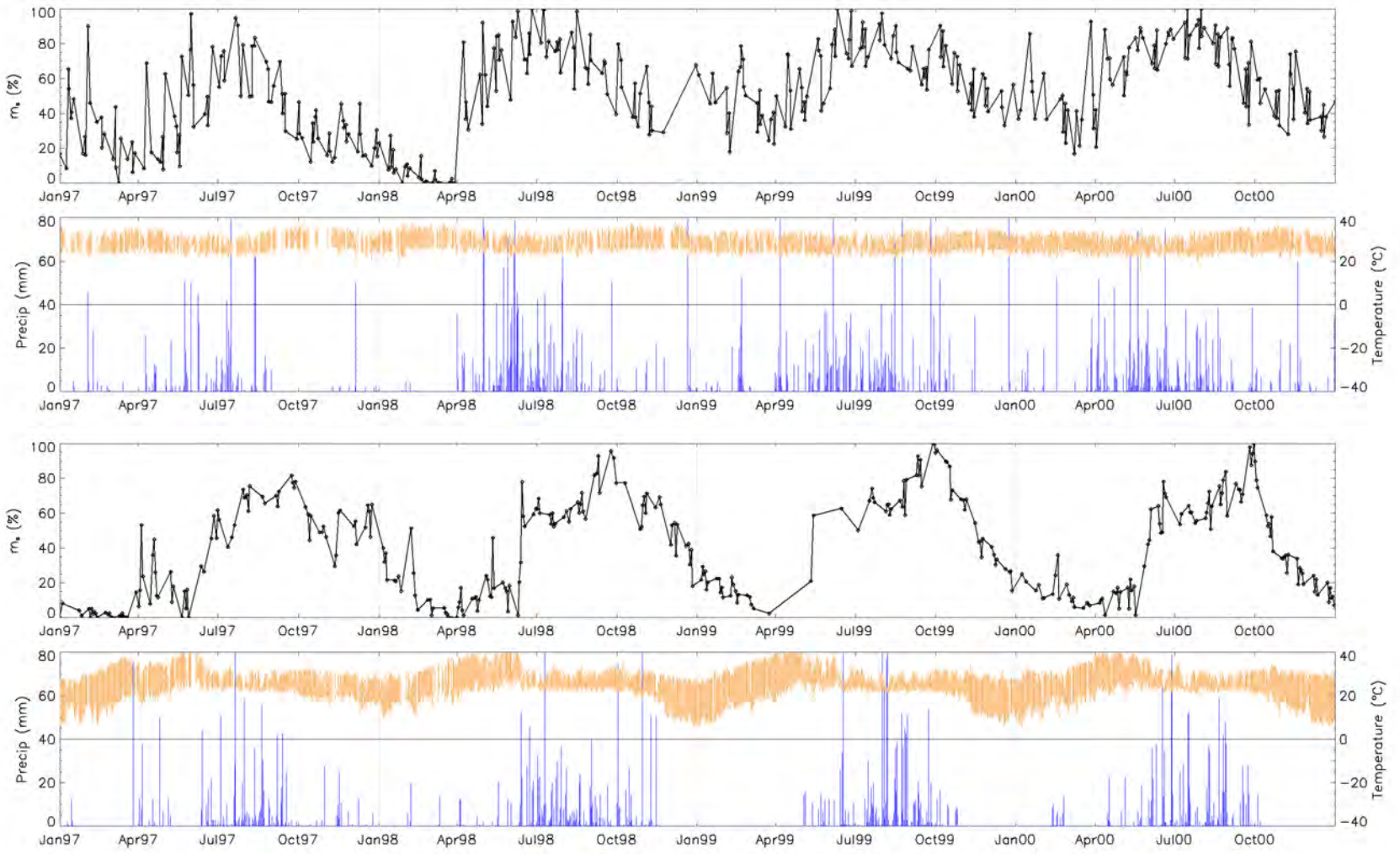

Figure 5-36: Degree of saturation of the top soil layer m_S *and meteorological records (rainfall, maximum and minimum temperature) for a Tropical Climate. Top: Boa Vista - Guyana (60.7°W, 2.9°N); Bottom: Jagdalpur - India (81.9°E, 19.1°N)*

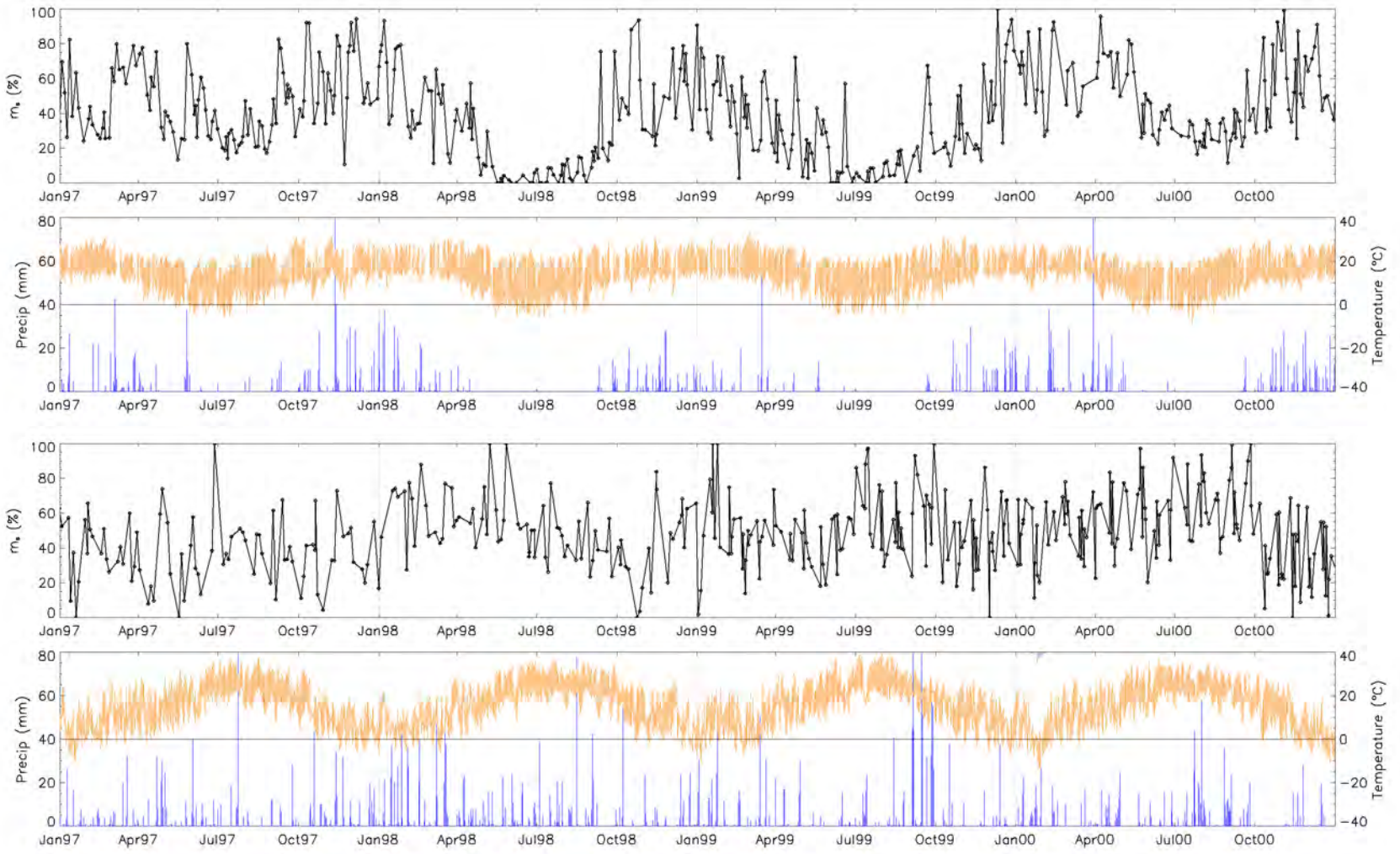

Figure 5-37: Degree of saturation of the top soil layer m_S *and meteorological records (rainfall, maximum and minimum temperature) for a Temperate Climate. Top: Bethal – South Africa (29.4°W, 26.4°S); Bottom: Raleigh-Durham - USA (78.9°W, 35.9°N)*

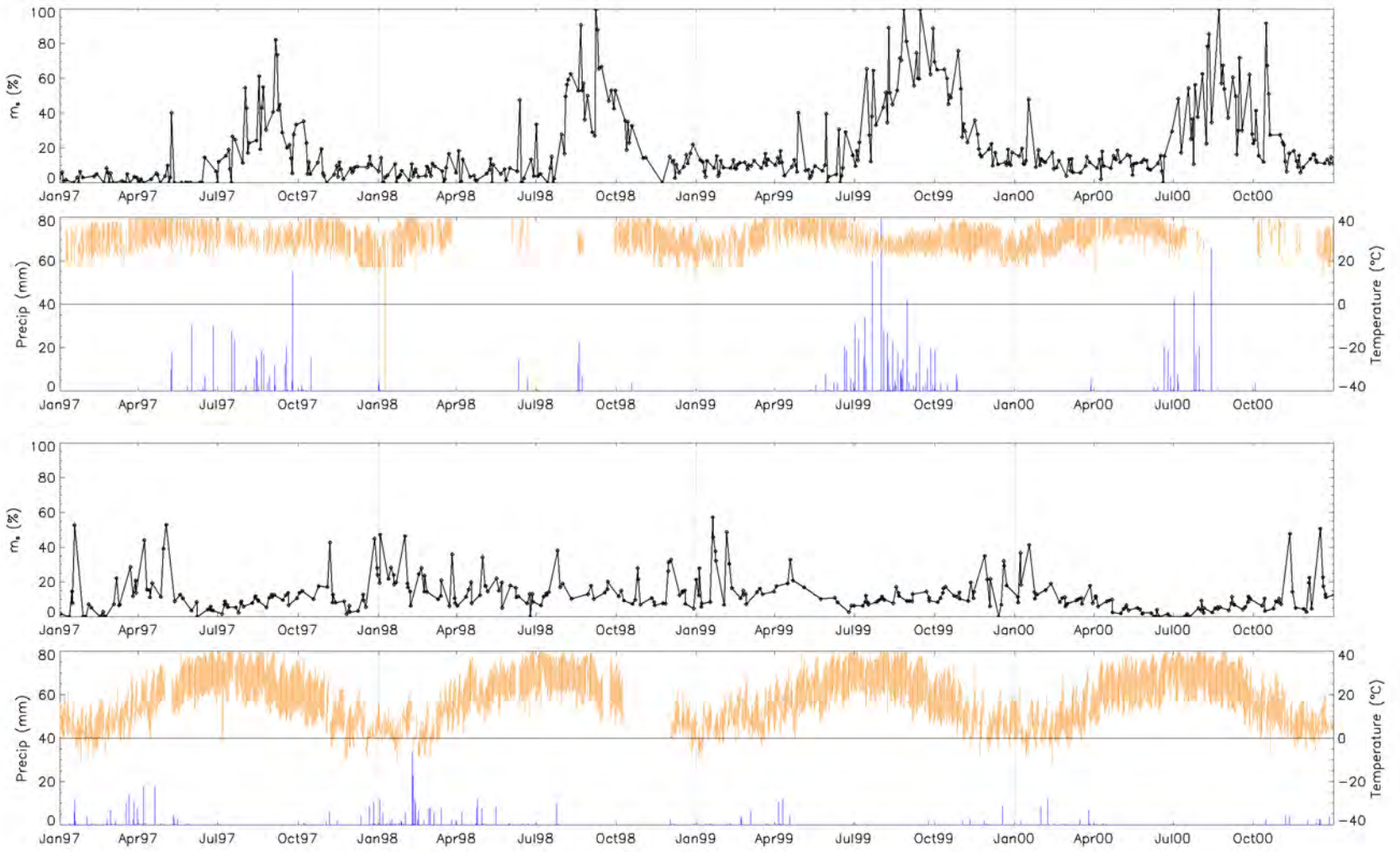

Figure 5-38: Degree of saturation of the top soil layer m_S *and meteorological records (rainfall, maximum and minimum temperature) for a Dry Climate. Top Yelimane - Mali (10.5°W, 15.1°N); Bottom: Burdylak – Turkmenistan (64.3°E, 38.4°N)*

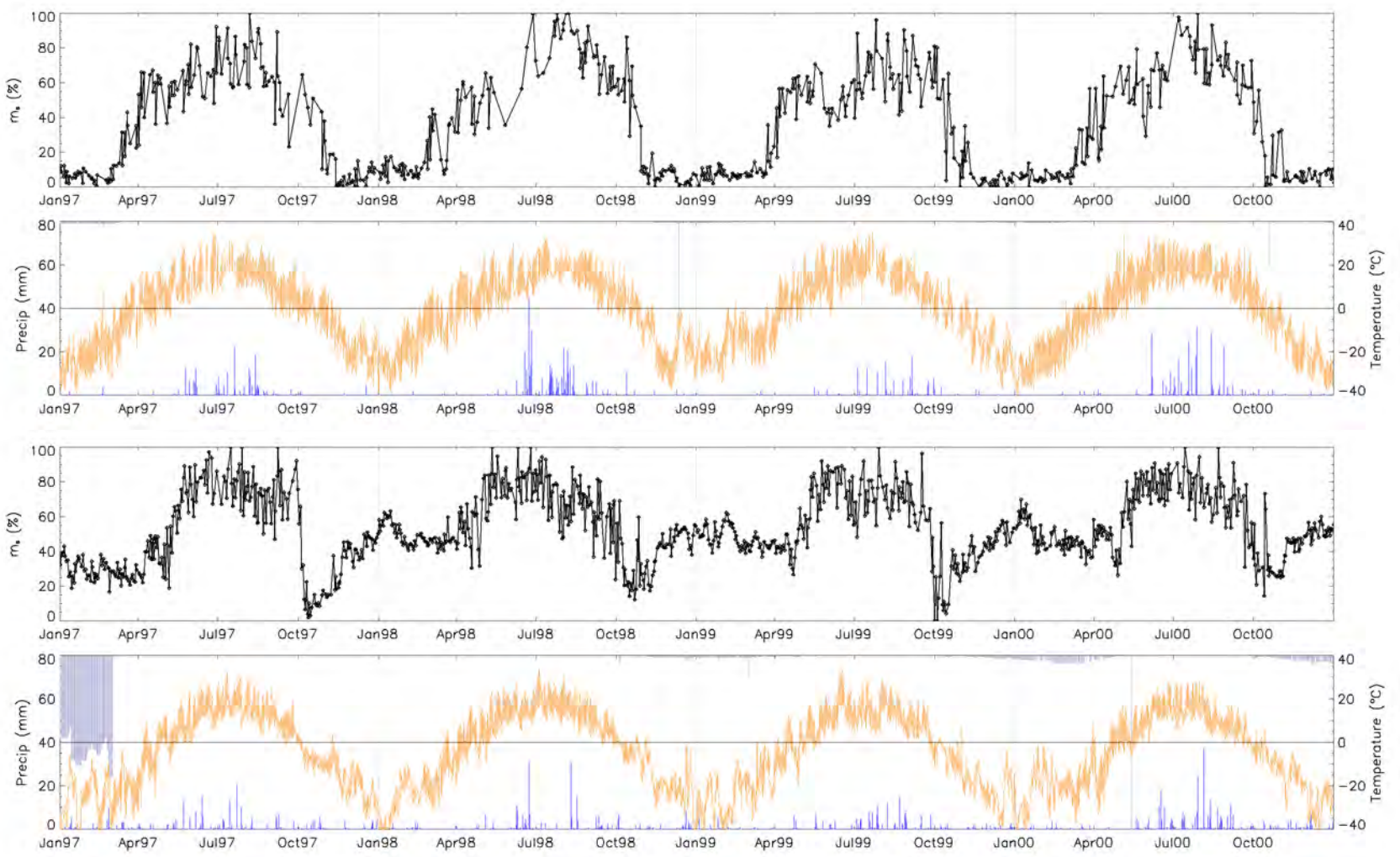

Figure 5-39: Degree of saturation of the top soil layer m_S *and meteorological records (rainfall, maximum and minimum temperature and snow depth) for a Cold Climate. Top: Karymskaya - Russia (114.5°E, 51.6°N); Bottom: Norman Wells - Canada (-126.9°E, 65.4°N)*

5.5.2 Freeze/Thawing

At microwave frequencies, freezing results in a strong decrease of the dielectric constant of soil and vegetation, which significantly alters their radar scattering properties. Therefore, it is not only possible to retrieve soil moisture information from scatterometer data but also information on the frost conditions of the land surface. Information on frost conditions is important in a number of scientific applications. Freeze/thaw cycles play a major role in high latitude terrestrial ecosystems. Freezing and frost drought result in potential damage to living plants and have a profound effect on the natural distribution of vegetation types and on their proliferation (Burke et al., 1976). Freezing and thawing also produce large changes in the heat balance between land and atmosphere during spring break up and fall freeze up, and dissipate more than half the annual heat balance in the arctic (Weller and Holmgren, 1974). More importantly, annual freeze/thaw cycles determine the length of the growing season for vegetation (Larcher, 1980). Knowing the length of the growing season is important for estimating annual productivity in boreal forests and in tundra, and for understanding biogeochemical seasonal and interannual cycles such as the exchange of atmospheric CO_2 with the northern high latitude terrestrial biosphere (Houghton, 1987; Sundquist, 1993; Tans et al., 1990; Waring et al., 1993).

Previous research has investigated the relationship between freeze/thaw state of snow and other materials and microwave backscatter. In general, it has been observed that transitions from a frozen to an unfrozen state, and vice versa, correspond to a shift in backscatter response. The magnitude and direction, positive or negative, of the backscatter shifts varies with the surface properties. Several authors have investigated the potential of simple change detection algorithms to detect frost conditions. Wismann (2000) investigated the capability of the ERS Scatterometer for detecting thawing of soil and vegetation in Siberia. A simple change detection method produced satisfactory results which were consistent with air temperature observations and SSM/I derived snow cover maps. Scipal (1999) investigated methods to detect freezing and thawing in Northern Canada. It was observed that the backscatter signal is not stable during winter for arctic regions characterised by myriads of small lakes. Over these regions, an increase in backscatter during winter was observed (see Figure 5-39) which required a more complex decision tree to detect frost conditions. Both studies concluded that retrieval of freeze thaw cycles from ERS scatterometer data is possible. However, these studies were limited to the high northern latitudes characterised by extreme winters. In Scipal (1999) it has been argued that only under such conditions proper detection of freeze thaw cycles is possible. In lower latitudes the estimates become questionable.

To detect freezing and thawing dates in this study m_S time series have been searched for distinct temporal patterns. To limit the search to the cold season and avoid misinterpretations mean climatic variables described in Chapter 4.4, have been used to get an initial estimate of the start and end dates of the frost season. Within a 3 month period of these estimates m_S time series have been searched for indicators of frost. The method is based on the observation that at the beginning of the frost period the degree of saturation is decreasing as soil freezes and is constantly low for frozen soils. Thawing is indicated by an increase in backscatter to very high values. After the onset of thawing the degree of saturation decreases as the melting water percolates into deeper layers or dry up by evaporation.

The starting point of the frost period was determined if following conditions were met:

1. Degree of saturation of instantaneous m_S less than 50%
2. Degree of saturation of two 7 day average m_S values before are above the instantaneous value
3. The absolute difference between instantaneous and following m_S is less than 20%.

Thawing was determined if:

1. Degree of saturation of instantaneous m_S above 50%
2. The following two 7 day average m_S values are below the instantaneous m_S value
3. The absolute difference between instantaneous and the m_S value before is less than 20%.

This method does not account for thawing and refreezing events during the cold period nor does it correctly capture an increase in backscatter during winter as observed in the Arctic regimes of Canada (Figure 5-39). Therefore, if the estimated freezing and thawing differed more than 6 weeks to the estimates of the mean climatic data they were rejected and the mean climatic estimates were used instead. Principally all measurements acquired between the estimated freezing and thawing date were marked as frozen/snow covered. Hence, the estimated freezing and thawing dates are rather conservative. However, the main concern of this study is to monitor soil moisture and it is more relevant to exclude frozen or snow covered soils from the soil moisture retrieval than to capture this geophysical process exactly, justifying this approach is.

5.5.3 Soil Water Index

Remote sensing by nature only provides information of the top soil layer. However often information on the soil moisture content of the soil profile up to a certain depth is required. To retrieve an estimate of the soil moisture content of the soil profile a simple two layer water balance model is applied. In the model, the water content in the surface layer is highly dynamic due to various processes such as precipitation, evaporation and surface runoff. The water content in the reservoir varies only slowly because its rate of change is limited by the amount of water that can be exchanged with the surface layer and is fully explained by the past dynamics of the surface soil moisture content. The conversion of the topsoil moisture content to the moisture content of the reservoir in this model can mathematically be described according to

$$SWI(t) = \frac{1}{T} \int_{-\infty}^{t} m_S(t') e^{-\frac{t-t'}{T}} dt' \qquad (5.6)$$

Where *SWI(t)* is the soil moisture content in the profile, $m_s(t)$ the surface soil moisture and *T* is a characteristic time variable increasing with depth of the soil layer and decreasing with the pseudo-diffusivity constant *C*, which depends on soil properties. *T*, set to 20 days, has been estimated empirically by maximizing the correlation between modeled data and *in-situ* data over the Ukraine (Wagner, 1998).

The discrete formulation of equation (5.6) is given in Table 5.2. *SWI(t)* has been calculated if at least four m_S value have been recorded in the period *T* (20 days) before the instantaneous measurement. The resulting parameter *SWI(t)* is the soil moisture content of the sub layer at time *t*. Like m_s, the moisture content in the subsurface layer derived according to the described model is only a trend indicator. Although the model is quite simple, assuming a standardized soil neglecting different climatic condition throughout the year the retrieved information is generally in good agreement with general climate regimes and comparable data such as gridded precipitation data. Chapter 6 and Chapter 7 are dedicated to a detailed analysis of the retrieved information. In the following general characteristics of the *SWI* will be discussed qualitatively. First, a review of continental climate patterns will be given followed of mean *SWI* maps for the respective continents. Information on general continental climate properties are taken from the online versions of the Encyclopaedia Britannica[4] and the World Book[5]. The *SWI* is calculated for

[4] http://www.britannica.com

the last day of each month and is averaged over the period 1992-2000, hence reflecting the mean annual cycle of soil moisture. Generally, the *SWI* depicts climatic conditions very well. Especially over the tropics characterised by the movement of the Intertropical Convergence Zone *SWI* maps compare favourable with the observed climatic cycles. The absolute value of the *SWI* might in some regions over or underestimate real conditions. Spatial patterns can therefore be inconsistent. Nevertheless, temporal variations are well reflected throughout the globe.

5.5.3.1 Africa

Most of Africa has a warm or hot climate, but the humidity and amount of rainfall vary dramatically from area to area. Africa has the largest tropical area of any continent. The equator runs through the middle of Africa, and about 90 per cent of the continent lies within the tropics. Temperatures are high the year around almost everywhere in Africa. The variations between summer and winter temperatures are slight. Africa's highest temperatures occur in the Sahara and in parts of Somalia. The coolest regions in Africa are the northwest, the highland areas of the east, and parts of the south. Frost and snowfall are common in the mountains of Africa. Rainfall is distributed very unevenly in Africa. Most areas receive either too much rain or too little. In parts of the west coast, for example, annual rainfall averages more than 250 centimetres. In contrast, more than half of Africa receives less than 50 centimetres of rainfall yearly. In parts of the deserts, rain may not fall for six or seven years in a row. Rain falls the year around in the forests of the Congo Basin and the coastal regions of western Africa. Almost all the rest of Africa has one or two seasons of heavy rainfall separated by dry periods driven by the movement of the Intertropical Convergence Zone. In some regions of Africa, the amount of rainfall varies sharply from year to year rather than from season to season.

Generally, it can be found that the *SWI* agrees well with climatic characteristics (Figure 5-40). Large-scale feature such as the movement of the Inter Tropical Convergence zone are well depicted in the maps. In addition, regional features such as the east Madagascan coast or the Ethiopian Highlands, being wetter then the surrounding areas are well depicted in the data. Even local features such as the Niger Delta in Mali being flooded every year and therefore staying longer wet then the surrounding areas are well reflected.

[5] http://www.worldbookonline.com

5.5.3.2 Asia

Because of Asia's tremendous size, its regions have a wide variety of climates. These varied climates include the polar north; the hot, dry desert environment of the center and southwest; and the hot, humid conditions of the tropical south. Winds called monsoons influence the climate of much of Asia. In winter, monsoons from the north move into East Asia and cause cold, dry weather. The wind switches in summer and blows from the seas that lie south and southeast of that region. It causes hot, humid weather. Monsoons from the northeast pass through South Asia and Southeast Asia from November to March. They cause the coolest weather in those two regions. From May to October, wet monsoons bring heavy rains from the south seas. Many of these monsoons cause floods. In Southwest Asia, monsoons affect only the southern and southwestern coasts of the Arabian Peninsula. Most of Southwest Asia has long, hot summers and mild winters. The region's heaviest rains fall in Turkey near the Black Sea and in the Caucasus region between the Black and Caspian seas. Some parts of the Arabian Peninsula receive no rain for several years at a time.

The *SWI* correctly depicts these conditions (Figure 5-41). East Asia is dry during the winter month and starts weeting up in March/April reaching a maximum during summer. Along the lower course of the Yangtze, unnatural dry spells can be observed during the summer months. Paddy rice fields frequently found in this region might cause these phenomena. In chapter 5.5.5.2 these phenomena will be discussed in more detailed. On the Indian subcontinent wetting up of soils is observed to start in June. Most parts of the Arabian Peninsula stay dry throughout the year. Central Asia and the Northern parts of the continent are characterised by the long cold winters. The movement of the cold front is correctly depicted in the data. After snow melt when soils are saturated with melting water the *SWI* reaches high values. During spring *SWI* decreases again but stays at mdium level. During this period, *SWI* might overestimate actual conditions.

5.5.3.3 Europe

Europe has a variety of climates, but most of the continent has mild weather. Europe's mild climate is caused by winds that blow across the continent from the Atlantic Ocean. In general, northern Europe has longer, colder winters and shorter, cooler summers than southern Europe. In addition, winters are longer and colder, and summers shorter and hotter, in the east than in the west. Most of Europe receives from 50 to 150 centimetres of precipitation each year. The greatest annual precipitation usually more than 200 centimetres occurs in areas just west of mountains. Such regions include parts of western Britain and western Norway. The continent's lightest annual precipitation usually less than 50 centimetres occurs in three general areas: (1) east

of high mountains, (2) far inland from the Atlantic Ocean, and (3) along the Arctic coast. Such regions include central and south-eastern Spain, northern Scandinavia, northern and south-eastern parts of European Russia, and western Kazakhstan.

Generally, the *SWI* depicts a clear seasonal trend over Europe (Figure 5-42). During winter most of the continent is wet during summer *SWI* reaches minimum values. Only over mountainous regions such as the Alps higher values can be observed. The south east of the continent is dry throughout the year, with higher values only observed during November to January.

5.5.3.4 North America

North America is the only continent that has every kind of climate, from the dry, cold of the Arctic to the steamy heat of the tropics. An icecap permanently covers the interior of Greenland, where the temperature almost never rises above freezing. In the North American tundra, the vast treeless plain of the far north, the temperature rises above freezing for only a short period each summer. In the low-lying areas of the far south, it is hot and rainy all the time. Most of the rest of North America is cold in the winter and warm in the summer, with moderate precipitation. Some areas have mild winters and long, hot summers. Other areas have harsh winters and short summers.

The general climatic regimes defined in Koeppen are well reflected in the *SWI* maps (Figure 5-43). In the southeast, defined as temperate climate soils generally stay wet and low levels of *SWI* are only reached during winter. The western interior of the United States and much of northern Mexico is characterised by mountains and deserts and generally receives small amounts of precipitation. In addition, the *SWI* is characterised by low values throughout the year. The Arctic, which receives relatively little precipitation, has generally high *SWI* values possibly influenced by melting water of the snow.

5.5.3.5 South America

South America has a wide variety of climates. They range from the dry desert conditions of northern Chile to the heavy rains along the windswept southwestern coast of the continent. Most of the continent receives ample rain. The Atacama Desert in northern Chile is one of the driest places on earth. In general, however, most of the continent has warm weather the year around. Rainfall is highest for the Northern coastal regions of the continent. However, even the wettest regions of the continent generally have a dry season. In southwestern Chile, humid westerly winds blow in from the Pacific and drop most of their moisture as rain before crossing the Andes.

As a result, the area east of the Andes is very dry. Coastal Peru and northern Chile are among the driest places on earth.

Over South America *SWI* depicts spatial patterns very well (Figure 5-44). For example, the plateaus of Patagonia, in southeastern Argentina receiving only about 25 centimetres of rain a year, are eminent dry regions in the *SWI* maps. In addition, the dry east of the Andes is well reflected in the data. Over the central parts of the continent, the *SWI* follows the movement of the Intertropical convergence zone.

5.5.3.6 Australia

In general, Australia has a warm, dry climate. However, the climate differs from one part of the country to another. The northern third of Australia lies in the tropics and so is warm or hot the year around. The rest of the country lies south of the tropics and has warm summers and mild or cool winters. About a third of the country is desert and receives less than 25 centimetres of rain a year. Much of the rest of Australia has less than 50 centimetres of rainfall annually. The heaviest rainfall occurs along the north, east, southeast, and extreme southwest coasts. The east coast of Queensland is the wettest part of the continent. Floods plague many parts of Australia during the wet season. However, droughts are usually a far more serious problem.

Generally, the *SWI* over Australia is low well reflecting the dry conditions encountered in the continent (Figure 5-45). Over northern Australia, belonging to tropical climate with distinct season, *SWI* depicts the wet and dry season very well. The wet season corresponds lasts from November through April, the dry season lasts from May through October.

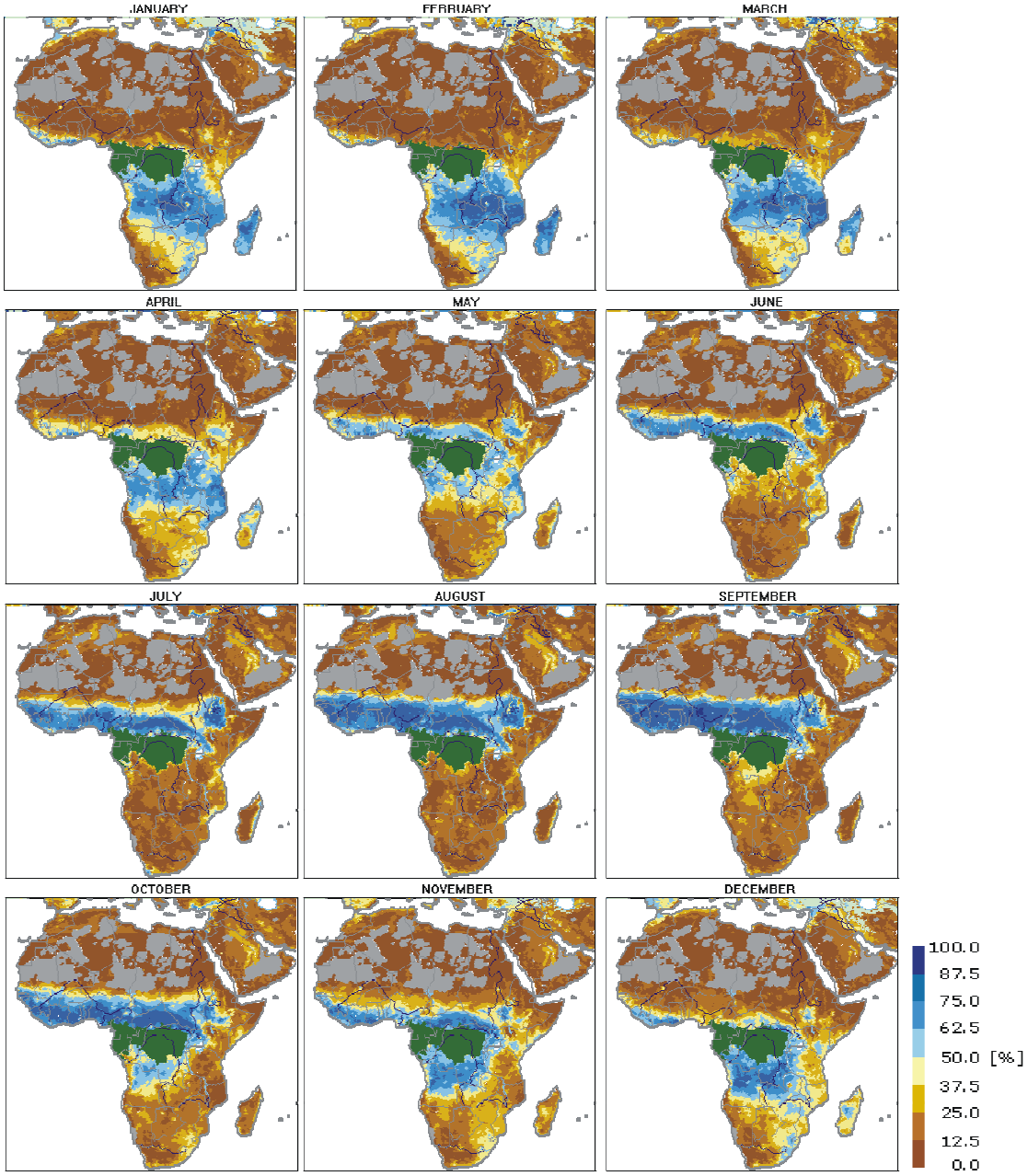

Figure 5-40: Mean SWI for Africa, calculated from monthly SWI values observed over the period 1992-2000. Brown colour tones indicate dry conditions, blue colour tones indicate wet conditions. Tropical forest are masked with green, areas of high azimuthal anisotropy with grey.

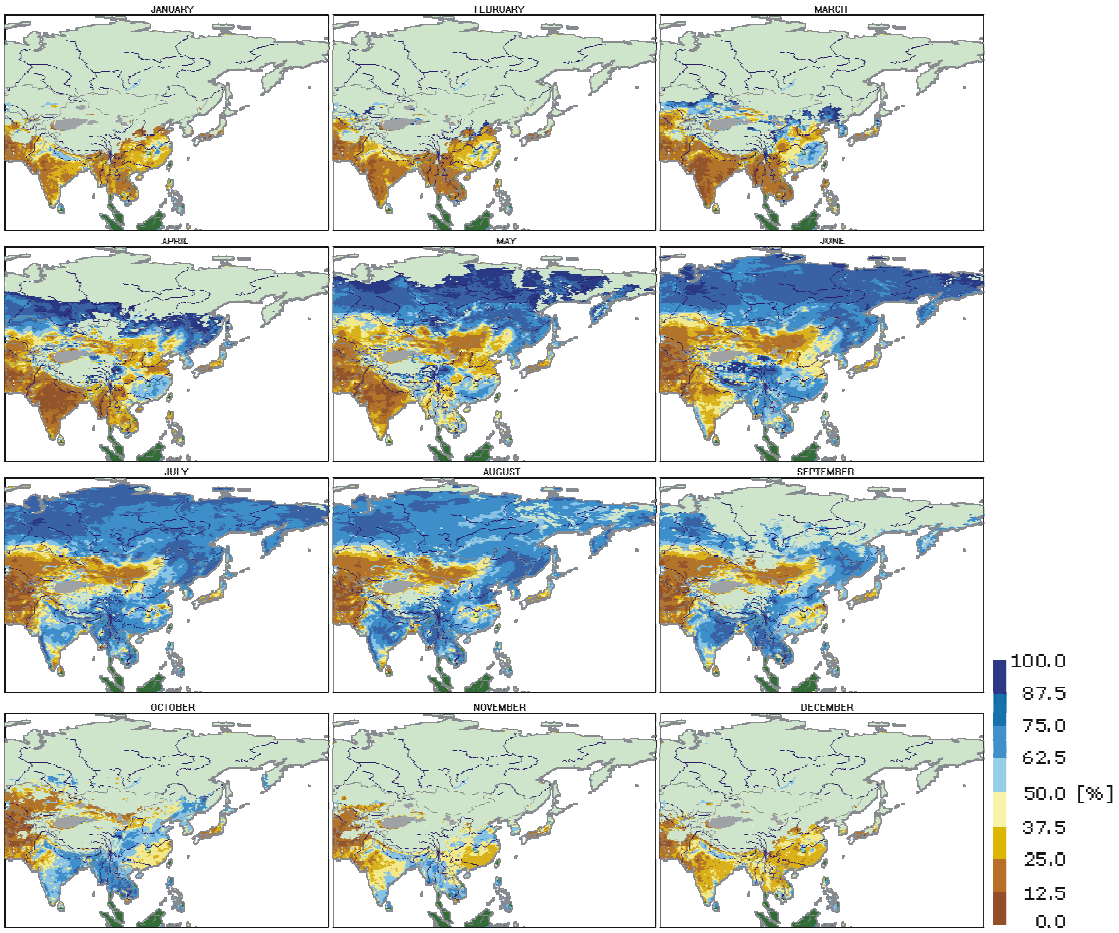

Figure 5-41: Mean SWI for Asia, calculated from monthly SWI values observed over the period 1992-2000. Brown colour tones indicate dry conditions, blue colour tones indicate wet conditions. Tropical forest are masked with green, areas of high azimuthal anisotropy with grey.

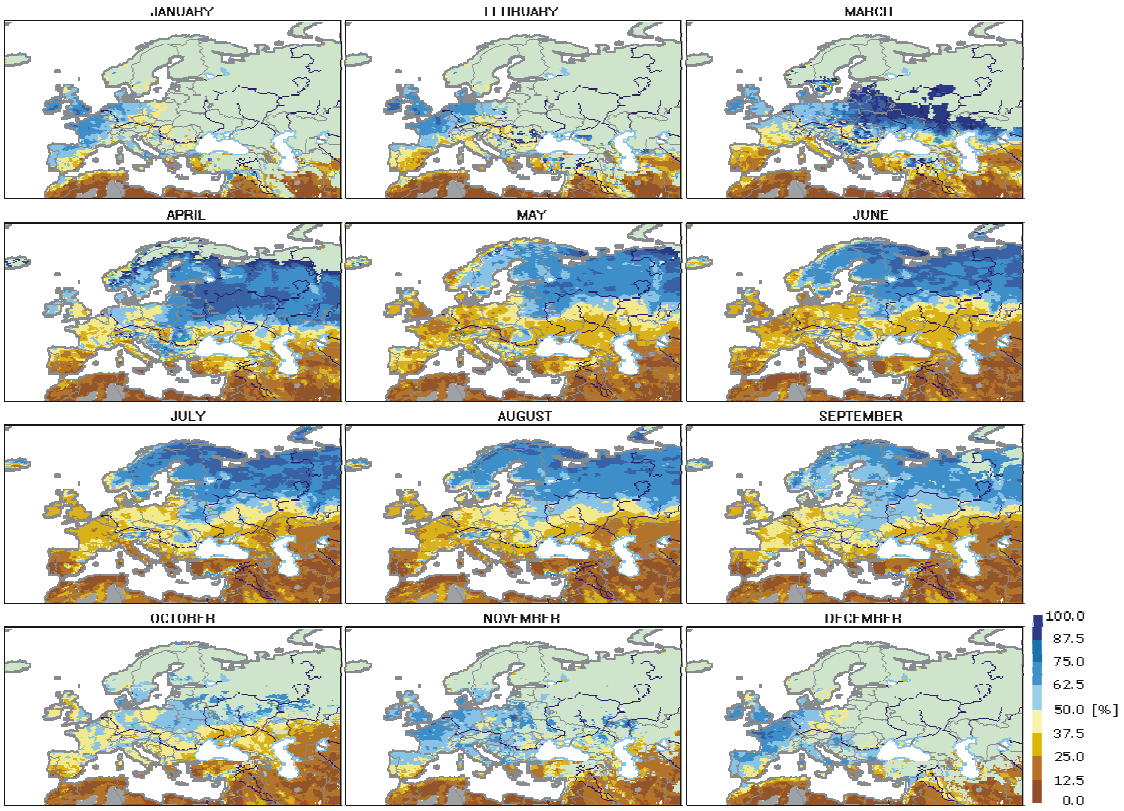

Figure 5-42: Mean SWI for Europe, calculated from monthly SWI values observed over the period 1992-2000. Brown colour tones indicate dry conditions, blue colour tones indicate wet conditions. Tropical forest are masked with green, areas of high azimuthal anisotropy with grey. Snow and Ice is indicated by light green

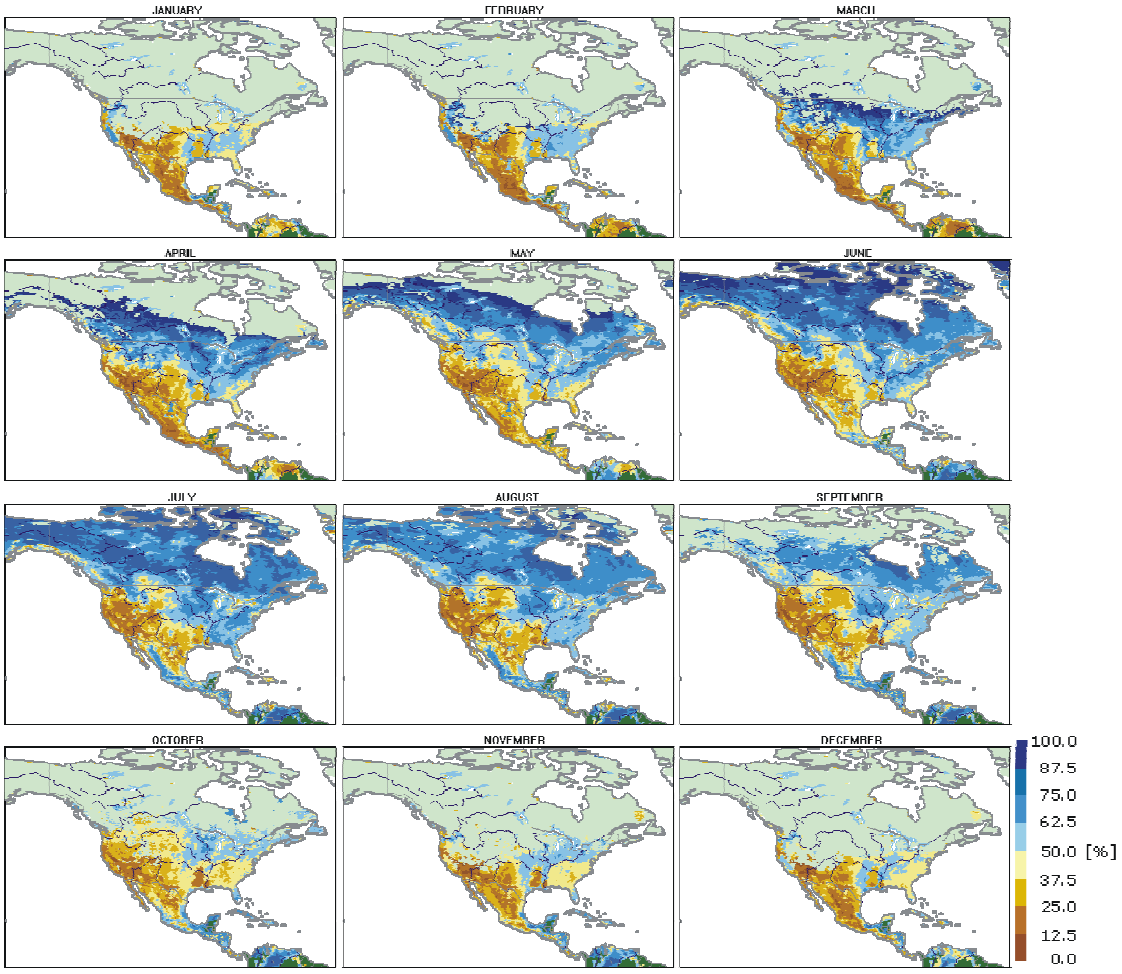

Figure 5-43: Mean SWI for North America, calculated from monthly SWI values observed over the period 1992-2000. Brown colour tones indicate dry conditions, blue colour tones indicate wet conditions. Tropical forest are masked with green, areas of high azimuthal anisotropy with grey. Snow and Ice is indicated by light green

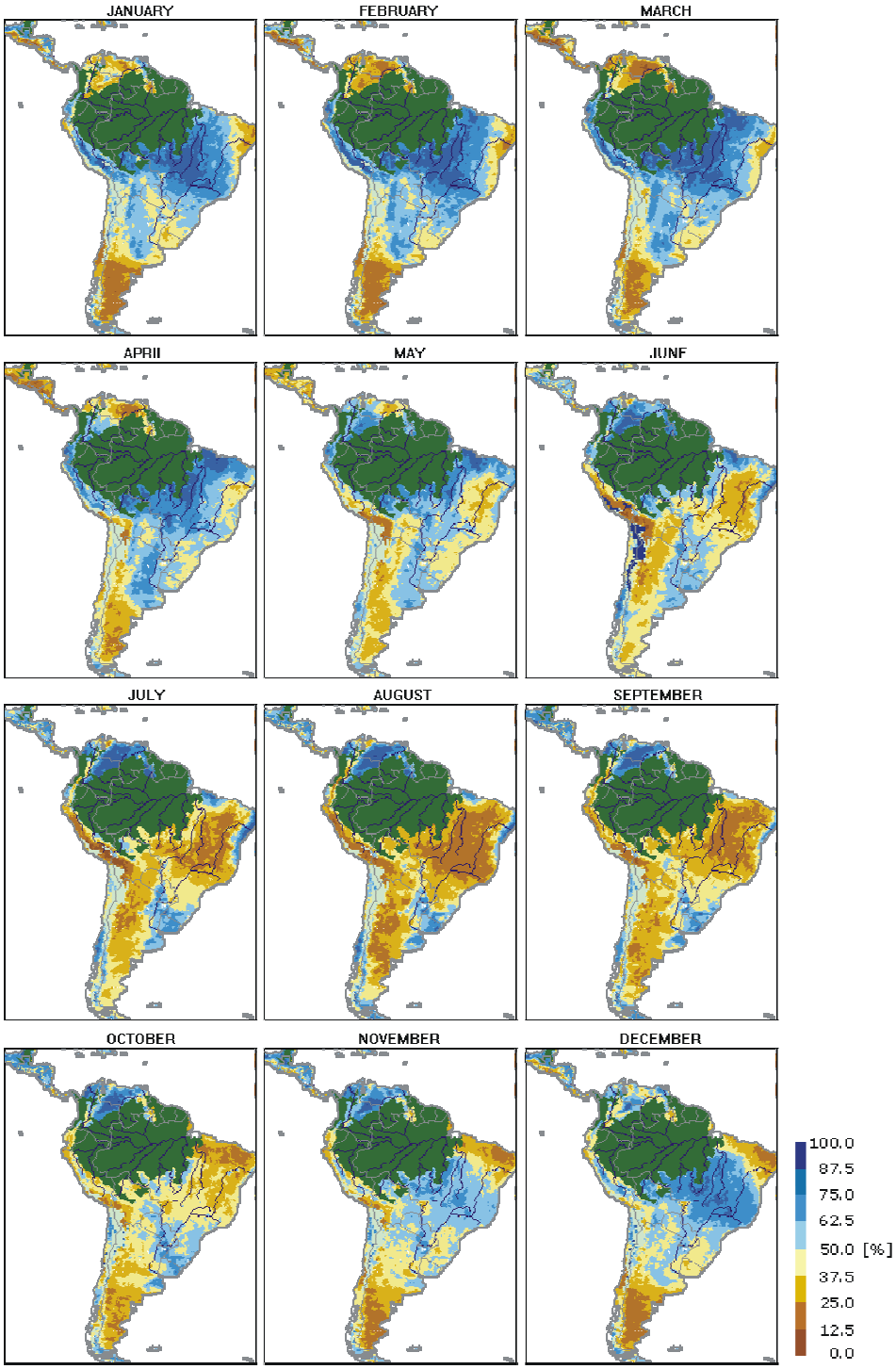

Figure 5-44: Mean SWI for South America, calculated from monthly SWI values observed over the period 1992-2000. Brown colour tones indicate dry conditions, blue colour tones indicate wet conditions. Tropical forest are masked with green, areas of high azimuthal anisotropy with grey. Snow and Ice is indicated by light green

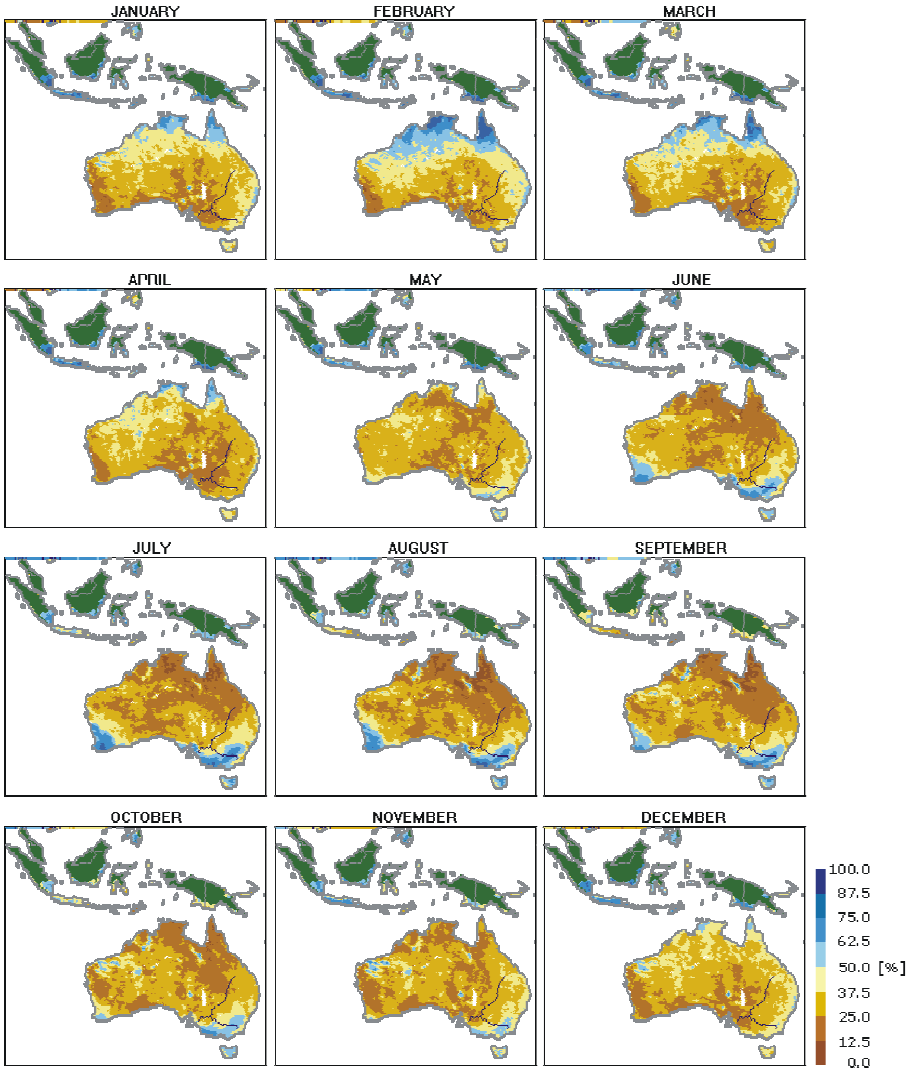

Figure 5-45: Mean SWI for Australia, calculated from monthly SWI values observed over the period 1992-2000. Brown colour tones indicate dry conditions, blue colour tones indicate wet conditions. Tropical forest are masked with green, areas of high azimuthal anisotropy with grey. Snow and Ice is indicated by light green

5.5.4 Volumetric Soil Moisture

The Soil Water Index *SWI* is a trend indicator ranging between 0 and 1. For estimating the water in deeper layers auxiliary information about the soil physical properties is needed. The idea is to define calibration points for dry and wet conditions. If W_{min} and W_{max} are the minimum and maximum soil wetness values that can occur in a particular soil and assuming further a linear relationship, the profile soil moisture content W at the time t may be estimated from *SWI* according to:

$$W(t) = W_{\min} + SWI(t) \cdot (W_{\max} - W_{\min}) \tag{5.7}$$

The soil parameters commonly used to define critical soil moisture values are the wilting level *WL*, the field capacity *FC*, and the total water capacity *TWC*. Over the Ukraine it was found that the water content of the soil profile can be estimated using *WL*, *FC* and *TWC* as calibration points and apply following formula

$$W(t) = WL + SWI(t) \cdot \left(\frac{FC + TWC}{2} - WL \right) \tag{5.8}$$

In Figure 5-46 it can be observed how calibration with soil properties influence the spatial patterns of soil moisture. For example in the southern African region, higher inland values are damped during November and values are left high only at the coast, giving a more realistic view of absolute soil moisture conditions.

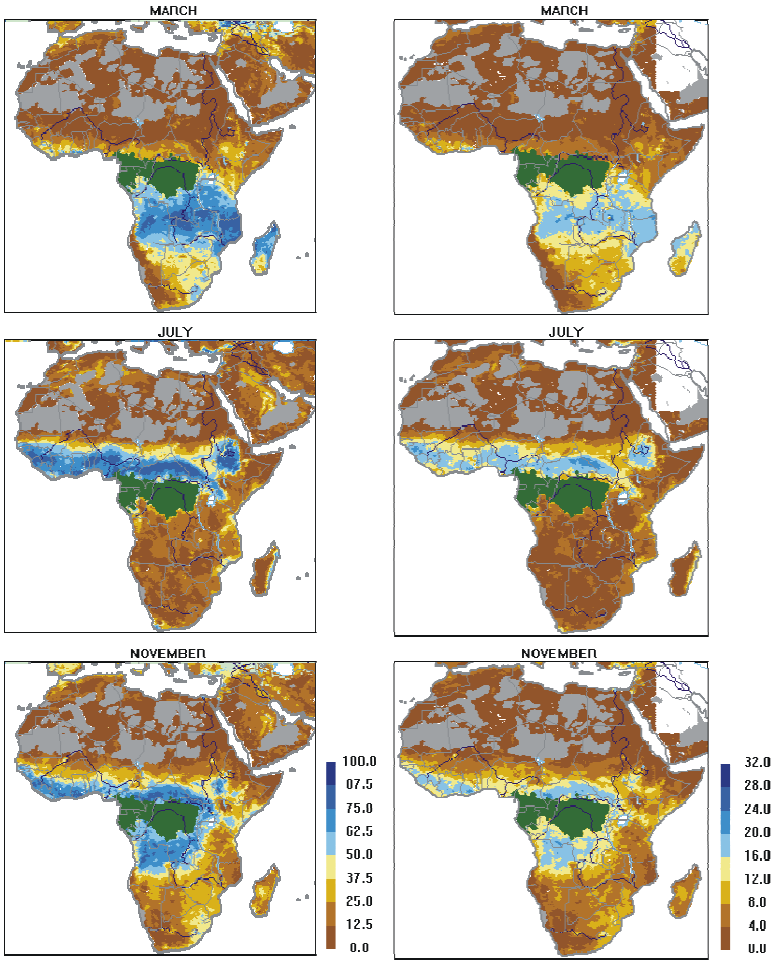

Figure 5-46 Mean Soil Water Index (left) and Mean Volumetric SoilMoisture(right) for the African continent. Volumetric Soil Moisture was calculate according to equation (5.8) ignoring the Total Water Capacity term with soil physical properties taken from the Soil Physical Properties Data Base.

5.5.5 Identified Problems

5.5.5.1 Azimuthal Effects

Figure 5-36 to Figure 5-39 present time series typically observed under normal conditions over most of the global land surfaces. However, it has been stressed in Chapter 5.3.1 that high azimuthal noise can introduce severe errors in the analysis of scatterometer data, raising the question about the influence of azimuthal noise on the retrieved degree of saturation. Very high azimuthal noise is for example evident in the Manchuria (North East of China). The observed values exceed the expected range by an order of magnitude. The respective area is characterised by agricultural fields and forests. The most plausible explanation for the high azimuthal noise are effects caused by systematic large scale topographic features consequently leading to a biased estimate of m_S. Figure 5-47 clearly shows the effect of the azimuthal noise immersed in the m_S series. Compared to precipitation records a coarse correlation can be deduced. During winter the region is gripped by temperatures far below 0°C. The long period of temperatures below 0°C let the soil freeze finally resulting in low m_S values. This "dry" period is correctly described by the m_s series. Also the increase in soil moisture after the onset of thawing when snow melts and the first rainfalls are wetting up the soil are correctly depicted in the data. Still due to the high noise a proper interpretation of m_s series and further information assessment is at least difficult and highly questionable. Another remarkable feature in the time series of Figure 5-47 is observed during the first quarter of 1994. This period was characterised by a calibration phase with a 3 day repeat cycle and therefore observations are taken at constant azimuth. Additionally climatic conditions were stable with average temperatures below zero and no precipitation resulting in very stable backscatter. Consequently, the signal should be comparably stable for all other years as similar climatic conditions prevail. This short period illustrates the effect of high azimuthal noise. The effects are significant and data over these regions has to be used with care. However, regions affected by azimuthal noise of this order are spatially limited and only observed over the Manchuria and some regions west of the Crimean peninsula.

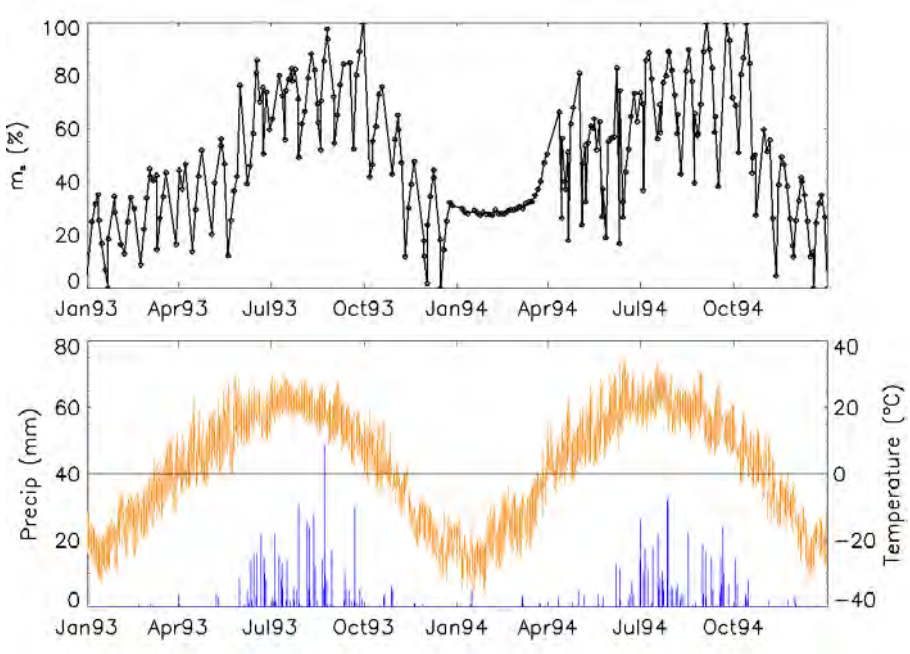

Figure 5-47: Degree of saturation of the top soil layer m_S and meteorological records (rainfall – blue, maximum and minimum temperature – red) for Keshan – China (125.9°E / 48.1°N).

5.5.5.2 Open Water Surfaces

Open water surfaces introduce errors in the estimation of surface soil moisture. Backscatter of open water surfaces depends mainly on surface roughness effects driven by wind. Backscatter is therefore highly variable and the requirement of stable surface roughness is violated. Generally open water should not effect the retrieval, if the percent area covered by the open water surface is small. Nevertheless, there exist regions were the area percentage of open water surfaces can reach a significant magnitude. Such is the case for paddy rice cultivation areas in Asia were the effect of open water bias the retrieved surface moisture estimates. For example along the lower course of the Yangtze, unnatural dry spells during the summer month are observed. Figure 5-48 shows the mean *SWI* for the month of August together with climographs for the synoptic weather station Hefei. Comparing the temporal evolution of the mean *SWI* to general weather data it becomes obvious that the observed drop during the second quarter of the year can not be explained by climatic effects. Rather the trend indicated by the *SWI* counter the trend given by precipitation records having a maximum during summer. The lower course of the Yangtze is a main cropping area of paddy rice where 70% of Chinese paddy rice is cultivated. There is evidence to believe that the regional rice cultivation practice has an influence on the measured $\sigma^0(40)$ and in consequence on the retrieved m_S and *SWI*. The effect of paddy rice fields on the backscattering coefficient has been addressed in a study of Leeuwen (1998) who investigated the

feasibility of using scatterometer data for wetland rice mapping. Scattering effects of inundated rice paddies might cause the decrease observed in the backscatter during summer. Scattering from open water surfaces can be low if the surface is smooth due to specula reflection. However, it is more likely that the low scattering is caused by the interaction of the impinging electromagnetic wave with the rice plants and the water surface. More detailed knowledge about the rice cultivation cycle and practice in the effected regions is required to conceive a clearer idea of this process. Nevertheless, a map showing the spatial distribution of paddy rice fields, principally correlating well with the spatial extend of the observed phenomenon (Figure 5-49) supports above statement.

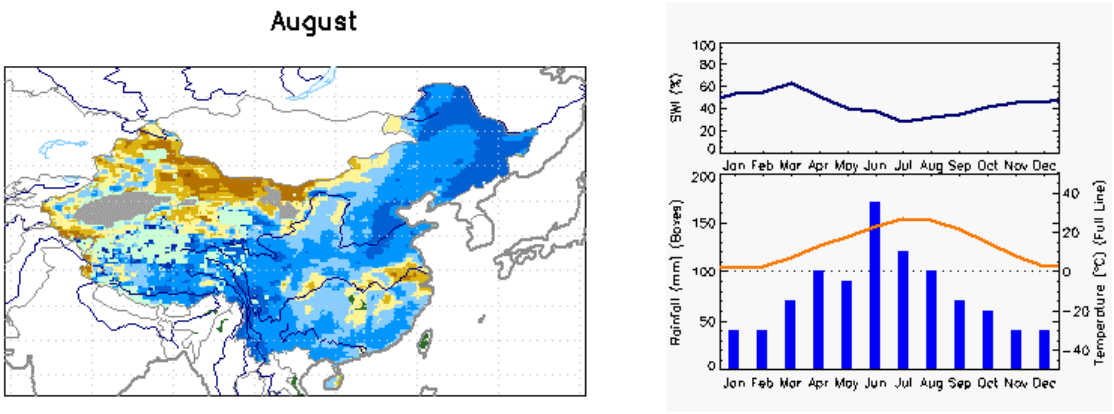

Figure 5-48: Unnatural dry spells during the summer months observed along the lower course of the Yangtze (left). Brown color tones indicate dry soil conditions blue tones wet conditions. Temporal evolution of the Mean SWI, together with climographs for the metstation Hefei / Luogang (117.1°E / 31.9°N)

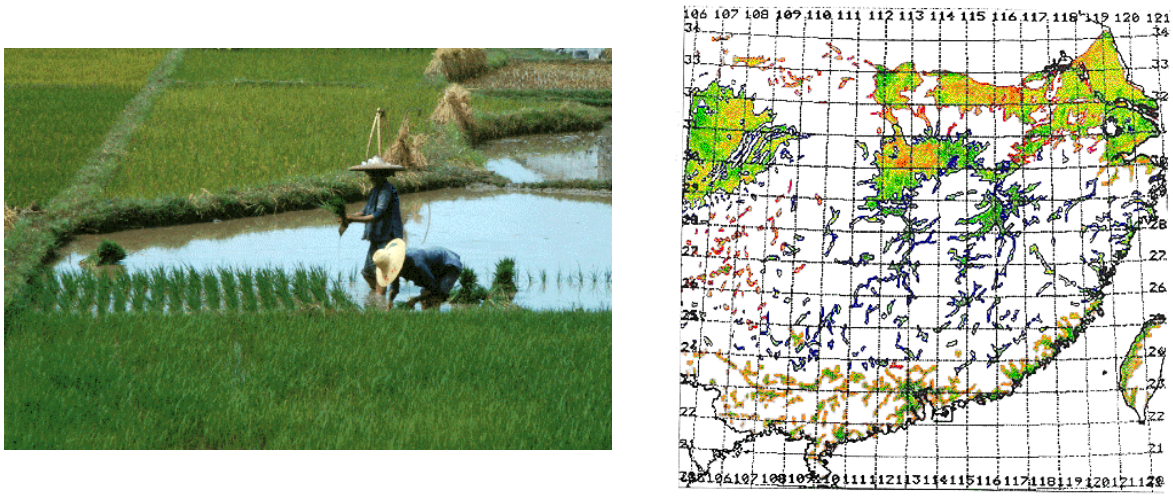

Figure 5-49: Typical rice paddy along the Yangtze (left) and spatial distribution of areas containing more than 50% rice paddies with superimposed 1km resolution NDVI.

6 STATISTICAL ANALYSIS

This chapter aims to analyse the temporal behaviour and summarise the dominant characteristics of the soil moisture field as observed with the scatterometer. In the course of the soil moisture retrieval process, vast amounts of numerical data are produced. Getting a feel and make sense of these numbers therefore becomes a significant task. Statistical methods like spectral analysis provide effective tools to support this analysis.

Analysis will focus on two aspects, climate "signals" and the underlying "noise". Separating these components is a major task of spectral analysis in climatic science. The separation is somehow arbitrary depending on the nature of analysis. The term signal most generally refers to a pattern in time, which is determined by system dynamics. Noise comprises all those features that are not considered to be relevant signals.

A high number of influencing variables, a complex interaction and response of the system characterize climatic processes, including hydrologic processes at the land surface. Many of the dominant dynamics generating climatic processes are fairly well understood ranging on temporal scales of a few minutes to millions of years. A well-known example of this variability is El Niño/Southern Oscillation (ENSO) phenomenon.

Beside the influence of geophysical variability, persistence is a major characteristic of the soil moisture field. Atmospheric variables generally exhibit statistical dependence with their own past. In atmospheric sciences, this dependence through time is usually known as persistence (Wilks, 1995). In this framework, persistence can be thought of as how long it takes soil moisture anomalies to disappear. As persistence is not regarded as a climatic signal, it is usually lumped into the noise term. A general model for underlying noise characterized by persistence will be presented in the next section.

Decomposition of the soil moisture time series in these two subspaces is done with the hope of identifying the physical processes responsible for the generation of the series and to learn about the process itself.

6.1 Signal and Noise

When analysing climatic time series the concepts of persistence and signals have to be considered integrative. The most common errors made in spectral analysis come from poor estimates of the effects of background as the level of confidence we attribute to a potential signal depend quite sensitively on our a priori assumptions regarding the nature of the background noise. The success

of signal detection hence hinge on the proper isolation of the underlying noise (Storch and Navarra, 1999).

Persistence in climate time series, generally expresses itself in enhanced low-frequency fluctuations. This may be because rapid variations are suppressed by the slow response components of the system, rather than because low frequencies are enhanced (Muller and MacDonald, 1995). Spectra derived from such processes are commonly referred as "red noise" spectra, compared to "white noise" spectra generated by random processes.

The simplest but still successful statistical model for a discrete finite red noise series is the first order autoregressive *AR(1)* process where fluctuations depend only on the own immediate past plus a random component (Gilman, 1963). The *AR(1)* process can be expressed as:

$$r_n = \rho \cdot r_{n-1} + \omega_n \tag{6.1}$$

where $n=1, .., N$ denotes the discrete time increment in units of the sampling interval Δt, $0 \leq \rho < 1$, the lag one autocorrelation coefficient, describing the degree of serial correlation in the noise and ω_n is a Gaussian white noise sequence with variance σ^2. For the *AR(1)* red noise process, autocorrelation decays exponentially as a function of time

$$\rho_n = e^{\left(\frac{-n\Delta t}{\tau}\right)} \tag{6.2}$$

where τ, being a measure for decay, is the characteristic descriptor of persistence.

Describing the underlying noise in climate processes with the *AR(1)* model was first introduced by Hasselmann (1976) and found wide application. Delworth and Manabe (1998) used the concept of Haselmann to theorize that soil moisture might be a variable whose long-term anomaly pattern are responses of the land surface layer to the random forcing of precipitation. Based on the analysis of results from the Geophysical Fluid Dynamics Laboratory General Circulation Model they developed the theory that soil moisture variations in time correspond to a first order Markov process, where the autocorrelation function $\rho(t)$ is exponential according to (6.2). They also determined that a good approximation of the persistence time scale is

$$\tau \approx \frac{W_f}{E_P} \tag{6.3}$$

where W_f is the field capacity and E_p is the potential evaporation. Using model data, τ was estimated to range from 1 month in tropical regions to extreme values of 10 months in the high

latitudes. However, Delworth and Manabes work is based on results of a bucket model, which is a simplistic approach to describe the land surface system and even though models in climatic science can be very impressive and give quite good approximations to atmospheric behaviour they are not complete and true representations of the governing physics. Hence one should be cautious inferring characteristics of a certain process from model data (Wilks, 1995).

Initial validation of Delworth and Manabes theory and formula for persistence using empirical soil moisture observations is found in Vinnikov and Yeserkepova (1991). This study presents results from analysis of data from 50 soil moisture stations in the Former Soviet Union, being in good agreement with the theoretical model. More recently results provided by Entin et al. (2000) analysing soil moisture data from China, Mongolia, Russia and India supported this theory. Entin estimated τ to range between 1-2.5 month depending on latitude. However, Vinnikov and Yeserkepovas (1991) and Entins (2000) work are limited by the restrictive distribution of the station network concentrating on mid-latitudes. Nevertheless, the *AR(1)* model has theoretical and empirical justification and it seems justified to apply this model in the following analysis as underlying "noise" model.

Spectral fluctuations significantly deviating from this model should be regarded as climatic "signals". However, not every "signal" observed in a spectrum, necessarily originates from geophysical dynamics. Hence if a signal is detected in the data it should also be identified as climatic signal (Storch and Navarra, 1998). In this respect, the analysis does not aim to track new, but to test the series for some well-known atmospheric phenomena. Atmospheric behaviour is well studied and synoptic variability of mid-latitude weather systems is known to occur on time scales of 3-7 days, 1-3 months (atmospheric low frequency variability), 30-60 days (Madden-Julian oscillation of winds and cloudiness in the tropics) or year to year variability dominated by ENSO related phenomena (Ghil, 2001).

6.2 General Considerations

6.2.1 Model Effects

The method to estimate profile soil moisture information from surface observations proposed by Wagner (1998) is based on a simple two-layer water balance model. Mathematically speaking, the profile soil moisture *SWI(t)* is determined by convoluting $m_S(t)$ with the transfer (filter) function $h(t')$ given by

$$h(t') = \frac{1}{T} e^{-\frac{t'}{T}} \qquad 0 \le t' \le \infty$$
$$h(t') = 0 \qquad t' < 0 \tag{6.4}$$

The power spectrum of the filtered time series *SWI(t)* is expressed as (Schlittgen and Streitberg, 1995)

$$\Gamma_{SWI}(\nu) = \Gamma_{m_S}(\nu) \cdot \left|\hat{H}_h(\nu)\right|^2 \tag{6.5}$$

or in words, the spectrum of the original series multiplied by the squared magnitude of the Fourier transform of the filter. The Fourier transform of the decaying exponential function *h(t´)* is

$$\hat{H}_h(\nu) = \frac{1}{1 + i2\pi\nu T} \tag{6.6}$$

To study the effect of the filter defined in (6.4) we plot the Gain Diagram defined as squared magnitude of the Fourier transform of the filter (see equation (6.5)). The gain diagram visualizes the effect of a filter with respect to its damping properties. If the gain for fixed *v* is lower than 1 the respective spectral component will be damped for values greater 1 the respective spectral component will be enhanced and a gain equal to 0 will result in a complete suppression.

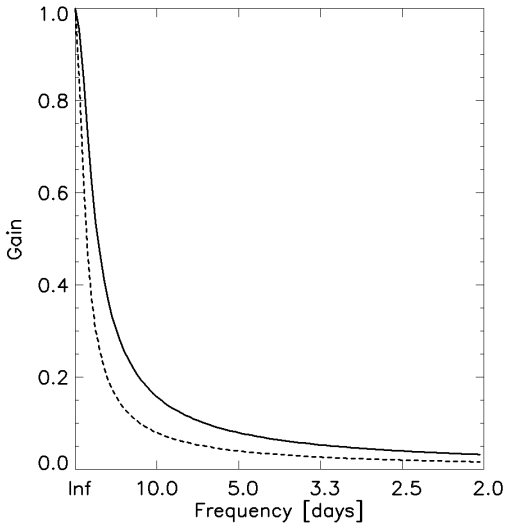

Figure 6-1: Gain Diagram of the filter function specified in equation (6.4). The solid line is representative for a characteristic time time length T=10; the dotted line for a characteristic time length T=20. For a definition of T see Chapter 5.3.2.

Figure 6-1 indicates that the filter function defined in (6.4) will generally damp all spectral components. However for frequencies less than ~$0.05t^{-1}$ damping is moderate. In the case of *SWI* determined with a frequency of ten days this corresponds to cycles above 200 days. To further

assess the effect of (6.4) on the *SWI* we assume that the top soil moisture content, sampled at irregular intervals by the ERS scatterometer is a highly variable nearly random process. This seems to be a severe simplification of reality. However, visual analysis of top soil moisture indicated the close link of top soil moisture to precipitation, which is often assumed to be a random process (Delworth and Manabe 1993). Hence assuming irregularly sampled top soil moisture data to be random is used as a working hypothesis. Applying above model to a pure random process will result in a power spectrum of *SWI(t)* of the form

$$\Gamma_{SWI}(\nu) = \frac{C}{1+(2\pi\nu T)^2} \tag{6.7}$$

In this expression C is the constant variance of the random top soil moisture process m_S. The effect of the filter function is therefore to give a power spectrum, that for large frequencies decays as ν^2. This becomes even more obvious when calculating the respective autocorrelation function, which is a decaying exponential:

$$\rho(\tau) = e^{\frac{-\tau}{T}} \tag{6.8}$$

The applied filter will hence enhance persistence of the time series where the characteristic time variable in equation (5.8) is the driving factor of the magnitude of the persistence time scale τ. In the current implementation of the model, T is kept constant, neglecting the influence of the variability of the soil layer on the temporal persistence τ. However, it should easily be possible to extend the current software implementation to a more realistic representation of the soil layer.

Setting T to a constant should result in constant estimates of τ. If however τ shows distinct spatial patterns than the assumption that surface soil moisture is a random process has to be rejected and replaced by a more realistic assumption.

6.2.2 Effect of Temporal Sampling

It is important to note that the persistence time τ estimated from the Fourier spectrum depends quite sensitively on the temporal sampling Δt of the analysed series. According to Storch and Navarra (1999), the persistence time τ is at least as long as the time increment Δt. The longer the time increment the larger the persistence τ. In case of a white noise process, τ is always equal to the time increment Δt. Storch and Navarra (1998) conclude that the absolute value of τ is of questionable informational value and only relative variations of τ can give useful information about the underlying process. Additionally they conclude that only a value well above the

sampling rate of the series has significant informational value. In our case, the estimated persistence time is therefore at least 10 days.

6.3 Analysis Methods

Fourier analysis provides tools to describe data series in terms of contributions occurring at different scales or characteristic frequencies, and is commonly applied in atmospheric science. The aim of these techniques is to summarize the dominant characteristics of a field, such as time patterns and discriminate between the signal of interest and the underlying process noise. In Fourier analysis theory the overall time series is regarded as having arisen from the combined effects of a collection of sine and cosine waves oscillating at different rates. The sum of these waves reproduce the original data, but it is often the relative strength of the individual component waves expressed in the power spectrum that is of primary interest. In the following, a short summary of Fourier analysis will be given and the most striking features will be discussed.

Let *h(t)* be a continuous function of time. According to Fourier theory this function can be completely specified in terms of a few underlying sinusoidal (sine and cosine) functions of particular wavelengths. The transform *H(ν)* being a function of frequency is called the Fourier spectrum of the function *h(t)* and defined as:

$$H(\nu) \equiv \int_{-\infty}^{\infty} h(t) e^{i2\pi\nu t} dt \tag{6.9}$$

Taking the transform according to (6.9) assumes that the function *h(t)* is both infinite and continuous. However real world data generally is finite and even worse only sampled at discrete points. Hence calculating the Fourier transform is obviously an ill posed problem. Estimating the Fourier spectrum of a finite time series by a discrete Fourier transform, one is confronted with the problems of bias (Is the estimate on average centred at the correct value?), leakage (How does variance at one frequency effect another?) and consistency (Does precision of the estimate improve when more data is analysed?). The retrieved estimate will be characterized by high variance about the true spectrum. A major problem of spectral analysis theory is therefore devoted to find a low variance estimate of *H(ν)*:

$$\hat{H}(\nu) \equiv \sum_{j=1}^{N} h_j e^{2\pi i \nu t_j} = \sum_{j=1}^{N} h_j \cos 2\pi\nu t_j + i \sum_{j=1}^{N} h_j \sin 2\pi\nu t_j \tag{6.10}$$

where h_j are discrete samples of the continuous function *h(t)*.

Traditionally, reducing variance in the spectrum estimate has been achieved by multiplying the time series with a data taper before performing a discrete Fourier transform. In the last couples of decades, new and more sophisticated methods of data analysis have increasingly been developed and applied in climatic sciences such as the Multi Taper Spectral Method (MTM) developed by Thomson (1982). MTM is especially well suited for short and noisy time series as observed in climatic science. Additionally to providing a low variance, leakage resistant spectrum estimate, statistical significance of spectral peaks can be inferred. However MTM can not be applied over the entire study area. Frozen and snow covered surfaces can not be used for the subsequent soil moisture retrieval, resulting in data gaps during the winter months in higher latitudes. In such case, MTM resting on the discrete Fourier transform, defined for equally spaced data without gaps, can not be applied. To receive a spectral estimate of soil moisture series for the entire globe a second method will be used in the course of the analysis, the Lomb Scargle Diagram LSD. LSD offers the possibility to estimate the spectrum of irregular sampled data and can hence be applied globally. Both LSD and MTM will be applied in an adopted way especially designed for the analysis of climatic time series characterized by an underlying "red noise" model.

6.3.1 Multi Taper Spectral Analysis

MTM provides a useful tool for spectral estimation of short and noisy time series containing both continuous and singular components characteristic for climatic time series (Thomson, 1982). In addition, MTM relaxes some of the strict stationary assumptions of common spectral analysis techniques. The idea of MTM is to multiply the data by a set of S leakage resistant orthogonal tapers a_s. This result in S tapered time series from one original data record. Taking the Fourier transforms of each of the S tapered time series, S estimates of the spectrum $H_s(v)$ are produced. The tapers a_s are called "eigentaper" since their construction involves an eigendecomposition. Similarly the spectra $H_s(v)$ are commonly called eigenspectra. The choice of the numbers of applied tapers depends on the analysis purpose and is a trade off between spectral resolution and the variance of the spectral estimate. Thomson (1982) pointed out that applying several different tapers and averaging the resulting power achieve the best sensitivity for finding a small signal in the presence of another signal, which has different frequency and much greater power. The multi taper spectral estimate is then formed as a weighted sum of the eigenspectra. However, averaging the power results in a degradation of resolution. Hence, MTM trades resolution for variance reduction. The more tapers used the better the variance properties but the lower the resolution of the spectrum estimate will be. In this study, five tapers have been found to obtain the best results.

As a positive side effect, MTM offers the possibility to calculate significance levels to test spectral peaks against white noise. For climate applications the traditional MTM method has been adopted by Mann and Lees (1996) to test spectral peaks against the null hypothesis of "red noise" estimated empirically from the data. To accommodate significance testing a robust estimate of the "red noise" background by minimizing the misfit between an analytical *AR(1)* red noise spectrum and the adaptively weighted MTM spectrum is calculated. MTM spectra are convoluted with a median smoother to insure that the estimated noise background is insensitive to outliers (most obviously peaks associated with signals) that should not influence the estimation of the global noise. Significance levels for harmonic or narrowband features relative to the estimated noise background can than easily be determined from appropriate quantiles of the chi-square distribution. Applying the adopted MTM the underlying noise and the spectrum estimate can be derived simultaneously.

6.3.2 Lomb Scargle Method

The major drawback of spectral analysis methods such as the MTM is the requirement of evenly spaced data. To cope with the problems of unevenly spaced data, Lomb (1976) and Scargle (1982) developed a different approach of estimating the spectrum.

Lomb (1976) and Scargle (1982) improved on the simple power spectrum by a slight alteration. They showed that if the cosine and sine coefficients are normalized separately then the classic power spectrum can be used with unevenly spaced data, and yet the statistical behaviour of the variance is identical to the behaviour we would expect if we had evenly spaced points. The Lomb-Scargle periodogram evaluates data, and sine and cosines, only at times t_i that are actually measured and is defined by

$$\Gamma(\nu) = \frac{1}{2\sigma^2}\left\{\frac{\left[\sum_k (y_k - \bar{y})\cos 2\pi\nu f(t_k - \Omega)\right]^2}{\sum_k \cos^2 2\pi\nu(t_k - \Omega)} + \frac{\left[\sum_k (y_k - \bar{y})\sin 2\pi\nu(t_k - \Omega)\right]^2}{\sum_k \sin^2 2\pi\nu(t_k - \Omega)}\right. \quad (6.11)$$

where $\bar{y}$ is the usual mean, σ^2 the variance and Ω a time constant defined for every frequency according to

$$\tan(4\pi\Omega) = \frac{\sum \sin(4\pi\nu t_k)}{\sum \cos(4\pi\nu t_k)} \quad (6.12)$$

(6.11) is less imposing than it looks. It has two terms, one for the cosine transform, the other for the sine transform. Each term is normalized separately. The only complication is that each frequency uses different time offsets Ω. The particular choice of Ω according to (6.12) has a deeper effect. It makes equation (6.11) identical to the equation that is obtained estimating the harmonic content of a data set, at given frequency ν, by linear least squares fitting to the model

$$h(t) = A\cos\nu t + B\sin\nu t \tag{6.13}$$

Other than these changes, the equation looks just like an ordinary digital Fourier transform. Schulz and Statteger (1997) and Schulz and Mudelsee (2001) expanded the traditional LSD with a Welch-Overlapped-Segment-Averaging procedure to retrieve consistent spectral estimates, a procedure to fit an analytical *AR(1)* noise model to the retrieved spectrum and to test for significant signals. Routines they make available will be used throughout the following analysis[6].

6.4 Spectral Properties of SWI Data

To study the statistical properties of soil moisture as observed with the scatterometer, *SWI* time series have been used with a decade temporal resolution. Calculation of *SWI* involves modeling the water flux of the observed topsoil moisture to deeper layers. Artefacts introduced by this transfer model have been discussed in Chapter 6.2. In the following, the retrieved spectral properties will be discussed.

6.4.1 Soil Moisture Persistence

Robustly estimated persistence time scales based on MTM are fairly constant over large parts of the globe ranging between 1-2 months (Figure). Over very dry regions with low rainfall, slightly higher values of 2-3 month can be observed. Delworth and Manabe (1988) speculate that over arid regions the precipitation spectrum takes on non-white, i.e. non-random characteristics where months can pass between consecutive rainfalls. In such a case, rainfall variability reduces and in consequence, soil moisture will show reduced variability. Persistence will hence not longer follow equation (6.2) but will be largely determined by the interval between consecutive rainfalls. Given that high τ values are not exclusively observed in arid regions and that large parts of the global deserts have constant low persistence a more realistic explanation of the observed high τ values might be enhanced long wave signals artificially introducing bias in the estimate of the background noise and hence the persistence timescale τ. The LSD gives a similar picture of the

[6] Code is available on http://www.uni-leipzig.de/~meteo/MUDELSEE/

persistence scale τ. Large parts of the globe are characterized by a temporal persistence of 1-2 months. Although it can be observed that the persistence time scale, derived using LSD, is systematically larger than the persistence time scale derived using MTM. This observation most likely arises from a well-known feature of the LSD. In contrast to classical Fourier transform, the LSD components are not necessarily independent of each other. Consequently, an estimated spectrum based on the LSD transform may be biased. In particular, spectral amplitudes at the high frequency end of a spectrum are often overestimated (Lomb 1976, Scargle 1982). According to Schulz and Mudelsee (2001), this bias can be reduced using a Monte Carlo simulation technique. However due to computational limitations this correction method could not be applied in a realistic time frame.

Both methods derive a persistence time scale τ of approximately 1-2 month. This value is somewhat higher than the characteristic time length *T,* which was set to 20 days. However, consideration concerning sampling interval and global homogeneity confirm that soil moisture variations at the surface layer are characterised by low persistence. However, it is stressed that the measurement process influences the statistical process properties. Surface soil moisture is a highly variable process. Fully capturing this process would require daily observations. With current sensors, this is not achievable. The ERS Scatterometer measures soil moisture approximately every 3-4 days sometimes even less often. Consecutive samples are hence not longer correlated, especially if the time between the measurements spans a longer period. It can therefore be assumed that the true persistence of surface soil moisture is larger than estimated from ERS scatterometer derived measurements and that the estimated persistence shows clearer spatial patterns.

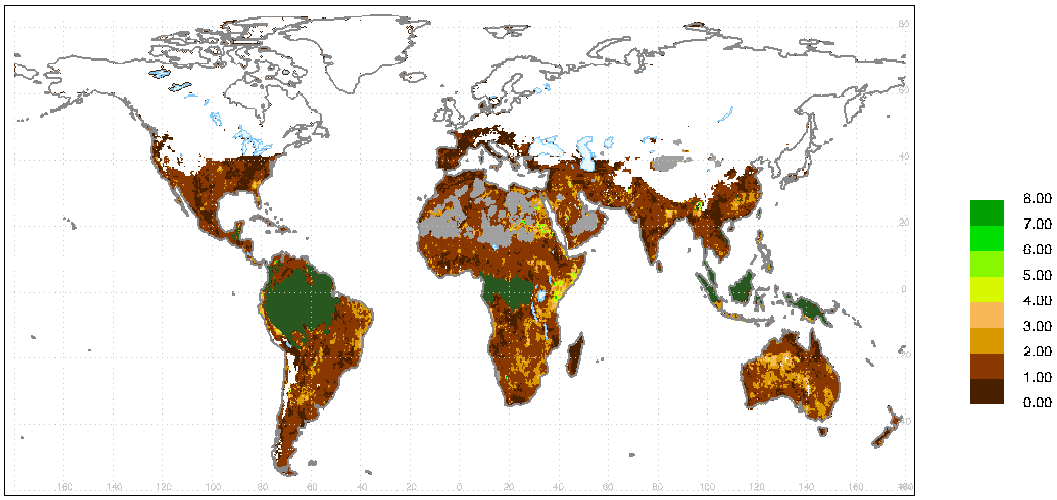

Figure 6-2: Persistence time scale τ estimated using MTM analysi. MTM could only be estimated for regions not effected by winter frost. Dark green indicates regions with dense tropical forest. Grey indicates regions of high azimuthal noise.

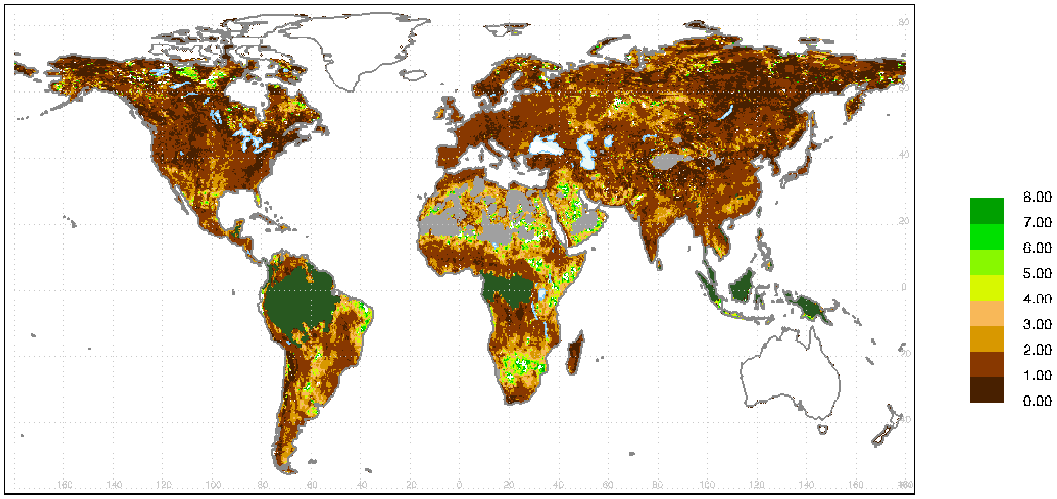

Figure 6-3: Persistence time scale τ estimated using LSD. LSD was not estimated for Greenland and Australia. Dark green indicates regions with dense tropical forest. Grey indicates regions of high azimuthal noise.

6.4.2 Significant Signals

A very prominent feature is the long time scale associated with all the soil moisture spectra. Large amounts of variance are located at periods of one year or more, suggesting that soil moisture may play a role in low frequency atmospheric variability (Delworth and Manabe, 1993). Beside this dominant feature, significant signals could mainly be identified at ~23 days and ~34 days. Variability occurring on scales of 1-2 month are known as the intraseasonal variability (atmospheric low frequency variability) influenced by the Madden Julian Oscillation of winds

and cloudiness in the tropics (Ghil, 2001). However, the cyclic feature can also be attributed to the orbit geometry of the sensor with a repeat cycle of 34 days. Beside these, no significant cycle features could be detected over large consistent regions.

The reason for not receiving a clearer picture of signals observed in the series might be the relative shortness of the available series spanning a period of only 9 years. In this case most known periodicities of climatic phenomena have far too few repetitions for good statistical localisation (Mann and Lees, 1996).

7 VALIDATION

A major task is to validate the retrieved products. Beside visual comparison geophysical parameters derived from scatterometer data with near surface synoptic weather records two validation strategies have been tracked. First, the comparison of monthly *SWI* anomalies with global gridded precipitation data and second, the comparison of scatterometer derived volumetric soil moisture time series with in-situ measurements. Analysis aims to provide an objective basis for methodological developments and to assess the quality of the retrieved products with emphasize on future applications.

7.1 Interpolated Precipitation Data

Although precipitation and soil moisture are two different geophysical quantities, in both data sets climatic anomalies should be well reflected. For this reason, global gridded precipitation anomalies have been compared to *SWI* anomaly maps.

Visual analysis affirms that climatic anomalies resulting in soil moisture deficits and surpluses can be depicted in the *SWI* anomaly maps and correlate well with precipitation anomalies. Problems are evident in regions with long lasting anomalies. For example the extreme 1999 drought hitting India, Pakistan and adjacent countries does not show up clearly in the *SWI* data. This drought persisted for several years resulting in biased (underestimated) normals for the period 92-00. Consequently, it has to be stressed that only extremes with regard to period 1992-2000 can be depicted correctly. Two examples of extreme events will illustrate the quality of derived products. Figure 7-1 shows an example of an extreme flood event. In 1998 China suffered massive flooding concentrated in three areas during the summer: along the Yangtze River in south central China; in the area around the Gulf of Tonkin in southern China; and across the north near the Russian border. The heaviest rainfalls were reported during the June-July period. According to official Chinese government reports, the floods, the second worst to hit the country in more than 130 years, have killed 3656 people. The floods have left 14 million people homeless, affected 240 million people, destroyed 5 million houses, damaged 12 million houses, flooded 25 million hectares of farmland, and caused over $20 billion ($US) in estimated damages [7]. These extreme events are well reflected in the soil moisture data for all three regions as can be observed in the sequence of the difference maps (deviation of the actual conditions to the 1992-2000 normals). The maps also compare very well to interpolated precipitation data.

[7] http://www.disasterrelief.org

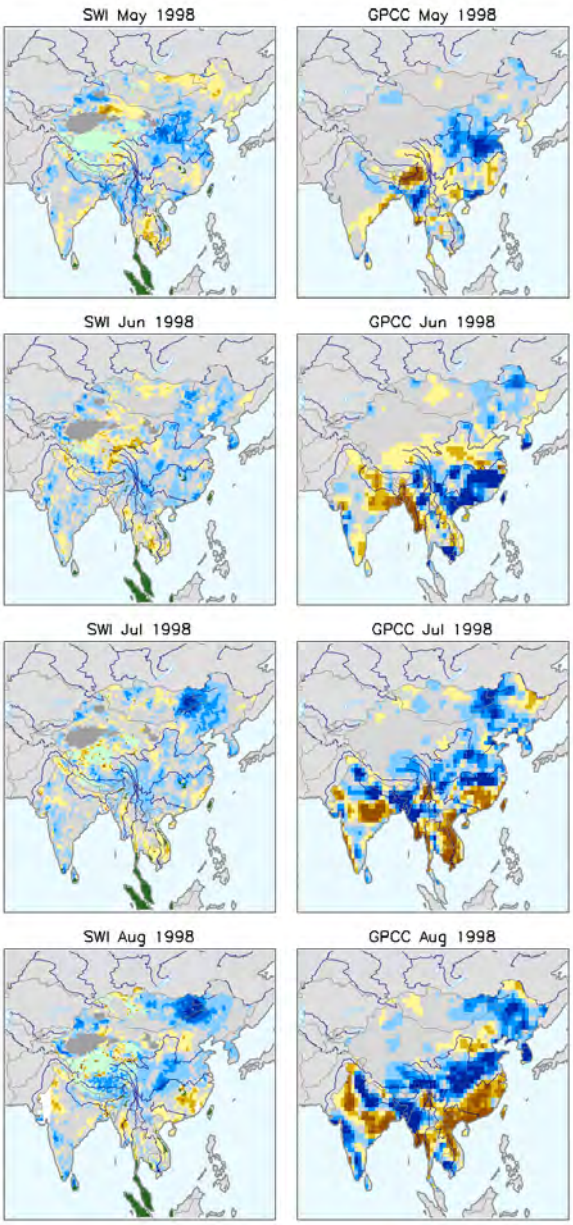

Figure 7-1: Difference of instantaneous soil moisture to the 1992-2000 normal (left) and difference of interpolated precipitation to the 1992-2000 normal (right). For the extreme summer flood of 1998. Blue tones indicate a surplus brown tones a deficit.

Figure 7-2: Destroyed houses in the Yangtze region caused by the massive summer flood of 1998.

In the following winter China experienced its worst drought in more than a decade, with 19 million residents lacking drinking water and more than 21.5 million acres of farmland parched [8].

In the northwest China's Qinghai province for example, more than 1000 lakes (which are the source of the Yellow river) have dried up because of deteriorating environmental factors and the lack of rain. After the flood of 1998 the country received very little rainfall from September 1998 onwards. Precipitation in most parts of China was more than 70 percent lower than the average for the same period in year before. These extreme events are again well reflected in the soil

[8] www.disasterrelief.org

moisture data as can be observed in the sequence of the difference maps (deviation of the actual conditions to the 1992-2000 normal). The maps also compare very well to interpolated precipitation data. Differences observed between the two sources of information have to be related to the different nature of the analysed data. While the highly variable precipitation process is more or less random, soil moisture shows a clear persistence of anomalies. The timescale of persistence has been estimated to be around 2-4 month depending on latitude (Entin et al. 2000). Soil moisture anomalies may therefore lack behind precipitation anomalies for several weeks.

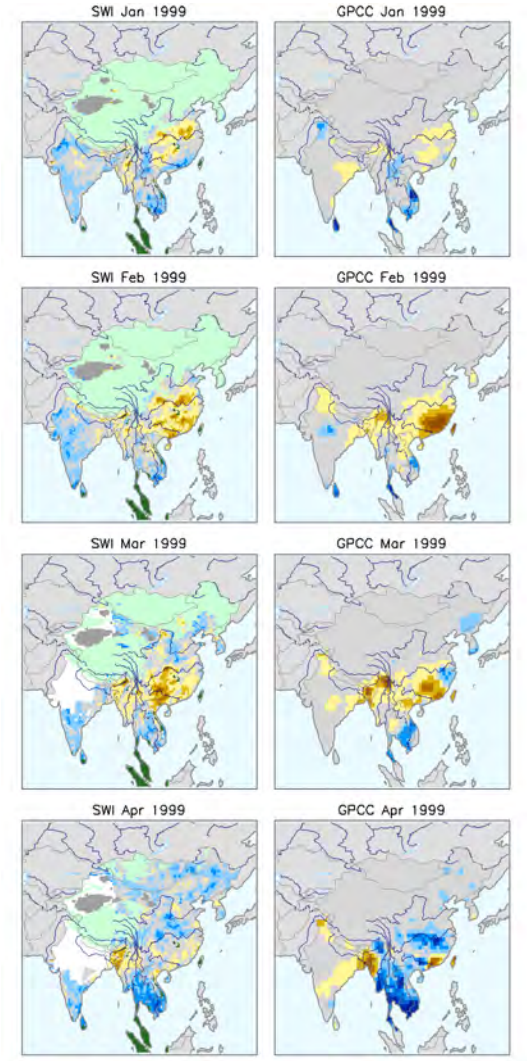

Figure 7-3: Difference of actual soil moisture to the 1992-2000 normal (left) and difference of interpolated precipitation to the 1992-2000 normal (right. Blue tones indicate a surplus brown tones a deficit.

Figure 7-4: Drought hit area in North West China

To quantify the observed parallels, *SWI* anomalies have been correlated with precipitation anomalies for the entire period 1992-2000. Figure 7-5 shows the global correlation. Generally, precipitation and soil moisture anomalies are positively correlated with high values reaching 80 percent. High correlation is observed over a wide range of land surfaces. Only in desert and

arctic regions areas with negative correlation can be depicted. In extreme climates, the extreme north and the dry lands of the African continent, correlation is observed to be not significant. It is noticeable that low correlation occurs mainly in data poor region, which might be an explanation (Figure 7-6). Finally, it is noted that the observed positive correlations over most of the global land surfaces indicate that the *SWI* fully capture the dynamics of the soil moisture process.

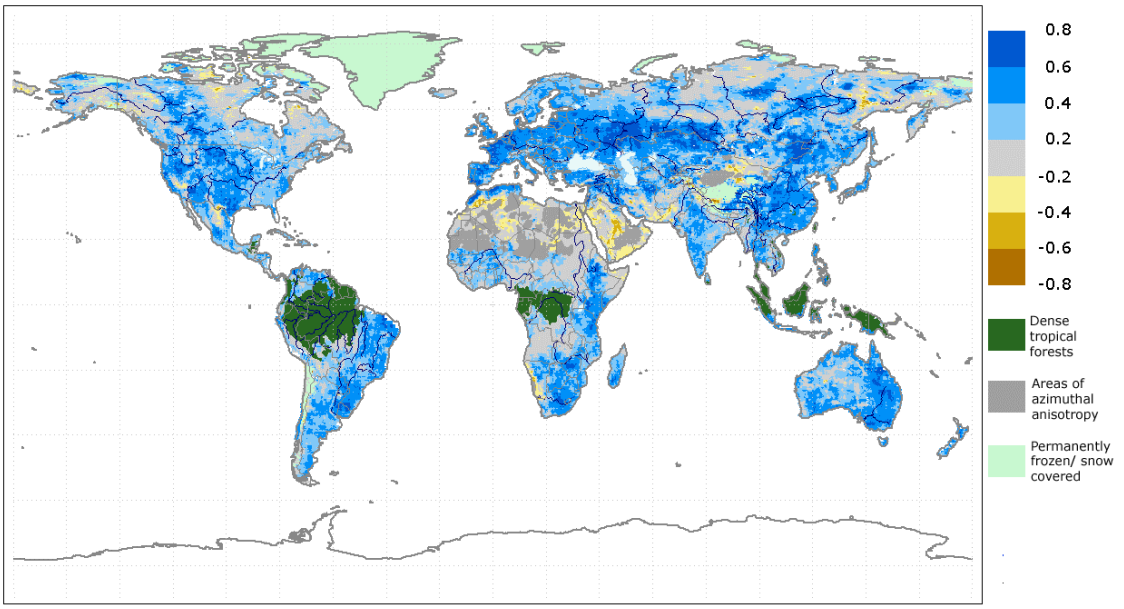

Figure 7-5: Correlation R between Global Gridded Precipitation anomalies and SWI anomalies for the period 1992-2000. Brown tones indicate negative correlation, blue tones positive correlation. Grey indicates that the estimated correlation coefficient was not significant at the α=0.01 level.

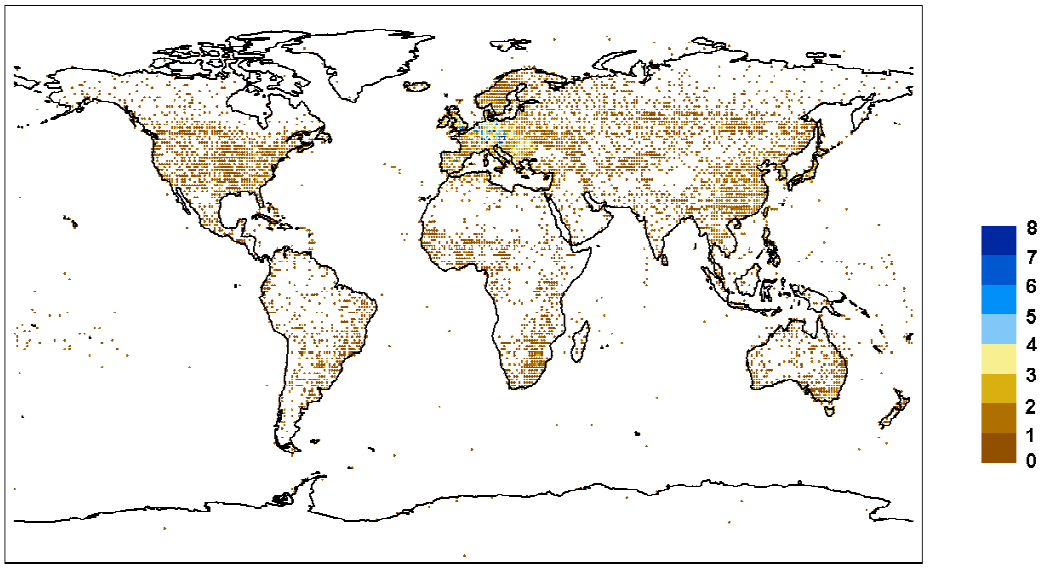

Figure 7-6: Average number of stations per grid for the period 1992-2000 used to derive global gridded precipitation estimates. Generally 1-2 stations are available. only in Europe a higher station density is pbserved. Large parts of the world have no synoptic weather staions.

7.2 In-Situ Soil Moisture Data

7.2.1 Methods

To receive a quantitative quality measure for the retrieved soil moisture information, products have been compared to an extensive data set of *in-situ* soil moisture measurements. The *in-situ* archive has been described in detail in Chapter 4.3. *In-situ* measurements are available in units of volumetric soil moisture. Comparative analysis therefore necessitates the conversion of the relative *SWI* to volumetric units. According to equation (5.8), conversion can be achieved if the *SWI* is calibrated with soil physical properties, encompassing wilting level, field capacity and total water capacity. Unfortunately, all three variables are only available for the soil moisture networks of Russia and the Ukraine. For India, Illinois and China only wilting level and field capacity is available. For these regions following relationship is assumed:

$$W(t) = WL + SWI(t) \cdot (FC - WL) \tag{7.1}$$

Volumetric soil moisture calculated according to (7.1) will systematically underestimate real soil moisture, which has to be considered during the interpretation. To get an estimate of the associated error, error analysis for the Russian and Ukraine station network is carried out using equation (7.1) and equation (5.8). Additionally for all networks, error statistics have been estimated for volumetric soil moisture based on a calibration with soil properties from the Soil Physical Properties database unfolded in Chapter 4.5.

To describe data quality four error quantities have been calculated: The *bias* as a measure of *tendency* describing if the scatterometer based estimates under or overestimate real conditions; The *standard deviation* as a measure of *precision* describing the scatter or variability of observations; The *correlation* as a reliable indication of overall method performance and finally the integrative error measure *root mean square error*.

7.2.2 Results of Error Analysis

Table 7-1 summarizes the error statistics for the station networks of Russia and the Ukraine. The statistics have been derived from more than 10000 samples for each station network. Volumetric soil moisture was calculated using the empirical relationship of equation (5.8) and soil physical properties accompanied with each *in-situ* station. Generally, the fit of the data is good, considering that scatterometer based estimates, represent a mean value of an area of 2500 km² compared to point measurements representative of individual fields. Wagner (1999c) showed that the variability of different fields within on resolution cell of the scatterometer can be as high as

the estimated variability between in-situ and scatterometer based soil moisture samples. The bias is near zero, the standard deviation is on the low side and correlation is generally high (Table 7-1). Figure 7-7 shows the favourable fit of the data. The estimated error quantities can be compared to specifications defined for the Soil Moisture and Ocean Salinity mission, a satellite mission dedicated to measure soil moisture over the land surfaces. In the mission objectives the required measurement accuracy was specified with a standard deviation of 4 % vol, only slightly lower than the accuracy of scatterometer derived soil moisture.

TABLE 7-1: Error statistics for scatterometer derived volumetric soil moisture compared to in-situ data from Russian and Ukraine. SWI has been converted to volumetric units applying equation (5.8) using soil physical properties from the soil moisture archive.

Station Network	No of samples	Bias (vol %)	StDev (vol %)	Correlation R	RMSE (vol %)
Russia	10287	-0.66	5.22	0.61	5.26
Ukraine	12877	0.38	5.10	0.61	5.12

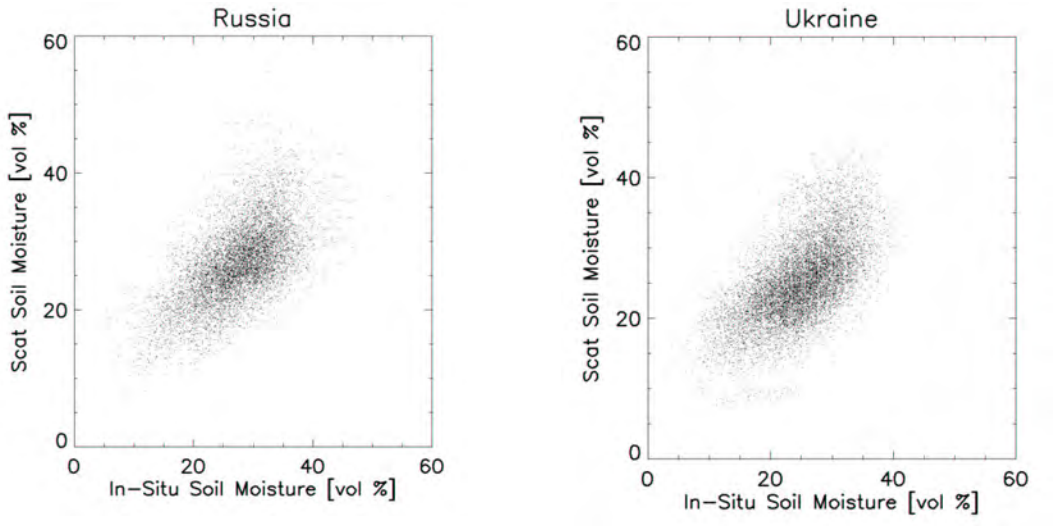

Figure 7-7: Scatteplots of scatterometer derived volumetric soil moisture calibrated with in-situ physical soil properties of wilting level, field capacity and total water capacity and in-situ samples.

Table 7-2 summarizes the error statistics for all station networks. Volumetric soil moisture was calculated using the simplified empirical relationship of equation (7.1). The estimated error quantities are generally higher than those specified in Table 7-1. Higher values can be attributed to violating the empirically determined relationship of equation (5.8) by assuming different calibration points, and to inaccuracies of the data sets. Highest error values are for example estimated for the Indian data set. For this data set, exact measuring dates are not available.

Arbitrarily defining a measurement date, likely introduces bias. However, the data is still in good agreement with *in-situ* observed records. Bias is in most instances negative, indicating that the applied method underestimates real conditions. It is stressed that neglecting total water capacity as calibration point causes part of this underestimation. The standard deviation is in the range 4.64 vol % to 8.34 vol %, correlation is generally above 50 %.

Error measures are generally higher for volumetric soil moisture based on a calibration with soil properties of the soil physical properties database. Differences can be significant. For example, the bias increases to high values of 11.9 % vol. for China and 9.4% vol for India using volumetric data based on the soil properties of the soil physical properties database. These high errors are associated with errors of soil properties inherent in the data base estimates.

TABLE 7-2: Error statistics for scatterometer derived volumetric soil moisture compared to in-situ data from all five networks. SWI has been converted to volumetric units applying equation (7.1) using soil physical properties from the soil moisture archive (indicated by in-situ) and soil properties from the global soil properties data base (indicated by DB).

Station Network		No. of samples	Bias (vol %)	StDev (vol %)	Correlation R	RMSE (vol %)
China	*in-situ*	20967	-2.32	5.80	0.55	6.25
	DB	21061	10.87	6.72	0.43	12.79
Russia	*in-situ*	11194	-5.32	4.64	0.67	7.06
	DB	11194	0.69	7.35	0.32	7.38
Ukraine	*in-situ*	12160	-3.76	4.26	0.70	5.69
	DB	12160	3.33	7.54	0.23	8.24
Illinois	*in-situ*	1375	-1.14	5.39	0.64	5.51
	DB	1375	-3.98	7.38	0.14	8.39
India	*in-situ*	2226	-3.23	8.34	0.65	8.94
	DB	2226	9.43	10.08	0.39	13.80

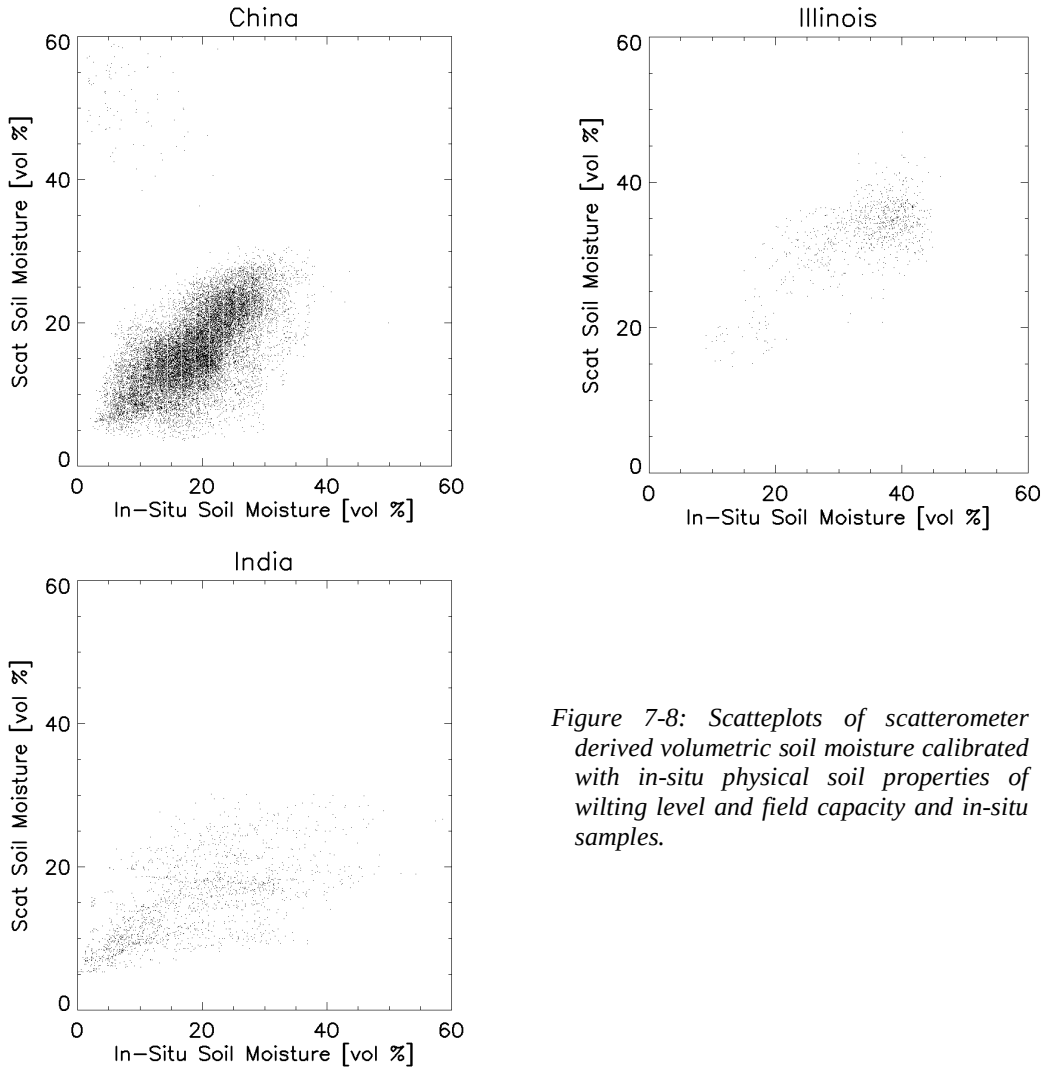

Figure 7-8: Scatteplots of scatterometer derived volumetric soil moisture calibrated with in-situ physical soil properties of wilting level and field capacity and in-situ samples.

Lumping all measurements of a region together and calculating the respective statistics resulted in the error quantities given in Table 7-1 and Table 7-2. This method is however sensitive to different bias observed at different stations. To study if site-to-site differences have significant impact on the retrieved error statistics, comparative analysis has been carried out specifically for each station and than averaged over all stations of a network. Table 7-3 and 7-4 summarize the results of this analysis. The error quantities are generally smaller indicating that the derived information is spatially slightly inhomogeneous. The bias reduces only slightly, however the standard deviation reduces significantly by a magnitudes up to 40% in the case of China. The correlation R increases which results from the lower number of measurements used during the calculation. Results indicate that anomaly time series are more accurate than the absolute series, and are therefore best used.

TABLE 7-3: Error statistics for scatterometer derived volumetric soil moisture compared to in-situ data from Russian and Ukraine. SWI has been converted to volumetric units applying equation (5.8) using soil physical properties from the soil moisture archive. Error statistics have been calculated specifically for each station and than averaged

Station Network	Bias (vol %)	StDev (vol %)	Correlation R	RMSE (vol %)
Russia	-0.32	4.12	0.49	5.20
Ukraine	0.28	4.31	0.51	5.05

TABLE 7-4: Error statistics for scatterometer derived volumetric soil moisture compared to in-situ data from all five networks. SWI has been converted to volumetric units applying equation (7.1) using soil physical properties from the soil moisture archive (indicated by in-situ) and soil properties from the global soil properties data base (indicated by DB). Error statistics have been calculated specifically for each station and than averaged

Station Network		Bias (vol %)	StDev (vol %)	Correlation R	RMSE (vol %)
China	*in-situ*	-1.81	3.71	0.27	5.25
	DB	11.04	4.18	0.27	12.21
Russia	*in-situ*	-5.14	3.68	0.50	6.71
	DB	0.78	4.02	0.50	6.72
Ukraine	*in-situ*	-3.81	3.84	0.52	5.58
	DB	3.34	4.18	0.52	7.61
Illinois	*in-situ*	-0.88	4.89	0.41	5.38
	DB	-3.26	4.89	0.41	7.99
India	*in-situ*	-3.12	6.23	0.60	8.04
	DB	9.59	6.16	0.60	12.92

Finally, it is checked if the estimated error quantities are time dependent. To estimate the time dependence, sample statistics have been calculated for each year and for each month. *SWI* has been converted to volumetric units applying equation (7.1) for Russia and Ukraine and equation (5.8) for India, Illinois and China with soil physical properties taken from the *in-situ* records.

Year to year differences are not evident in the data. However, an annual cycle can be determined (Figure 7-10). The standard deviation is relatively constant throughout the year. However, the bias and the correlation show a clear trend. Soil moisture is underestimated during the winter months indicated by negative bias. During the summer month, the soil moisture is correctly depicted for China and Russia and slightly overestimated for Illinois and Ukraine. India has a contrary trend underestimating soil moisture throughout the year with lower bias during winter than summer. Possible sources of error are for example the simplified model relating the observed surface soil moisture to the profile soil moisture. This model does not account for

varying climatic conditions. Further, the model does not consider evaporation. For example, it can be assumed that evaporation rates are lower during spring than during winter with distinct effect on soil moisture persistence.

Figure 7-9 and Figure 7-10 also illustrate that the quality of data is spatially consistent. Higher values are only observed for the Indian data, however this is attributed to *in-situ* data inaccuracies. Lowest error estimates are observed for the Ukraine and Russia data set. It is stressed that the higher errors of the Indian, Illinois and China data set are influenced by the simplified calibration given in equation (7.1).

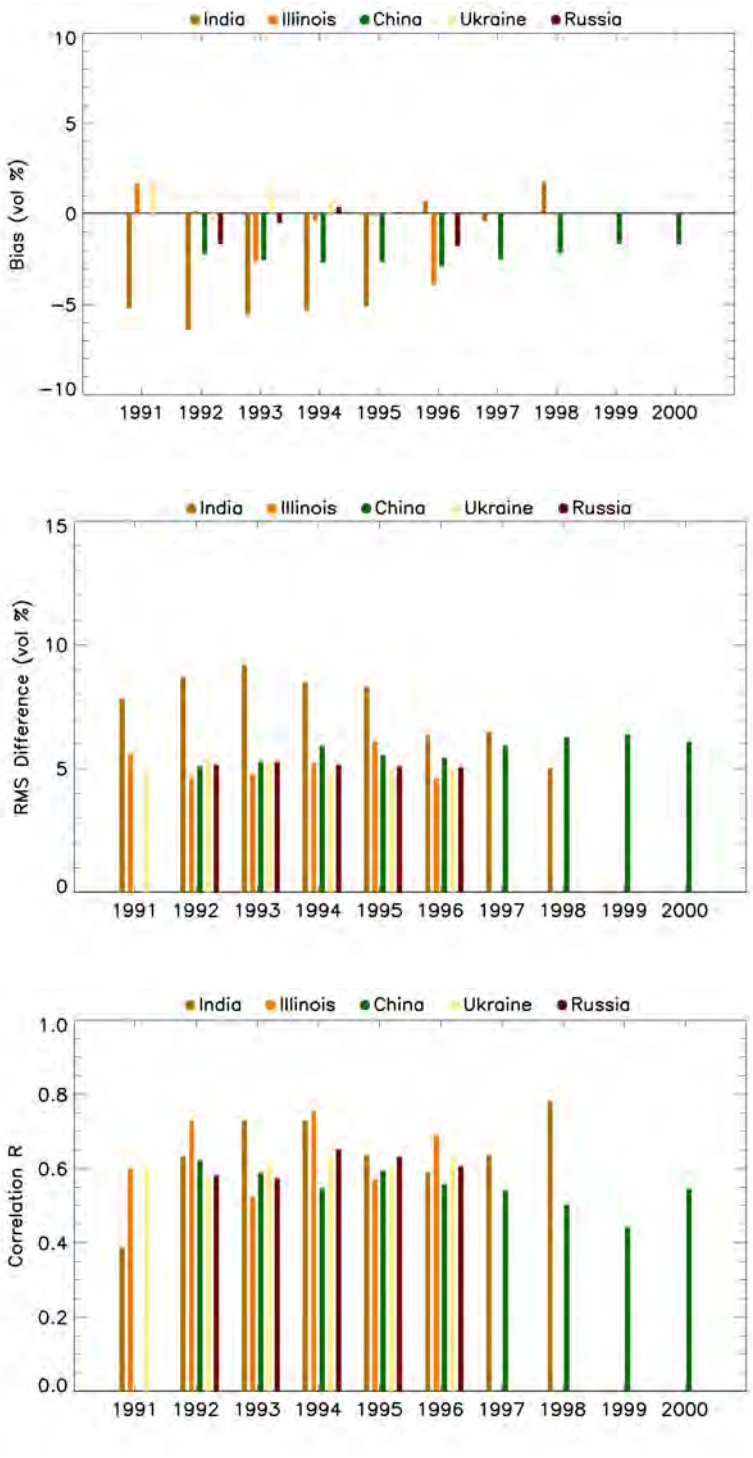

Figure 7-9 Year to year variations of error statistics between scatterometer derived volumetric soil moisture and in-situ. Shown are the bias, the standard deviation (RMS Difference) and the Correlation R.

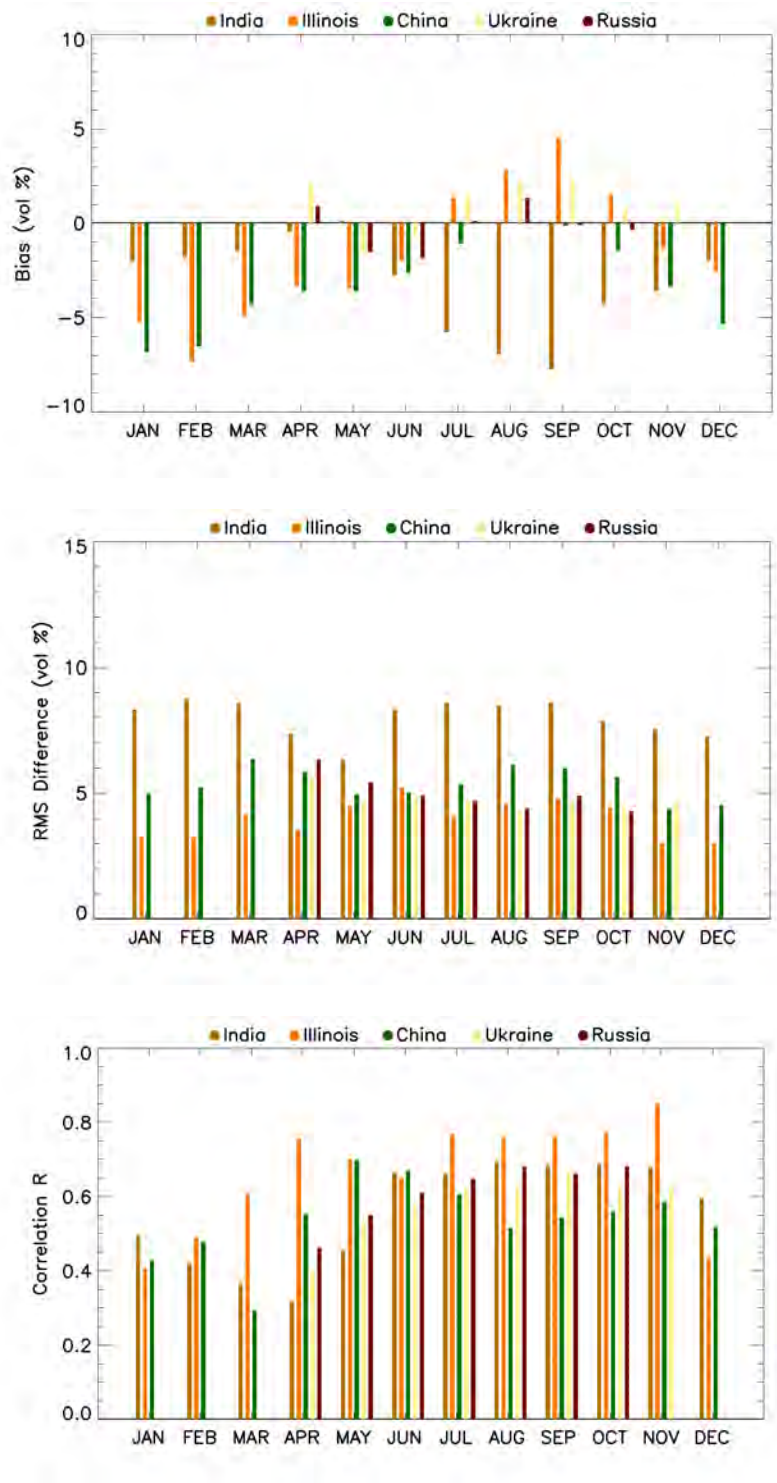

Figure 7-10 Annual variations of error statistics between scatterometer derived volumetric soil moisture and in-situ. Shown are the bias, the standard deviation (RMS Difference) and the Correlation R.

8 CONCLUSIONS AND FUTURE DIRECTIONS

8.1 Summary

The thesis was concerned with the global application of a new technology to derive soil moisture information from ERS scatterometer data. The method is a combination of an empirical model describing basic scattering processes of land surfaces and a change detection method to retrieve geophysical parameters. Based on the analysis of scatterometer data a global soil moisture archive has been set up and validated.

The applied methodology, developed under specific natural conditions was successfully applied to global land surfaces. The retrieved parameters of the empirical model generally depict basic scattering properties evident from theoretical reasoning well. The distinct influence of vegetation on scattering properties was shown based on a comparative analysis with potential biomass and land cover types. Retrieved geophysical parameters include a trend indicator for surface and profile soil moisture, volumetric soil moisture and information on freeze/thaw cycles. Geophysical parameters were validated extensively using gridded precipitation data and *in-situ* soil moisture data from five different agro meteorological networks.

Comparison with global gridded precipitation data indicates that the soil moisture trend is correctly captured by the applied method. Negative correlation can only be found over limited regions in desert climates. In extreme climates, such as the Arctic North and the dry regimes of Africa, correlation was found to be insignificant. A possible reason for the low correlation is the sparse station network in these areas resulting in questionable gridded precipitation estimates. Overall the correlation is high given that soil moisture and precipitation are different climatic processes.

To receive a quantitative measure of quality scatterometer based soil moisture has been compared to *in-situ* soil moisture measurements of five different agrometeorological networks. In total, data from 493 stations encompassing more than 48000 soil moisture samples have been compared. The estimated error is in the range 5-6 vol % indicating the reliability of the applied method.

Analysis has shown that there is still potential for improvements. Following problems should be addressed in future work

- In the current formulation of the model, surfaces are assumed to be azimuthal anisotrop, i.e. backscatter is independent of the azimuthal look direction. It has been shown that this assumption is valid for most of the land surfaces, introducing only little additional error.

However, over specific regions strong azimuthal effects are observed, therefore necessitating a correction procedure for azimuthal variations.

- The applied method assumes that at least once the land surface is observed under completely dry and wet conditions. In very dry climates, this assumption is violated, as soils might never reach saturation. Based on an empirical relationship a simple correction method has been implemented. The correction method will however result in biased estimates if the surface is rough. Based on model simulations an improved method should be developed, which can be applied to a wide range of surfaces.
- The method developed to account for vegetation cover works effective over a wide range of land surface types. Nevertheless it has been observed, that over specific landscapes mainly found on the African continent the modelled vegetation influences may be questionable. Currently it is difficult to properly attribute the observed phenomena to natural processes, as reference data over the respective area is widely unavailable. Reanalysis over these regions should lead to an improved understanding of vegetation phenology and of the effect of vegetation on the backscatter signal.

8.2 Future Directions

Initially designed to measure winds over the oceans, scatterometer instruments turned out to be a valuable instrument for land applications. The results of first explanatory land studies were promising and in the meantime a number of unforeseen applications with exciting results have emerged. History has shown that with the availability of a new generation of sensors, scientific research and application have revives. It is therefore expected that recently started and future low resolution microwave missions will push developments in this area to new frontiers. Three mission will be in the spotlight of future developments, Seawinds on Quickscat and its successor on ADEOS, the Advanced Scatterometer on METOP and the Soil Moisture and Ocean Salinity mission.

8.2.1 The Seawinds Sensor

SeaWinds is a Ku-band scatterometer built by the Jet Propulsion Laboratory (JPL). The instrument uses a rotating dish antenna with two spot beams that sweep in a circular pattern, covering a swath of 1800 km for the outer beam. The first SeaWinds instrument has been launched on board of the QuikSCAT satellite in June 1999, the second will follow when ADEOS II will be launched, now foreseen in November 2002. The increased attenuation of K_u-band electromagnetic waves by vegetation will probably limit possible applications to vegetation

sparse seasons or regions. Figure 8-1 and Figure 8-2 illustrate the potential of this sensor for land applications. Remarkably is the high temporal sampling rate of Seawinds. In both regions, Seawinds better captures temporal dynamics of relevant geophysical processes. The ERS scatterometer sometimes misses single rainfall events or short melting events during the cold season. However, the influence of vegetation on backscatter in K_u-band still has to be investigated in more detail before this sensor can be used for wide spread operational applications. Nevertheless, comparing data from the ERS scatterometer and from Seawinds can significantly extend our knowledge of global scattering properties of the land surface. Simultaneous analysis of time series will give insight into the potential and synergistic use of multipolarization and multifrequency data and their sensitivity to geophysical processes. The time series of Figure 8-1 and Figure 8-2 also illustrate the importance of temporal resolution if geophysical properties of the land surface hydrology should be fully captured, and indicate the potential of the future ASCAT mission.

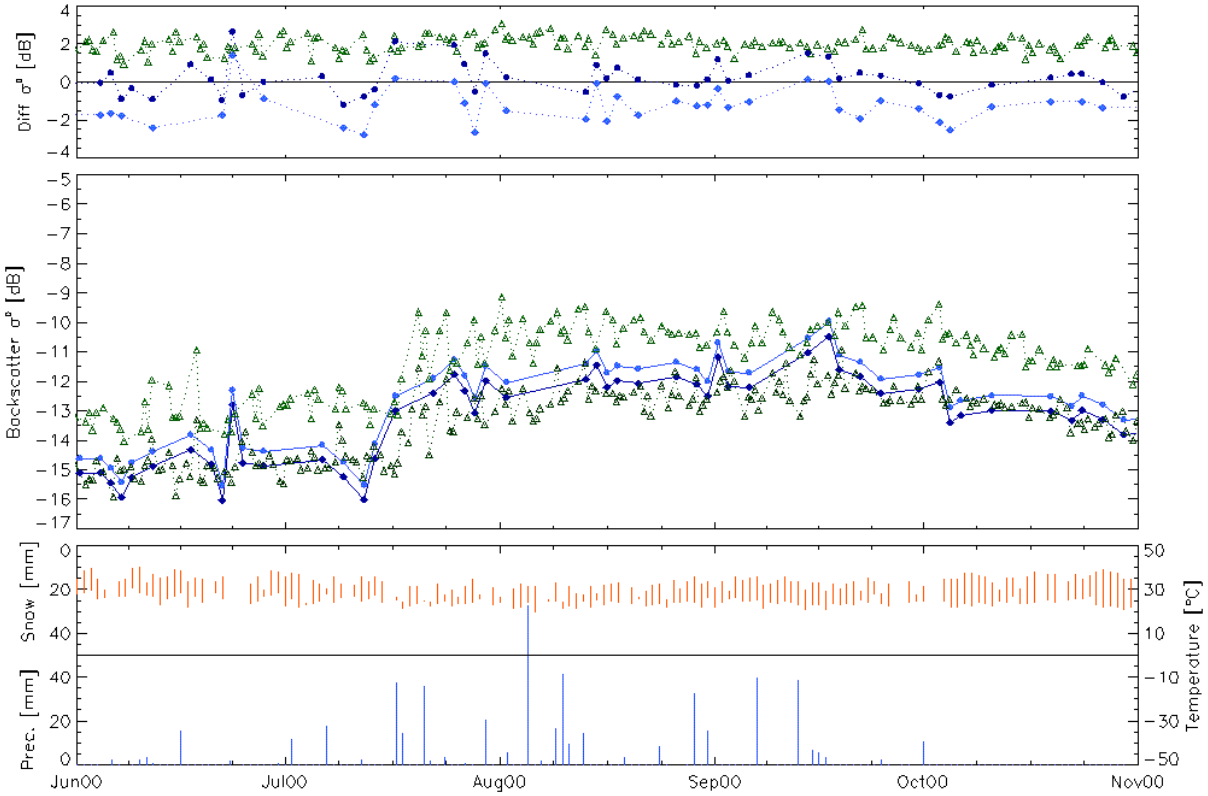

Figure 8-1: σ^0 and meteorological time series for San/Mali (4.1°W, 14.6°N). Bottom: synoptic meteorological data (minimum/maximum temperature and precipitation); Centre: C-band σ^0_{VV} extrapolated to 46° (blue dots) and σ^0_{VV} extrapolated to 54° (dark blue diamonds), K_u-band $\sigma^0_{HH}(46)$ (green triangles) and $\sigma^0_{VV}(54)$ (dark green triangles); Top: difference C-band $\sigma^0_{VV}(46)$ and K_u-band $\sigma^0_{HH}(46)$ (blue dots), difference C-band $\sigma^0_{VV}(54)$ and K_u-band $\sigma^0_{VV}(54)$ (dark blue diamonds), K_u-band $\sigma^0_{HH}(46)$ and $\sigma^0_{VV}(54)$ (green triangles).

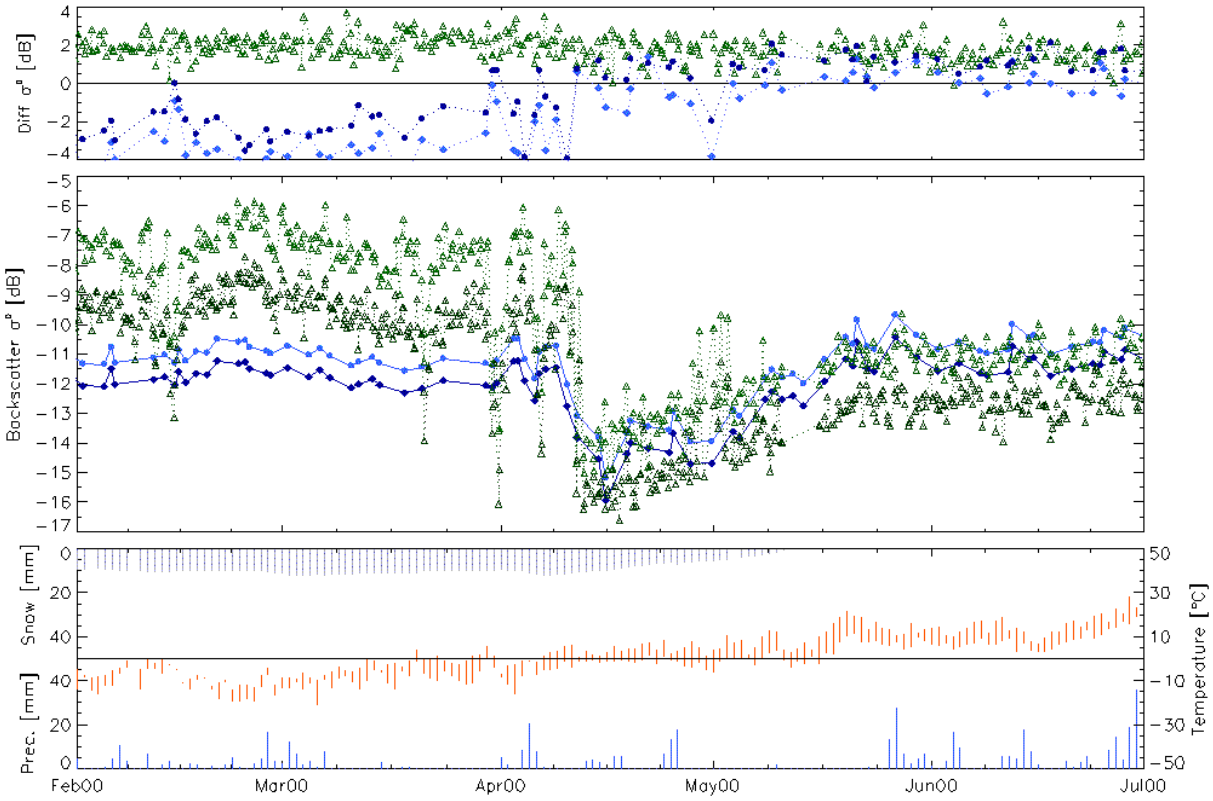

Figure 8-2: Same as Figure 8-1 but for Rovaniemi/Finland (25.8°E, 66.6°N).

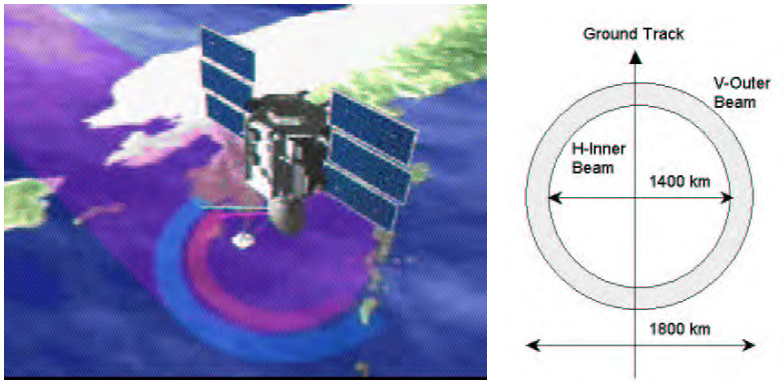

Figure 8-3: The Seawinds sensor onboard of Quikscat and the satellite geometry.

8.2.2 The Advanced Scatterometer

The Advanced Scatterometer (ASCAT) is a C-band scatterometer and has six antennas that look at the surface from different viewing directions. It is the direct successor of the ERS Scatterometer. It will be flown on a series of three METOP satellites, which are planned to be operated over a period of 14 years, starting with the launch of METOP-1 in 2005. Due to the six

antennas of the sensor, daily global coverage will be 82%, further the senor offers an improved resolution of 25 x 25 km². The expected merits are an improved view on the land surface through the daily coverage. As the sensor design is similar to the ERS scatterometer sensors, there is evidence to believe that methods and knowledge currently available can directly be used for ASCAT data analysis.

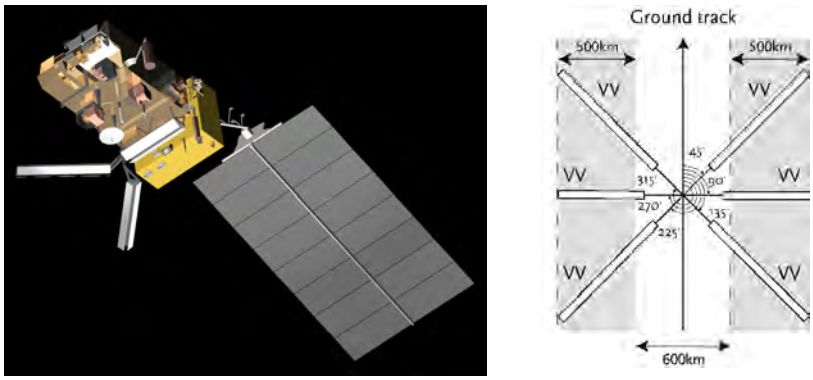

Figure 8-4: The Advanced Scatterometer onboard of METOP and the satellite geometry.

8.2.3 The Soil Moisture and Ocean Salinity Mission

The SMOS Mission is an Earth Opportunity mission of the European Space agency dedicated to the monitoring of soil moisture monitoring and ocean salinity. It is the first satellite mission specifically dedicated to monitoring the soil moisture process on a global scale. The instrument is a passive microwave radiometer operating in L-band with a spatial resolution of about 50 km. The sensor will be launched in 2006 and is planned to operate for 3 years. A passive microwave concept was chosen for SMOS because it is currently held, that passive sensors are more suited to measure soil moisture over land surfaces as they are insensitive to surface roughness effects. Still data has to be corrected for temperature and vegetation cover effects. SMOS will throw attention of the scientific community on the topic of large scale soil moisture monitoring, from which also the active microwave community will profit.

9 REFERENCES

Attema E.P., F.T. Ulaby (1978) Vegetation modeled as a water cloud, *Radio Science, Vol. 13, pp. 357-364.*

Bindlish R., A. P. Barros (2000) Multifrequency Soil Moisture Inversion from SAR Measurements with the Use of IEM, *Remote Sensing of Environment, Vol. 71, pp. 67-88*.

Blöschl, G., M. Sivapalan (1995) Scale issues in hydrological modelling: A Review, *Hydrological Processes, Vol. 9, pp. 251-290.*

Champion I. (1996) Simple Modeling of Radar Backscattering Coefficients over a Bare Soil: Variation with Incidence Angle, Frequency and Polarization, *International Journal of Remote Sensing, Vol. 17, pp. 783-800.*

Clevers J.G.P., H.J.C. van Leeuwen (1996) Combined optical and microwave remote sensing data for crop growth monitoring, Remote Sensing of Environment, *Vol. 56, pp. 42-51*.

Cookmartin G., P. Saich, S. Quegan, R. Cordey, P. Burgess-Allen, A. Sowter (2000) Modeling microwave interactions with crops and comparison with ERS-2 SAR observations, *IEEE Transactions Geoscience and Remote Sensing, Vol. 38, pp. 658-669.*

Cramer, W., D. W. Kicklighter, A. Bondeau, B. Moore III, G. Churkina, B. Nemry, A. Ruimy, A Schloss and the participants of the Potsdam NPP Model Intercomparison (1999) Comparing global models of terrestrial net primary productivity (NPP): overview and key results, *Global Change Biology, 5(suppl. 1):1-15.*

Davidson M.W.J., T. Le Toan, F. Mattia, G. Stalino, t. Manninen, M. Borgeaud. (2000) On the characterization of agricultural soil roughness for radar remote sensing studies, *IEEE Trans. Geoscience and Remote Sensing, Vol. 38, pp. 630-640.*

Dawson M.S., A.K. Fung, M.T. Manry (1997) A Robust Statistical-Based Estimator for Soil Moisture Retrieval from Radar Measurements, *IEEE Transactions. Geoscience and Remote Sensing, Vol. 35, pp. 57-67*

Delworth T.L., S. Manabe (1988) The influence of potential evaporation on the variabilities of simulated soil wetness and climate, *Journal of Climate, Vol. 1, pp. 523-547*

Delworth T. L., S. Manabe (1993) Climate Variability and Land-Surface Processes, *Advances in Water Resources, Vol. 16, pp3-20*

Dirnmeyer, A. P. (1995) Problems in Initializing Soil Wetness, Bulletin of the American Meteorological Society, Vol. 76, No. 11, pp. 2234-2240.

Dobson M.C., F.T. Ulaby (1986) Active Microwave Soil Moisture Research, *IEEE Transactions. Geoscience and Remote Sensing, Vol.. 24, pp. 23-35.*

Dobson M.C., F.T. Ulaby (1998) Mapping Soil Moisture Distributions With Imaging Radar. *In "Principles and Applications of Imaging Radar – Manual of Remote Sensing" 3rd edition, Volume 2, John Wiley & Sons, ISBN 0-471-29406-3.*

Dubois P. C., J. van Zyl, T. Engman (1995) Measuring Soil Moisture with Imaging Radars, *IEEE Transactions Geoscience and Remote Sensing, Vol.. 33, pp. 915-926.*

Engman E. T., N. Chauhan (1995) Status of Microwave Soil Moisture Measurements with Remote Sensing, *Remote Sensing of Environment, Vol. 51, pp. 189-198*.

Entin J.K, A. Robock., K.Y. Vinnikov, S. E. Hollinger, S. Liu, A. Namkhai (2000) Temporal and spatial scales of observed soil moisture variations in the extratropics. *J. Geophys. Res*., 105, 11,865-11,877.

Entin, J. K., A. Robock, K. Y. Vinnikov, V. Zabelin, S. Liu, A. Namkhai, and Ts. Adyasuren (1999) Evaluation of Global Soil Wetness Project soil moisture simulations. J. Meteorol. Soc. Japan.

ESA (1992) ERS-1 System, *ESA SP-1146, ESA Publications Division, Noordwijk, September 1992.*

ESRI (1993) The digital chart of the World for use with ARC/INFO, Data Dictonary, *Environmental Systems Research Institute Inc., 380 New York Street, Redlands, CA 92373 USA.*

Frison P.L., E. Mougin (1996) Monitoring global vegetation dynamics with ERS-1 wind scatterometer data, *International Journal of Remote Sensing, Vol. 17, pp. 3201-3218.*

Frison P. L., E. Mougin, P. Hiernaux (1998) Observations and Interpretation of Seasonal ERS-1 Wind Scatterometer Data over Northern Sahel (Mali), *Remote Sensing of Environment, Vol. 63, pp. 233-242.*

Fung A.K. Z.Li and K.S. Chen (1992) Backscattering from a randomly rough dielectric surface, *IEEE Trans. Geoscience and Remote Sensing, Vol. 30, pp. 356-369.*

Fung, A. K., and G.W. Pan (1987) A scattering model for perfectly conducting random surfaces: I. Model development, *International Journal of Remote Sensing, Vol. 8, pp. 1579-1593.*

Georgakakos, K.P., O.W. Baumer (1996) Measurement and utilization of on-site soil moisture data, *J. Hydrology, Vol. 184, pp. 131-152*

Ghil M., (2001) Natural climate variability, in *Encyclopedia of Global Environmental Change*, T. Munn (Ed.), Vol. 1, J. Wiley & Sons, Chichester/New York, in press.

Gilman D.L., F.J. Fuglister, J.M. Mitchel, (1963) On the power of "red noise", *Journal of the Atmospheric Sciences, Vol 20, pp. 182-184*

Global Soil Data Task (2000) Global Gridded Surfaces of Selected Soil Characteristics (IGBP-DIS). International Geosphere-Biosphere Programme - Data and Information Services. Available on-line [http://www.daac.ornl.gov /] from Oak Ridge National Laboratory Distributed Active Archive Center, Oak Ridge, Tennessee, U.S.A.

Goutorbe, J.-P. (1997) An overview of HAPEX-Sahel: A study in climate and desertification, *J. Hydrology., 188-189*, pp. 4-17.

GPCC (1998) The Global Precipitation Climatology Centre. Information on World Wide Web under http://www.dwd.de/research/gpcc

Grassl, H., and L. Bengtsson, (2001) personal communication, *EURISY summer school, Budapest, Hungary, September 2001*

Hasselmann K. (1976) Stochastic climate models. Part I, Theory, *Tellus, 28, 473-485.*

Hillel D. (1982) Introduction to soil physics, *Academic Press, San Diego, California, ISBN 0-12-348520-7*

Hollinger, S.E., S. A. Isard (1994) A Soil Moisture Climatology of Illinois, *J. Climate, Vol. 7, pp. 822-833*

Jackson. T. J., D. M. LeVine, C. T. Swift, T. J. Schmugge, and F. R. Schiebe, Large area mapping of soil moisture using the ESTAR passive microwave radiometer, *Remote Sens. Environ., 53*, pp. 27-37, 1995.

Jackson T. J. (Ed.) (1999) Soil Moisture Research Mission (EX-4) A report from the NASA Post-2002 Land Surface Hydrology Planning Workshop, Irvine, CA, April 12-14th, 1999, http://lshp.gsfc.nasa.gov/Post2002/smm3.html

Köppen, W., 1923: Die Klimate der Erde. Walter de Gruyter, Berlin

Kunch T., B. Frazier, W.L. Pan, A.M. Smith (2001) Satellite radar assessment of winter cover types, *Canadian Journal of Remote Sensing, Vol. 27, pp. 603-615.*

Leemans, R. and Cramer, W., 1991. "The IIASA database for mean monthly values of temperature, precipitation and cloudiness on a global terrestrial grid". Research Report RR-91-18. November 1991. International Institute of Applied Systems Analyses, Laxenburg, pp. 61.

Leeuwen, H., R. Verhoeven, H. Denier van der Gon, H. van der Woerd, L. Janssen, J. Tjalling (1998) Feasibility study in using scatterometer data for wetland rice mapping yielding methane emission indicators for global applications, *Workshop on Emerging Scatterometer Applications: From Research to Operations, ESTEC, Noordwijk, The Netherlands, 5-7 October 1998, ESA-SP-424, pp. 45-48*

Lecomte, P., W. Wagner (1998) ERS Wind Scatterometer Commissioning and in-flight Calibration, *Workshop on Emerging Scatterometer Applications: From Research to Operations, ESTEC, Noordwijk, The Netherlands, 5-7 October 1998, ESA-SP-424, pp. 261-270.*

Lieth, H., 1972. "Modelling the primary productivity of the earth. Nature and resources", UNESCO, VIII, 2:5-10.

Lomb N.R. (1976) Least-squares frequency analysis of unequally spaced Data, *Astrophysics and Space Science Vol. 39, pp. 447-462*.

Long, D., M. R. Drinkwater (2000) Azimuth Variations in Microwave Scatterometer and Radimoter Data Over Antarctica, *IEEE Trans. Geoscience and Remote Sensing, Vol. 38, pp.1857-1870.*

Loveland, T.R., Reed, B.C., Brown, J.F., Ohlen, D.O., Zhu, J, Yang, L., and Merchant, J.W. (2000) Development of a Global Land Cover Characteristics Database and IGBP DISCover from 1-km AVHRR Data, *International Journal of Remote Sensing , Vol. 21, no. 6/7, p. 1,303-1,330*.

Magagi R.D., Y.H. Kerr (1997) Retrieval of soil moisture and vegetation characteristics by use of ERS-1 wind scatterometer over arid and semi arid areas, *J. Hydrology, No. 188-189, pp. 361-384.*

Magagi R.D., Y.H. Kerr. (2001) Estimating surface soil moisture and soil roughness over semiarid areas from the use of the copolarization ratio, *Remote Sensing of Environment, Vol. 75, pp. 432-445*

Major D.J., A.M. Smith, M.J. Hill, W.D. Willms, B. Brisco and R.J. Brown (1994) Radar backscatter and visible infrared reflectance from short-grass prairie, *Canadian Journal of Remote Sensing, Vol. 20, pp. 71-77.*

Mann M.E., J.M. Lees (1996) Robust Estimation of Background Noise and Signal Detection in Climatic Time Series, *Climate Change Vol 33 pp. 409-445*

McNairn H., R.J. Brown, J. Ellis and D. Wood (1998) Extraction of crop information from RADARSAT-1 imagery, *Proceedings, ADRO Final Symposium, Montreal, Canada, Oct. 12-15. (CD-ROM).*

Moran M.S., A. Vidal, D. Troufleau, Y. Inoue, T.A. Mitchell. (1998) Ku-band C-band SAR for discriminating agricultural crop and soil conditions, *IEEE Trans. Geoscience and Remote Sensing, Vol. 36, pp. 265-272.*

Moran M. S., D. C. Hymer, J. Qi, E.E. Sano (2000) Soil Moisture Evaluation Using Multi-Temporal Synthetic Aperture Radar (SAR) in Semiarid Rangeland, *Agricultural and Forest Meteorology Vol. 105, pp. 69-80.*

Muller R.A., G.J. MacDonald (1995) Ice Ages and Astronomical Causes – Data Spectral Analysis and Mechanisms, *Springer-Praxis Books in Environmental Science, Springer Verlag, ISBN 1-85233-634-X*

Narayanan R. M., P. P. Hirsave (2001) Soil Moisture Estimation Models Using SIR-C SAR Data: A case study in New Hampshire, USA, *Remote Sensing of Environment, Vol. 75, pp. 385-396.*

Oevelen, P. J. van, D. H. Hoekman (1999) Radar Backscatter Inversion Techniques for Estimation of Surface Soil Moisture: EFEDA-Spain and HAPEX-Sahel Case Studies, *IEEE Trans. Geosci. Remote Sensing, Vol. 37, pp. 113-123.*

Oh Y., K. Sarabandi, F.T. Ulaby (1992) An Empirical Model and an Inversion Technique for Radar Scattering from Bare Soil Surfaces, *IEEE Transactions Geoscience and Remote Sensing, Vol 30, pp. 370-381*.

Pulliainen, J. T., T. Manninen, M. Hallikainen (1998) Application of ERS-1 Wind Scatterometer data to soil frost and soil moisture monitoring in boreal forest zone, *IEEE Trans. Geosci. Remote Sensing, Vol. 36, pp. 849-863.*

Prevot L., I. Champion, G. Guyot. (1993a) Estimating surface soil moisture and leaf area index of a wheat canopy using a dual-frequency (C and X bands) scatterometer, *Remote Sensing of Environment, Vol. 46, pp. 331-339.*

Prevot L., M. Dechambre, O. Taconet, D. Vidal-Madjar, M. Normand, S. Galle (1993b) Estimating the characteristics of vegetation canopies with airborne radar measurements, *International Journal of Remote Sensing, Vol. 14, pp. 2803-2818.*

Quesney, A., S. Le Hégarat-Mascle, O. Taconet, D. Vidal-Madjar, J. P. Wigneron, C. Loumange, M. Normand (2000) Estimation of watershed soil moisture index from ERS/SAR data, Remote Sens. Environment, Vol. 72, pp. 290-303.

Quilfen, Y. (1995) ERS-1 Offline Wind Scatterometer Products, *IFREMER, Ref. No. C1-EX-MUT-CD0000-03-IF, Version 1.1, December 1995.*

Robock A., K. Y. Vinnikov, G. Srinivasan, J. K. Entin, S. E. Hollinger, N. A. Speranskaya, S. Liu, A. Namkhai (2000) The Global Soil Moisture Data Bank. *Bull. Amer. Meteorol. Soc., 81, pp. 1281-1299.*

Rombach, M., W. Mauser (1997) Multi-annual analysis of ERS surface soil moisture measurements of different land uses, *3rd ERS Symposium on Space at the service of our Environment, Florence, Italy, 14-21 March, European Space Agency, SP-414, pp. 27-34*

Rott, H., W. Rack (1995) Characterisation of Antarctic Firn by Means of ERS-1 Scatterometer Measurements, *IGARSS'95, pp.2041-2043*

Rudolf, B., H. Hauschild, W. Rueth and U. Schneider (1994): Terrestrial Precipitation Analysis: Operational Method and Required Density of Point Measurements. In: Global Precipitations and Climate Change (Ed. M. Desbois, F. Desalmond), NATO ASI Series I, Vol. 26, Springer-Verlag, p. 173-186.

Scargle J.D. (1982) Studies in Astronomical Time Series Analysis. II. Statistical Aspects of Spectral Analysis of Unevenly Spaced Data, *The Astrophysical Journal, Vol. 263, pp. 835-853*

Schlittgen R., Streitberg H. (1995) Zeitreihenanalyse, *Oldenburg Verlag, München, ISBN 3-486-23408-0*

Schmullius, C. (1997) Monitoring Siberian forests and agriculture with the ERS-1 Windscatterometer, *IEEE Trans. Geoscience and Remote Sensing, Vol. 35, No. 5, pp. 1363-1366.*

Schulz M., Statteger K., (1997) SPECTRUM: Spectral Analysis of unevenly spaced paleoclimatic time series, *Computer & Geosciences Vol 23., No. 9 pp. 929-945*

Schulz M., Mudelsee M., (2001) REDFIT: Estimating red-noise spectra directly from unevenly spaced paleoclimatic time series, *Computers and Geoscience, in press.*

Scipal, K. (1999) Monitoring Thaw Freeze Cycles over Northern Canada using ERS Scatterometer Data, *M.Sc. Thesis, Vienna University of Technology, October 1999, 80 p.*

Shi J., J. Wang, A. Y. Hsu, P. E. O'Neill, E. T. Engman (1997) Estimation of Bare Surface Soil Moisture and Surface Roughness Parameters Using L-band SAR Image Data, *IEEE Trans. Geoscience and Remote Sensing, Vol. 35, pp. 1254-1266*

Schmugge, T., T. J. Jackson, and H. L. McKim, 1979. Survey of In-Situ and Remote Sensing Methods for Soil Moisture Determination. *Satellite Hydrology, American Water Resources Association.*

Schulin, R., H. Flühler, H. M. Selim, B. Sevruk, P. J. Wierenga, (1992) Soil Moisture, Part III, In Snow cover measurements and areal assessment of precipitation and soil moisture, edited by B. Sevruk, WMO, Operational Hydrological Report, No. 55, pp. 219-283.

Srinivasan, S. (2001) personnel communication

Storch von H., A. Navarra (1999) Analysis of Climate Variability - Applications of Statistical Techniques, *Springer Verlag, ISBN 3-540-66315-0*

Taconet O., M. Benallegue, D. Vidal-Madjar, L. Prevot, M. Dechambre, M. Normand (1994) Estimation of soil and crop parameters for wheat from airborne backscattering data in C and X bands, *Remote Sensing of Environment, Vol. 50, pp. 287-294.*

Thomson D.J. (1982) Spectrum Estimation and Harmonic Analysis, *IEEE Proc., Vol 70, No 9, pp. 1055-1096*

Touré A., K.P.B. Thomson, G. Edwards, R.J. Brown, B. Brisco (1994) Adaptation of the MIMICS backscattering model to the agricultural context: Wheat and Canola at L and C bands, *IEEE Trans. Geoscience and Remote Sensing, Vol. 32, pp. 4761*.

Ulaby F. T., P.C Dubois, J. van Zyl. (1996) Radar Mapping of surface soil moisture, *Journal of Hydrology, Vol. 84, pp. 57-84*

Ulaby F.T., K. Sarabandi, K. McDonald, M. Whitt, M.C. Dobson (1990) Michigan microwave canopy scattering model, *International Journal of Remote Sensing, Vol. 11, pp. 1223-1253.*

Ulaby F. T. (1998) SAR Biophysical Retrievals: Lessons Learned and Challenges to Overcome, *Applications Workshop on Retrieval of Bio- and Geo-Physical Parameters from SAR Data for Land, ESTEC, Nordwijk, The Netherlands, 21-23 October 1998.*

Vinnikov K. Y., I. B. Iserkepova (1991) Soil Misture: Empirical data and model results, *J. Climate, Vol. 4, pp. 66-79*

Wagner, W., K. Scipal (2000) Large-Scale Soil Moisture Mapping in Western Africa using the ERS Scatterometer, IEEE Trans. Geosci. Remote Sensing, Vol. 38, pp. 1777-1782.

Wagner, W., J. Noll, M. Borgeaud, H. Rott (1999a) Monitoring Soil Moisture over the Canadian Prairies with the ERS Scatterometer, *IEEE Trans. Geosci. Remote Sensing, Vol. 37, No. 1, pp. 206-216*

Wagner, W., G. Lemoine, M. Borgeaud, H. Rott (1999b) A Study of Vegetation Cover Effects on ERS Scatterometer Data, *IEEE Trans. Geosci. Remote Sensing*, Vol. 37, No. 2, pp. 938-948

Wagner, W., G. Lemoine, H. Rott (1999c) A Method for Estimating Soil Moisture from ERS Scatterometer and Soil Data, *Remote Sens. Environ.*, Vol. 70, pp. 191-207

Wei, M.-Y., Ed., (1995) Soil Moisture: Report of a Workshop held in Tiburno, California, 25-27 January 1994, *NASA Conference Publication 3319, 80 pp*

Wilks D.S. (1995) Statistical Methods in the Atmospheric Sciences, *Academic Press, ISBN 0-12-751965-3*

Wismann V., I. Woodhouse (2000) Monitoring of seasonal thawing in Siberia with ERS scatterometer data *IEEE Trans. Geoscience and Remote Sensing, Vol. 38 No. 4, pp. 1804 -1809*

Wismann V., I. Woodhouse (2001) Evaluation of Operational Land Applications of Scatterometers, Final Presentation held at EUMETSAT, Darmstadt, June 8, 2001.

Woodhouse I. H., D. H. Hoekman (2000a) Determining land-surface parameters from ERS Wind Scatterometer, *IEEE Trans. Geoscience and Remote Sensing, Vol. 38, No. 1, pp. 126-140*.

Woodhouse I. H., D. H. Hoekman (2000b) A model-based determination of soil moisture trends in Spain with the ERS-Scatterometer, *IEEE Trans. Geoscience and Remote Sensing., Vol. 38, No. 4, pp. 1783-1793.*

Xu H., M.D. Steven, K.W. Jaggard (1996) Monitoring leaf area of sugar beet using ERS-1 SAR data. *International Journal of Remote Sensing Vol. 17, pp. 3401-3410*.

Yanasse C.C.F., S. Quegan, R.J. Martin (1992) Inferences on spatial and temporal variability of the backscatter from growing crops using AgriSAR data, *International Journal of Remote Sensing, Vol. 13, pp. 493-507.*